Regulator Control of a Short-Radius Centrifuge and Subjective Responses to Head Movements in a Rotating Environment

by

Carol C. Cheung

S.B. Aeronautics and Astronautics
Massachusetts Institute of Technology, 1998

Submitted to the Department of Aeronautics and Astronautics in partial fulfillment of the requirements for the degree of

MASTER OF SCIENCE IN AERONAUTICS AND ASTRONAUTICS
AT THE

MASSACHUSETTS INSTITUTE OF TECHNOLOGY

June 2000

Author .....
Department of Aeronautics and Astronautics

Certified by .....
Laurence R. Young
Apollo Program Professor of Astronautics
Thesis Supervisor

Accepted by .....
Professor Nesbitt Hagood
Chairman, Departmental Graduate Committee

Regulator Control of a Short-Radius Centrifuge and Subjective Responses to Head Movements in a Rotating Environment

by

Carol C. Cheung

Submitted to the Department of Aeronautics and Astronautics on May 19, 2000 in Partial Fulfillment of the Requirements for the Degree of Master of Science in Aeronautics and Astronautics

Abstract

Artificial gravity is made through the centripetal force from a rotating chair or short-radius centrifuge. It is a very promising countermeasure, as it alone should remove all the adverse effects of microgravity. In order to effectively use artificial gravity as a long-duration space flight countermeasure, the effects of artificial gravity on the human body must be investigated. If artificial gravity is created by use of a short-radius centrifuge, the high angular velocity required, about 23 rpm, causes unexpected and illusory body motions when making head turns. My work in artificial gravity consisted of two parts, a study that investigated the vestibular response to head movements during centrifugation and regulator feedback control of the centrifuge.

This experiment studied the perceived illusory body sensations and heart rate changes induced by head movements in both the yaw and pitch planes while supine during centrifugation. Yaw right, yaw left, and pitch head movements yielded successively significantly higher heart rate than baseline. Results show that 68% of subjects in the yaw plane and 48% of subjects in the pitch plane experienced illusory body tilt as predicted by a model of the vestibular system while 13% in yaw and 40% in pitch experienced body tilt in the opposite direction from the predicted model. Pitch head movements yielded significantly higher magnitude and duration of illusory tilt. These side effects are serious and will need to be controlled if short-radius centrifugation is to be a successful countermeasure.

Regulator feedback control has been implemented on the centrifuge with both an optical encoder and an accelerometer. Tachometer development, automatic control, and classical PID control theory was used to develop the gain and integrator time constants, which lead to K=1.5 and Ti=1 sec. This results in an improved steady state error by 99.8% and a more accurate response of the centrifuge by 5.7% for the accelerometer and 52% for the encoder feedback system from the open loop system.

Thesis Supervisor: Laurence R. Young
Title: Apollo Program Professor of Astronautics, MIT

This work was supported by the National Space Biomedical Research Institute through a cooperative agreement with the National Aeronautics and Space Administration (NCC 9-58).

Acknowledgements

I would like to thank most my advisor Professor Larry Young who permitted me to do research in the area that interested me most. Also, for being so flexible with my thesis topic, permitting me to search for myself a subject, and do research with a wonderful research group. Your guidance and gentle push to keep the end in sight were invaluable and much appreciated.

Thank you to Heiko Hecht whose vision and crafted eye for interesting issues to pursue made research interesting, lively and always active. Thank you for your guidance in the ever confusing area of statistics of goodness of fits.

I would like to thank Jessica Kavelaars who made the lab a wonderful friendly, amiable place to come to every day. Jessica, together you and I designed and implemented Large N with grace and ease. Thank you for your excellent explanation of the protocol to these unknowing victims and your true partnership throughout the experiment.

Huge thanks to Chris Albert, the equipment wizard of the centrifuge. Thank you so much for all the work that you helped me with and the equipment that you added to the centrifuge. You went far beyond the call of duty and we researchers at the MVL are extremely grateful.

I'd like to thank Lisette Lyne for introducing me to the equipment and helping me sort through the madness. Thank you to Kathy Sienko for putting together the centrifuge and always being wary of its equipment. You were a brave pilot subject for 12 days of repeated artificial gravity exposure. And a special thanks to all of you from the MVL for the company. My time in research has been too short, and I will really miss coming to lab.

All my thanks to National Space Biomedical Research Institute whose vision and mission have funded this research and numerous other worthwhile pursuits in furthering the possibility for long-duration manned space flight missions.

Many credits to Erik Bailey whose Framemaker knowledge and template artistry and everlasting openness for haggling lends himself a great friend and indisposable for the accomplishment of this beast.

Thanks to Marsha Warren whose master knowledge of the inner workings of the MVL never permitted me to slip through the paper cracks.

To the MIT staff, the best staff I've known, you make being at MIT clear of red tape. Eileen Dorschner thank you for all those article searches, ancient or ambiguous, you found them all. Dick Perdichizzi, thank you for all your tachometer contributions and help in trying to control the bed.

And to my parents. You two are awesome. It's wonderful to be at the stage where you are my supports and my compass and always a welcome, familiar sound. Thank you.

Table of Contents

List of Figures

List of Tables

"Space and Time: It's the best relationship you can ever have. It will never leave you, lie to you, or turn back on you. And it will give you *everything*."

Milton Meyers
Jacob's Pillow, 1992

Chapter 1.0

Artificial Gravity Introduction

1.1 Thesis Introduction

This thesis includes two topics in the context of exploring artificial gravity as a countermeasure to the harmful effects of long-duration space flight. The first section describes an experiment concerning the subjective self-perceived illusory tilt, motion sickness, and heart rate following head turns in the yaw and pitch axes while supine during centrifugation. The second section documents the methods and analysis of the hardware equipment and regulator feedback control that has been implemented on the Man-Vehicle Lab's short-radius centrifuge.

1.2 Motivation

Short-duration space flights to the Moon have been successfully accomplished, and the new frontier is to further human exploration of other planets. To achieve this the physiological and psychological challenges of long-duration space flight and effective long-term countermeasures to maintain health must be acknowledged. A mission to Mars would require a travel duration of at least 6 months for lowest spaceflight energy consumption. However, one year would pass before Mars reaches a similar orientation to Earth in orbit for the return flight. Therefore, a round trip to Mars would take 2 years, 1 year at 3/8 g and a total of 1 year at 0 g.

NASA's Human Exploration and Development of Space Enterprise has an initiative to achieve advanced biomedical knowledge and technologies to maintain human health and performance on long-duration missions before the year 2008 (http:// www.hq.nasa.gov/office/nsp/hedsroad.htm, 2000). Particularly, if manned missions are to explore other gravitational bodies, i.e. planets and moons, human health, mobility and functional control are a major concern. Humans may be able to tolerate missions up to 15 months while in microgravity. However, upon return to gravitational

environments, adverse symptoms of diminished orthostatic tolerance, deterioration of the musculoskeletal system, and posture and gait instability severely reduce the astronaut's ability to function (Young, 1999). Various countermeasures are in development to address the adverse effects of microgravity while in space, but accomplishments are limited in maintaining human health in a condition to function safely and effectively in a gravitational environment following exposure to microgravity. This may be due to the difficulty in conditioning the body for constant gravitoinertial forces like gravity while in a microgravity space environment.

Artificial gravity, though the idea has been around for almost a century, has unclear short- and long-term effects on humans. It is theoretically an ideal countermeasure since it systematically reverses the adverse effects to humans by replacing the source of problem, a missing gravitoinertial field. Although science fiction has illustrated engineering feats of rotating spacecraft and tethered modules, existing test facilities explore artificial gravity with rotating rooms and short-radius centrifuges. It is important to study the side effects of human centrifugation in determining the feasibility of short-radius centrifugation for maintaining the functionality of the vestibular, cardiovascular, and skeletal system.

1.3 Adverse Effects of Microgravity & Countermeasures

A number of programs are currently underway to develop methods to counteract the deleterious effects of microgravity. This section discusses some of the issues affecting the astronaut while in space, which would effect the functional ability upon the return to Earth.

1.3.1 Muscular Atrophy

In microgravity, the human body no longer works against the continual force of gravity to remain upright or ambulate, so muscle atrophy occurs without intervention. Humans are subject to acute and extreme loss of gravitational loading on bone and muscle. Cardiac and skeletal muscle deconditioning occurs in microgravity even if extrememly strenuous exercise programs are used (Landauer and Burke, 1998). Experiments with

space flown rats showed a doubling of nonmyofiber area in the adductor longus muscles, measured after 2.3 hours postflight from Spacelab Life Sciences-1 and -2 missions (Riley, Ellis, Slocum, Sedlack, Bain, Krippendorf, Lehman, Macias, Thompson, Vijayan, 1996). A rigorous exercise regime for astronauts has been corrective, as after a 120-day spaceflight, astronauts have walked off the Orbiter without medical attention. Additionally, a drug called dobutamine (a synthetic adrenomimetic) improves exercise performance by mechanisms that prevent the decline in peak O_2 consumption and reduce the concentration of lactic acid measured in the blood and may be used for use in microgravity to reduce the rate of muscle atrophy (Tipton and Sebastian, 1997).

1.3.2 Space Motion Sickness

Space motion sickness can occur abruptly when the astronaut is suddenly overcome with an orientation conflict. While in space, the astronaut develops a sense of direction by synthesizing which way is "down". However, when the astronaut sees an object normally perceived as upright, like another astronaut, which is now inverted; suddenly the astronaut's conception of "down" is conflicted. This is called the inversion illusion (Oman, 1990), and is often accompanied by motion sickness. Pharmaceutical drugs, such as promethazine, though not completely successful, have improved the nausea and sickness symptoms that can sometimes immobilize an astronaut's productivity.

1.3.3 Bone Loss

One particularly deleterious effect is reduced bone density, as there is no evidence from space missions that bone density loss has been reduced by current countermeasures. Data from Mir missions document bone loss in microgravity even through an aggressive countermeasure program. Average losses were 0.35 % per month, however, load bearing areas lost more than 1 % per month. If unabated, this rate of degradation would lead to osteoporosis (Bucky, 1999). However, pharmaceutical agents in a research enviorment such as androgens have shown to counteract this loss. The use of testosterone improved bone mass density by 85 % while the use of nandrolone decanoate improved bone mass density by 76 %

(Wimalawansa, Chapa, Wei, Westlund, Quast, Wimalawansa, 1999). However, the use of these drugs have yet to be implemented in space.

1.3.4 Cardiovascular Deconditioning

Similarly, research to counteract the deconditioning effects of microgravity to the cardiovascular system is being explored. Microgravity simulation by hindlimb unweighting of rats for 20 days showed a reduction of contractility in arteries but generally had no effect on veins (Purdy, Duckles, Krause, Rubera, Sara, 1998). Human cardiovascular changes that occur in microgravity reduce extracirculatory tissue pressures which elevates cardial transural pressures, increasing central circulation. Reduced postural baroflex stimulation appears to reduce heart rate and its variability in spaceflight (Watenpaugh, Smith, 1998). Different methods of exercise, such as isometric contractions, lead to the activation of threshold chemosensitive receptors (P-receptors), which induce sympathetic excitation resulting in increases of heart rate, vascular resistance, arterial pressure, and breathing depth (Tallarida, 1991). Also, drugs such as Dextroamphetamine, are undergoing research to reduce symptoms of post-flight orthostatic intolerance (Snow, 1995).

1.3.5 Degraded Immune System

The immune system is also known to have changes in T-cells due to exposure to microgravity. A Space Shuttle Endeavor (STS-77) experiment flew 12 rats on a 10-day mission to study the effect of microgravity on the immune system. The percentage of cytotoxic/suppressor (TCR+/CD8+) T-cells increased significantly, and decreases in splenic helper (TCR+/CD4+) T-cells and (CD11b+) macrophages, showing the rats considerable decrease in the ability for rats to mount an immune response (Pecaut, Simske, Fleshner, Zimmerman, 1997). Recently, the use of insulin-like growth factor-1 (IGF-1) was shown to attenuate induced changes in the immune system from a 10-day exposure to space microgravity in rats (Chapes, Forsman, Simske, Bateman, Zimmerman, 1999).

1.3.6 Space Radiation

Another concern of human space flight is radiation exposure. Without an atmosphere, humans are susceptible to much more harmful radiation particles: gamma rays, cosmic rays, solar particles, and heavy ions. Long duration space missions preclude particularly harmful prolonged exposures to this radiation leading to genetic mutations, increased probability for cancer and genetic diseases. Factual evidence of the harmful effects of space radiation is limited and is perhaps in the earliest stages of research (NASA report 19980024368, 1998; Ohnishi, Wang, Fukuda, Takahashi, Ohnishi, Nagaoka, 1998).

1.3.7 Vestibular Disturbances

Astronauts have experienced acute vestibular disturbances, leading to duress and a loss of performance while in space. A common symptom is space motion sickness that affects approximately 50 % of all astronauts and cosmonauts (Cowings, 1994). Countermeasures such as Dextroamphetamine and autogenic feedback training have been explored and reduced the extent of these disturbances. Although vestibular adaptation occurs in the weightless environment within 2-4 days, the mechanisms responsible for the disturbance and the vestibular adaptation are unknown. To understand vestibular function in space and normal gravity-dependent conditions, the basic physiological mechansism of vestibular function must be understood (Dickman, 1998).

1.4 Artificial Gravity Countermeasure

While most countermeasures attempt to rectify a particular degradation of the human condition, there is one countermeasure that is theoretically ideal -- artificial gravity. If artificial gravity were to completely replace the missing stimulus that is the cause of these adverse side effects, then artificial gravity alone would be needed for astronauts to sustain functional and physiological well-being. Artificial gravity is accomplished by the centripetal force of a rotating body to "pull" a person "downward". Two main

designs have been considered, a large radius rotating spacecraft or a short-radius centrifuge for at most a few persons.

Artificial gravity has proven to counteract the effects of cardiovascular decompensation. The stimulus of artificial gravity can be likened to orthostasis when going from a supine to a standing position. Burton and Meeker (1992) showed that a short-radius centrifuge is capable of eliciting a vigorous stimulation of the baroreceptors to tolerate almost 2 g over a gradual onset of 0.1 g/s to rapid onset of 1 g/s. Periodic exposure to artificial gravity would expose astronauts to cardiovascular stimulation similar to maintain orthostatic tolerances.

1.4.1 Short-Radius Centrifuge for Artificial Gravity

While a large radius spacecraft results in a smaller differential g-loading along the human body and the spacecraft would be able to rotate at a slower rate than a short-arm centrifuge for the same inertial force, the complexity of engineering construction and controlling a spacecraft that size is currently too costly for materials standards today.

However, a short-arm centrifuge is comparatively practical in terms of implementation. Its small size, between a 2-5 m radius, low power supply, controllability, and comparable low cost make a short-radius centrifuge ideal in the current budget-tight agenda for research in the applicability of artificial gravity as a countermeasure for long-duration manned missions.

1.4.2 Problems with Artificial Gravity

Although artificial gravity through short-radius centrifugation may replace gravity in a 0-g environment, there are a number of considerations that need to be taken into account. Since it is not reasonable for an astronaut to remain on a short-radius centrifuge for the complete duration of the mission, a short-arm centrifuge implies an intermittent, non-continuous exposure to artificial gravity. This raises the question, when would astronauts be exposed to artificial gravity and for how long? And what would they do while on the centrifuge: sleep, exercise, read, or perhaps initially

perform physiological/psycho-physical experiments to measure its effectiveness as a countermeasure?

Coriolis forces affect all movements made in an artificial gravity environment. Thus, a person needs to adapt to a new set of motor sensory mechanisms for handling objects, ambulating, and executing head movements during centrifugation. Coriolis force is a transient force, that is absent at the beginning and end of the motor movement because at those times, the linear velocity is zero. The motor sensory mechanism quickly adapts. In an experiment, in which reaching movements were performed while being rotated at 10 rpm, after 15-20 movements, subjects were back to straight and accurate reaching movements despite the absence of visual and tactile feedback about reaching accuracy (Lackner, DiZio 1997). With use of full vision, these movements were lowered to 8-10 attempts, and again they were making straight reaches accurately to the targets. It is important to note this adaptation was context-specific. During the first reaching movements while being rotated, subjects felt the Coriolis force deviate their arm. With continued reaches, the Coriolis force was no longer "felt" by the reaching arm, although still present at the same magnitude. The movements seemed completely normal. Since the subjects then fully adapted their arm movements to the rotating environment, a residual learning would result in the subject inaccurately reaching for an object in a normal Coriolis-free environment. The subject must re-adapt the motor skills following centrifugation. A short-radius centrifuge, though it would reduce the potential for space motion sickness by creating a radial acceleration to stimulate the otolith organs as studied by Benson, Guedry, Parker, and Reschke (1997), it also increases the possibility for cross-coupled angular motions, which cause disorientation and discomfort.

1.4.3 Cross-Coupling Illusion

In order to produce 1 g at the foot of a short-radius centrifuge, the angular velocity of the centrifuge must be relatively high. This high angular rate is undesirable since the strength of the cross-coupling illusion is correlated to angular rate. This illusion is caused by simultaneous stimulation of the semicircular canals in two planes. If angular

motion about one axis is performed and quickly thereafter, within 5-7 seconds, rotation is performed about another axis, there is no conflict (Young, 1977). However, if the angular motion about the initial axis is constant and lasts longer than 30 seconds, the semicircular canals (Section 2.2.2), behaving like angular accelerometers, will equilibrate and no longer be stimulated. Then when a second head rotation about another other axis is executed, the cross-coupled response of the semicircular canals (Section 1.4.10) to the two-axis angular velocities produces an illusion of angular motion about the third axis. The cross-coupled angular velocities are called Coriolis angular acceleration. If the head is permitted to move on the centrifuge, then the resultant total angular velocity of the head is expressed in Equation (1.1). ω_H is the total angular velocity of the head in inertial space, ω_C is the angular velocity of the centrifuge, and $\omega_{H|C}$ is the angular velocity of the head with respect to the centrifuge.

$$\vec{\omega}_H = \vec{\omega}_C + \vec{\omega}_{H|C} \tag{1.1}$$

Differentiating Equation (1.1), the angular acceleration of the subject's head is in Equation (1.2) where α_H is the total angular acceleration of the head in inertial space and $\alpha_{H|C}$ is the angular acceleration of the head with respect to the centrifuge.

$$\vec{\alpha}_H = \vec{\alpha}_{H|C} + \vec{\omega}_C \times \vec{\omega}_{H|C} \tag{1.2}$$

Then the Coriolis angular acceleration is the vector cross product of the two angular velocities about the two axes, which explains the resultant cross-coupled illusion of motion about the third axis (1.3).

$$\vec{\alpha}_{Coriolis} = \vec{\omega}_C \times \vec{\omega}_{H|C} \tag{1.3}$$

1.4.4 Sensory Conflict

Once a person is accustomed to the constant rotation of the centrifuge, the person feels stationary. During passive or active head movements on the centrifuge, this cross-coupled illusion is often disturbing and disorienting, primarily because the direction of motion is highly unanticipated. This unanticipated motion is not only due to conscience expectation, but also due to somatosensory cues, otolith cues, and visual cues. During the head movement, the semicircular canal experiences this Coriolis

acceleration without any otolith time-varying signals nor somatosensory responses that communicate an acceleration in this third axis of rotation. If the visual field is available, another sensory mechansism would conflict with the illusory motion about the third axis. Young (1977) argued that the source of the discomfort and symptoms of motion sickness are not from the unexpected illusory sensations caused by the Coriolis acceleration but from the conflict between the semicircular canals and the nonconfirming otolith cues. Probably the additional conflicting cues of the proprioceptive muscles in the neck and somatosensory cues in the body, which transmit a signal congruent to the otolith cues, contribute to the incongruency to the canals' cross-coupled acceleration.

An additional sensory conflict that occurs for a longer period of time than the duration of the head turn is the sensory conflict from the dynamical behavior of the semicircular canals and their response to moving into and out of the plane of rotation. Following the cross-coupled angular acceleration caused by the canals, the head rotation has caused the semicircular canals into a different orientation with respect to the plane of rotation. If a head movement was made about an axis other than the axis rotation of the centrifuge, then the effective canals whose plane of rotation did not correspond to the head movement will receive different stimuli while the effective canal that did correspond with the head movement plane of rotation receives the same stimulus before the head movement. The result is an illusory tilt, a motion that is felt in body coordinates, although the origin of the perceived motion is in head coordinates. For example, if the body is supine and the head is yawed to the right, the pitch canal of the head is stimulated; therefore, the person feels a whole body pitch, although the effective pitch canals are in the same plane as body roll, the head now in the "look right" position. This lasting sensation, about 8-10 seconds, provides a longer stimulation that further conflicts with the otolith, proprioceptive, somatosensory, and visual stimulation.

The magnitude of this sensation should correspond to the angular velocity input, and the duration of the sensation is the time constant for the canal that is being stimulated. Figure 1.1 shows an idealized response of the canals to both the cross-coupled

stimulation and the canal endolymph absorption of the angular rate of the plane in which it is located. As documented by Peters (1969) and Pancratz, Bomar, and Raddin (1995), the semicircular canals each have different time constants for the three orthogonal canals. However, instead of the characterizing time constants for each semicircular canal, the time constants described the three effective canals in body coordinates of pitch, roll, and yaw. They are 6.1 seconds for roll, 5.3 seconds for pitch, and 10.2 seconds for yaw. It is noted that although the time constants for the semicircular canals are not equal, they produce the same magnitude of illusory tilt for the same stimulus. The differences in time constants will be exposed in the duration of the perceived motion to the same stimulus.

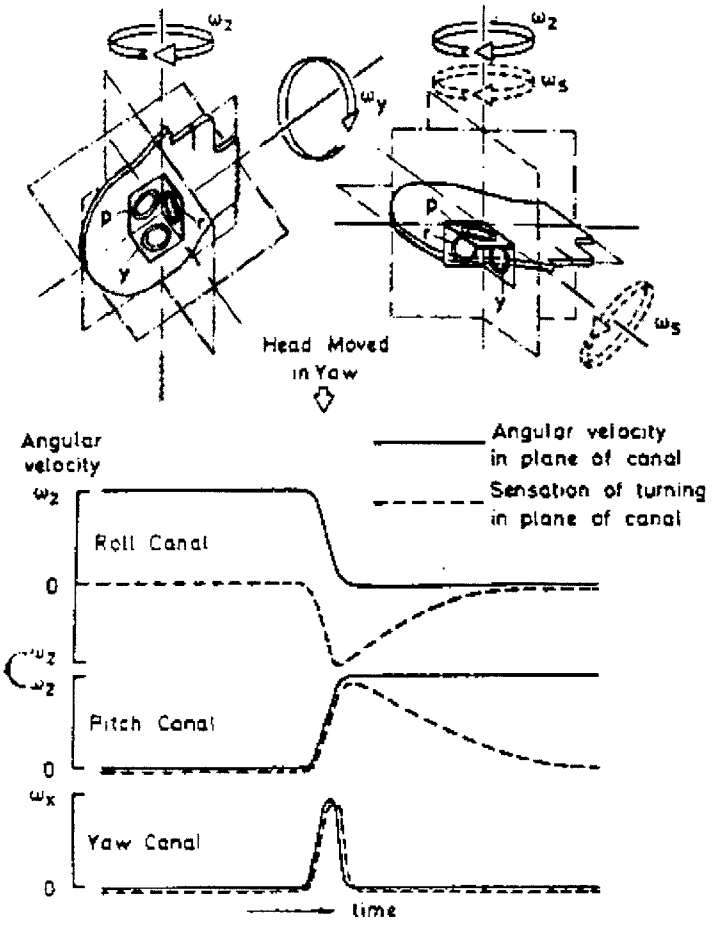

Figure 1.1 Response to Cross-Coupled Stimulation to the Semicircular Canals (Young, 1977, p. 1053)

This conflict often evokes motion sickness symptoms and a vestibular-ocular reflex characterized by nystagmus, a beating of the eyeball, either rotary or linearly. This nystagmus also affects the visual scene as well as balance ability. While motor skills are quickly adaptable, vestibular adaptation requires a slow physiological adaptation in the afferent firing response. A pilot study was performed to ascertain the level of vestibular adaptation when exposed to ten minutes of daily centrifugation for 12 consecutive days. It was noticed that by the fifth day, the subject no longer experienced oscillations or scrolling of the visual scene upon making a head movement at the end of the ten-minute adaptation period. It was also noted that the subject required only one to two head turns to eliminate the nystagmus-inducing visual scrolling following the fifth day.

In order to better understand the actual response of the vestibular conflict, the perceived illusory tilt from head turns during centrifugation was studied for vestibular, proprioceptive, and autonomic interactions.

Chapter 2.0

Large N Study

2.1 Introduction

In a pilot study of short-radius centrifugation, subjects perceived differing directions of illusory tilt, both in the 3-axes body coordinates and inversion along one axis, to the same yaw head movements and the same direction of stimulation. Although there exists a semicircular canal model that can predict the stimulation of the canals and the directions one should feel, these pilot studies showed that not all people felt sensations in the same direction. In light of achieving vestibular adaptation through performing repeated head movements during centrifugation (Lyne, 2000; Sienko, 2000), understanding the response of the vestibular system to head movements in this rotating environment is in order.

One primary topic of my thesis is to further understanding of the artificial gravity countermeasure. Artificial gravity, by replacing the missing stimulus with the man-made version of the same stimulus, potentially is the most ideal countermeasure. To fully understand all the impacts of artificial gravity, the physiological responses to intermittent exposure to centrifugation need to be characterized. In particular, the subjective illusory tilt, duration of motion, motion sickness, and heart rate were measured during yaw and pitch head movements during rotation in the roll axis human body.

2.2 Background

The vestibular system, composed of linear and angular accelerometers, is the primary orientation sensor of the human body. They are located just inside the inner ear on both the left and right sides of the head, adjacent to the auditory system. The linear and angular accelerometers of the head are called the otolith and semicircular canal

system, respectively. The vestibular system with the auditory system compose the labyrinth (Figure 2.1).

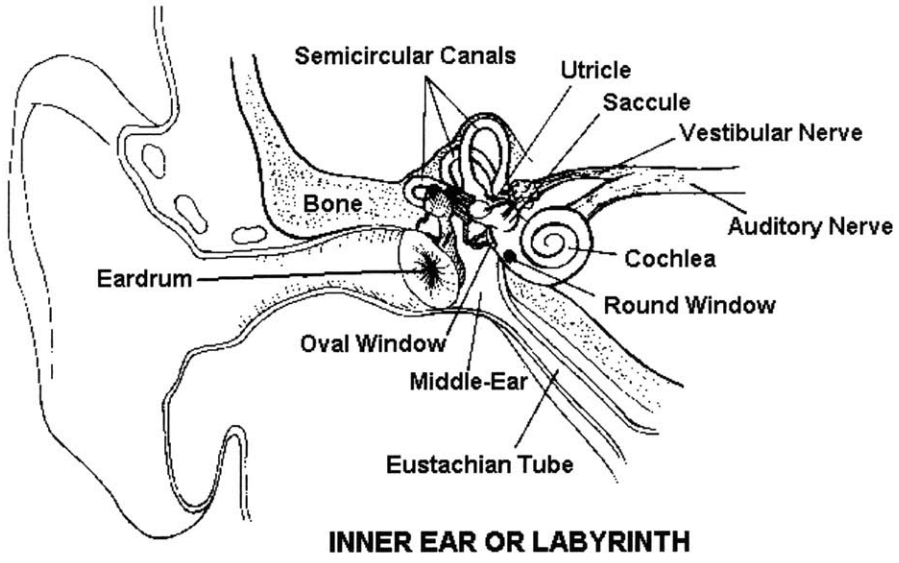

Figure 2.1 The Labyrinth (Courtesy of Department of Psychology, McMaster University, Hamilton, Ontario, CA)

2.2.1 The Otolith System

The vestibular system's linear accelerometers are two organs: the utricle and saccule (Figure 2.2). Each organ has a sheet of hair cells, the macula, whose cilia are embedded in a gelatinous mass. This gel has a clump of small crystals embedded in it, called an otolith. When the head is accelerated, the inertia of the otoliths resist this motion, and the otolith-gel mass pulls on the haircells. However, if the stimulus comes to a constant linear velocity, the otoliths come to equilibrium. Motion is no longer perceived. It must be kept in mind that otoliths respond to the specific force, the projection of the gravitoinertial acceleration. Therefore, if there is only constant linear velocity, the otoliths are still acted upon by gravity.

The hair cells in the utricle and saccule are polarized, but they are arrayed in different directions so that a single sheet of hair cells can detect motion forward and back, side to side. Each macula can therefore cover two dimensions of movement. The utricle lies

pitched back 20-25 degrees from the head horizontal position in the ear and effectively, detects motion in the horizontal plane. Similarly, the saccule is oriented 20-25 degrees off of the earth vertical axis, and detects motion in the sagittal plane (up and down, forward and back). A major role of the saccule and utricle is to maintain stability vertically with respect to gravity and assist the body in postural adjustments.

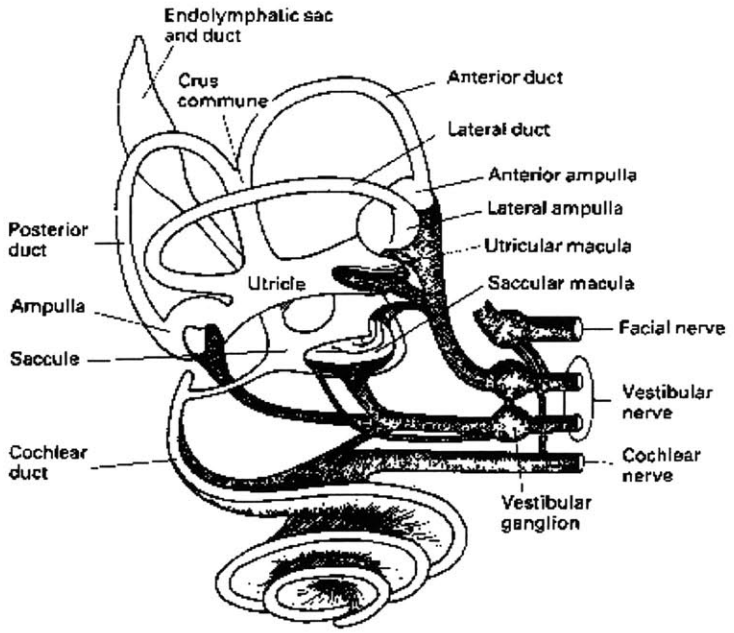

Figure 2.2 The Otolith and Semicircular Canals (Ernsting, Nicholson, Rainford, 1999)

The dynamic mathematic model of the otolith response has a first order term representing the dynamics with an affferent processing term (Figure 2.3). In addition the saccular otoliths are modelled with a non-linear term that adjusts for the direction of the perceived earth vertical. Output of the otolith model is the Afferent Firing Rate (AFR), which is the change in a baseline rate of theoretical impulses to the brain. It has units of impulses per second. The model also outputs an estimate of the local down direction.

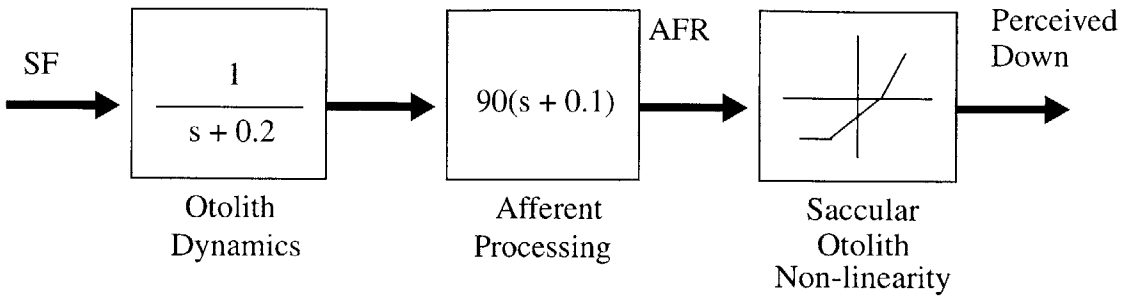

Figure 2.3 Otolith Model Block Diagram (Pancratz, et al, 1994)

2.2.2 The Semicircular Canals

The semicircular canals are composed of three rings, the lateral, posterior, and anterior canals (Figure 2.2). The lateral canal is 25 degrees tilted from the vertical, and the anterior and posterior canals are perpendicular to ground horizontal. The anterior canals are tilted forward 45 degrees from the coronal plane, and posterior canals are tilted 45 degrees aft. The cilia, hair-like cells, extend into the cupula that forms a virtually fluid-tight gate across the ampulla. The cupula is hinged at the crista and is able to move in response to the movements of the endolymph.

In-plane clockwise rotations would result in an inertial lag of the endolymph that forces the cupula to be displaced counterclockwise (Figure 2.4). The highly viscous fluid of the endolymph relative to the inertial forces cause the semicircular canals to act as approximate integrators. This cupula-endolymph mechanism has dynamics which are modeled as a heavily damped torsion pendulum. Therefore, for all frequencies of stimulation, except at the low range of 0.1 Hz (Young, 1977), their output reflects angular velocity rather than angular acceleration of the head with respect to inertial space. After a short period at constant angular velocity, the subject no longer feels rotated, rather only the otoliths orient the subject in a slightly pitched forward position due to the centrifugal centripetal acceleration. The transfer of energy from angular acceleration to electrical energy in the semicircular canals is very

different from the otolith counterpart. In addition, gravity, which has a large affect on cilio-otolith stimulation, is normally negligable for semicircular canal stimulation.

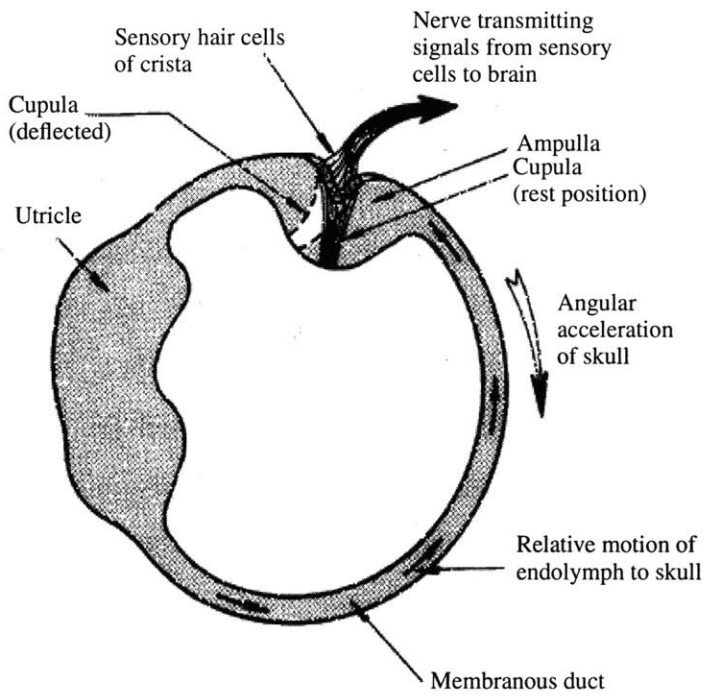

Figure 2.4 A Plane of the Semicircular Canals (Ernsting, et al, 1999)

The canals act as angular accelerometers for low frequency stimuli less than 1Hz and angular velocity transducers for high frequency stimuli. The dynamics of the canal are modelled as an overdamped torsional pendulum, which has different time constants for each canal. An adaptation term is often used by researchers to account for the highly resilient behavior in humans to become less sensitive to repeated angular acceleration stimulus over time. The final term is a lead processing term to account for rate sensitivity. The semicircular canal block diagram model is in Figure 2.5. The output of this canal model is a theoretical afferent firing rate.

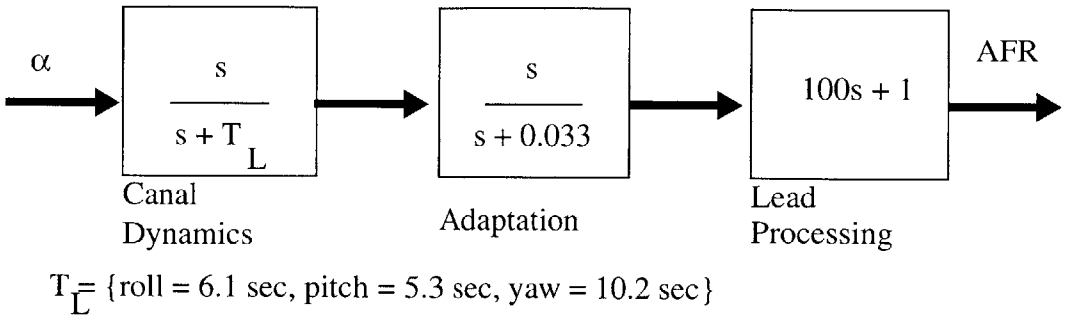

Figure 2.5 The Block Diagram of the Semicircular Canals (Pancratz, et al, 1994)

2.2.3 Semicircular Canals on the Centrifuge

Consider the 3-axis angular acceleration sensors on the centrifuge. For simplicity, although the semicircular canals are not located exactly in each of the transverse, coronal, and sagittal planes, the canals are approximately orthogonal from each other and effectively act as accelerometers in each of the body planes; such that when motion is resolved, it is in these three planes. Head movements and perceived motions in these planes can be derived as yaw, roll, and pitch, respectively.

2.2.3.1 Semicircular Canal Stimulus

At a particular orientation of the head, any canal that is in the plane of rotation will pick up its angular velocity and the endolymph will cause the cupula to deflect and stimulate the vestibular nerve. After 20-30 seconds at constant velocity, the endolymph will be rotating with the angular speed of the rotating plane. The cupula will equilibrate and no longer signal, although it is still being rotated.

At this time, if the head is turned about an axis perpendicular to the rotating axis, the canal whose endolymph was rotating with the plane of rotation is taken out of that plane. That canal suddenly receives no velocity stimulus and is no longer rotating in inertial space. The endolymph's inertia keeps rotating in the non-rotating canal, which stimulates the cupula. The subject suddenly feels rotated in the opposite direction from the direction the endolymph is stimulating the cupula. The person experiences a rotation in the opposite direction that the cupula is deflected. Now, the complication

here is that there is a second canal, once the head is turned, is then put into the plane of rotation. This second canals effectively receives a step input of the centrifuge's angular velocity. Inversely, this canal's endolymph is takes about 0.1 sec (Peters, 1969) to pick up the plane's angular velocity and deflects its cupula while the endolymph picks up the speed of the rotating plane.

2.2.3.2 Response to Semicircular Canal Stimulus

While the cupula is being deflected, the subject reacts with both a vestibular-ocular reflex in the form of nystagmus, vertical beating displacements of the eye, and a perceived rotary motion or illusory tilt is felt. The nystagmus is composed of a fast phase velocity, a resetting of the eye, and a slow phase velocity, whose magnitude is related to the angular acceleration stimulus (Sienko, 2000). This illusory tilt is experienced in two planes, one in the plane of the canal being accelerated by the centrifuge rotation, and one in the plane of the other canal being decelerated. The duration of this transient response of the cupula in relation to the velocity step input to the canals is called "subjective cupulogram" (Meiry, 1965). Peters notes that the subjective cupulogram differs depending on the axis of stimulation and the subjective inertial orientation with respect to gravity. Table 2.1 shows average subjective cupulogram and nystagmus cupulogram for different experiments and axis of stimulation where the time is the exponential decay time constant of the ratio of viscous damping torque of the endolymph and the stiffness, torque per unit angular deflection of the cupula.

Table 2.1 Average Cupulogram (s)

Experiment	Axis	Subjective Cupulogram	Nystagmus Cupulogram
Van Egmond, Groen, and Jongkees, 1949	Yaw	8 sec normal subjects 10 sec sensitive subjects	
Groen, 1960	Yaw	8 sec normal subjects 6 sec 18 experienced aviators	16 sec normal subjects 8 sec 18 experienced aviators
Jones, Barry, and Kowalsky, 1964	Yaw Pitch Roll	10.2 +/- 1.8 sec 5.3 +/- 0.7 sec 6.1 +/- 1.2 sec	15.6 +/- 1.2 sec 6.6 +/- 0.7 sec 4.0 +/- 0.4 sec

Table 2.1 Average Cupulogram (s)

Experiment	Axis	Subjective Cupulogram	Nystagmus Cupulogram
Meiry, 1965	Roll	7 sec	

2.3 Stimulus Considerations

2.3.1 Ground-Based Experiments for Space Applications

Although artficial gravity is for a space, microgravity application, experiments must first be run on Earth, a 1 g environment. Because the semicircular canals are angular acceleration sensors, the same environment conditions that stimulate the canals exist both in space and Earth. "Rotations of the head would provide stimulus to the canals the same as under terrestrial conditions." (Graybiel, 1973, p. 111) The vestibular otolith organs respond to gravitoinertial forces. Although otoliths would be stimulated by gravity while the head is fixed; in space, the absence of gravity, the otoliths would not be stimulated. The semicircular canals, however, would respond similarly in either case. Therefore, studying the response of the semicircular canals to the stimulus of turning the head on the centrifuge while on the Earth's ground is a helpful study for artificial gravity applications in space.

2.3.2 Otolithic Contribution to Illusory Tilt

In 1g it is difficult to study true otolith contributions to the vestibular system response during artificial gravity in microgravity. The otoliths measure linear acceleration while the semicircular canals are angular accelerometers and integrators, however, both constitute the vestibular system to place the person in one orientation. Therefore, perceived motion and orientation may be studied in terrestrial 1 g conditions, but it should be kept in mind the response of the vestibular system would not be exactly the same in space due to the different stimuli on the otoliths. Currently, the extent of otolith effects are not clearly defined. It has been remarked by Berthoz, Grandt, Dichgans, Probst, Bruzek, and Vieville (1986) that under 1 Hz, the semicircular canals dominate the vestibular-induced motions, so the vestibular response to centrifugation should be similar under both 1 g and 0 g.

Chapter 3.0

Large N Experimental Methods

3.1 Design

To understand the effectiveness of artificial gravity as a countermeasure, how the vestibular system responds to centrifugation and how head movements affect this vestibular response is studied. Large N measured the perceived motion, the duration of motion, motion sickness, and heart rate to head movements in pitch and yaw during centrifugation. The instigation of this experiment was brought upon by the hypothesis that perceptions of illusory body tilt caused by head movements during centrifugation are not completely predicted by the idealized semicircular canal model (Section 2.2.2). The experimental objective was to record subjective responses to yaw and pitch head movements while supine on the centrifuge. These subjective responses were perceived magnitude, direction of motion, and duration of the perceived motion. Additional measures were heart rate, perceived room orientation while being rotated, body tilt without making head movements, and a 0-20 verbal motion sickness rating (Lyne, 2000). These measures were taken prior to and during the experiment. Experienced body tilt was categorized into 4 subcategories of motions about the three body axes: clockwise/counterclockwise yaw about the body's longitudinal axis where clockwise is to the subject's right, clockwise/counterclockwise roll where clockwise denoted a cartwheel-like motion to the left side, and forward/backward pitch. Experienced pitch was separated into two distinct motions: tilting for motions where the pitch remained fixed at a distinct angle and tumbling in which pitch was a constantly increasing angular motion. Additionally, to explore the cause of subjective differences, handedness, eye dominance, and activities that would enhance vestibular orientation and function were recorded.

3.1.1 Subjective Measures

Four subjective measures were addressed: motion sickness, subjective inertial orientation, illusory tilt without head movements, and illusory tilt immediately after head movements and were taken intermittently throughout the experiment. These subjective sensations of illusory tilt refer to the whole body motions about the center of the body whose stimulus were purely head movements during centrifugation. A pilot study exposed the difficulty in communicating subjective orientation and the direction of illusory tilt. Therefore, a puppet was used as a tool to train the subjects beforehand in an effort to avoid miscommunication.

3.1.1.1 Motion Sickness

The subject may experience symptoms of motion sickness as described in Section 1.4.4, similar to those experienced during seasickness. Stomach awareness, sweating, yawning, flatulation, and nausea are the typical symptoms of motion sickness. Therefore, the subject was asked to give a self-assessment rating on a scale of 0 to 20 to represent the overall feeling of discomfort. A score of 0 represented 'I am fine' and a score 20 represented vomiting. The motion sickness rating was taken throughout the experiment.

3.1.1.2 Subjective Orientation

During a pilot study, subjects reported a conflicting orientation with respect to the room in inertial space while on the centrifuge. Although subjects were cognizant that they were rotating on a centrifuge, once head movements were made, they felt oriented in the room in a certain direction, such as their head felt pointed toward the blackboard at one end of lab (Figure 3.1). We felt it was worth exploring because this cognizance of being rotated conflicted with the sensation of being stationary once the cupula had returned to equilibrium. Then when a head turn was performed, a vestibular orientation conflict may occur, whereby the mind may regress to the last clear orientation when stationary before the ramp up of the centrifuge to resolve this conflict.

From a total of 20 subjects, 10 subjects (5 males, 5 females) were randomly assigned to orient their feet initially toward the blackboard, and 10 subjects were randomly assigned to initially point their feet toward "You", the experimenters.

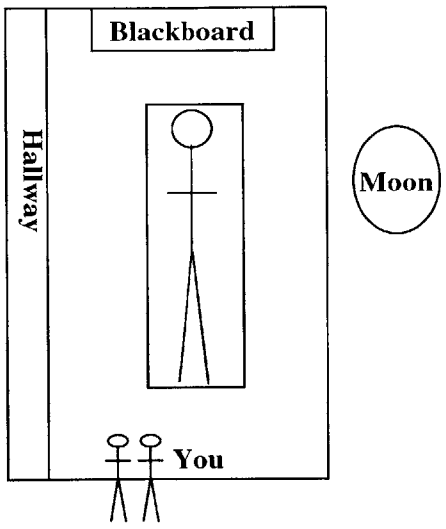

Figure 3.1 Four Possible Subjective Inertial Orientations

3.1.1.3 Persistence of Illusory Tilt

To measure the duration of the perceived motions after making head movements, subjects were required to say "stop" when the illusory tilt died out for every head movement made. This was not consistently the best method since subjects would at times forget to say, "stop".

3.1.1.4 Illusory Body Tilt Description

Because the intent of the study was to determine subjective motion direction, duration, and magnitude of illusory body tilt when making head movements in a rotating environment, definitive vocabulary was crucial to the correct communication of direction and accurate, bias-free data collection. Motions in the pitch, roll and yaw plane were explained with the establishment of a vocabulary convention for the subject (Appendix B). The vocabulary for roll motions consisted of "feet to the left or to the right", and yaw motions were expressed as "spinning to the left or to the right". Pitch

motions were distinguished between two distinctly different motions. Tilt was used to denote pitch where the illusory tilt remains at a fixed angle and tumble was used to denote pitch where the motion was a constantly increasing angular continuous motion. "Tumbling forward and backward" or "tilting head up and down" denoted pitch motion. Magnitude of motion perceived was given by degrees or revolutions. In this way, perceived angular velocity may be determined by the persistence of the illusory tilt by the estimated verbal magnitude.

3.2 Subjects

Twenty healthy human subjects (10 males, 10 females), ranging in the age from 18 to 32 yrs (24 +/- 0.8 yrs), participated in the experiment. The subjects had no prior experience with centrifuges or other rotating devices in a research environment. Subjects were not on any medication, nor did they have a history of neurological, cardiovascular, respiratory, or ear-related problems. Prior to the run subjects underwent a medical examination for eye dominance and vestibular function, using the Rhomberg test. The subjects did not to consume alcohol and caffeine 24 hours prior to the experiment.

A written informed consent and a medical consent form affirming healthy condition (Appendix A) was provided before the experiment by each subject. The MIT Committee on the Use of Humans as Experimental Subjects approved the experiment.

3.3 Equipment

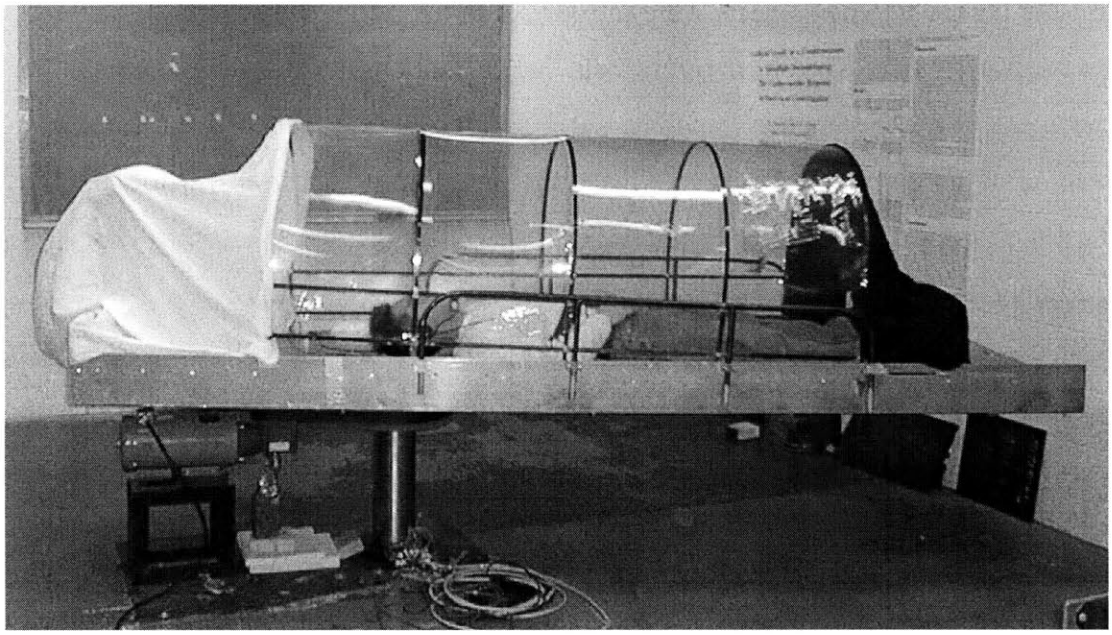

Figure 3.2 Short-Radius Centrifuge with Canopy (Not Light-Proofed)

3.3.1 Short-Radius Centrifuge

The MIT short-radius centrifuge was used has been in use since 1988 for various artificial gravity experiments. (Diamandis, 1988). The centrifuge is 2 m in length with a rotation radius of 1.55 cm. A Browning 1 hp dc motor drove the bed and was controlled by a Browning LWS Series LW second generation DC Motor Controller. The controller produced an input profile providing a constant linear ramp-up from 0 rpm to a constant angular velocity of 138 deg/s or 23 rpm at an acceleration rate of 5.52 deg/s^2 or 0.92 rev/s^2. The participant lay supine with the head at the axis of rotation and nose pointing toward the ceiling. At 23 rpm, the centrifugal force caused a 100 % gradient of 0 g at the head and 1 g for a 5'6 (1.68 m) participant at the feet. An on-board video camera monitored the subjects from a distance of 40.5 inches for the duration of the experiment to monitor their well-being and head movements. Additionally, an audio tape recorder was on-board to record all verbal responses. To remove wind cues, a light-proofed canopy was attached over the subjects's head and

torso. However, for purposes of ventilation and lighting, the foot of the canopy was left open. To eliminate visual cues, subjects wore a blindfold and all of them reported complete darkness. The subjects were introduced to the safety equipment on board: a power cut-off safety switch, a safety belt, and a motion sickness bag. During the experiment, the experimenters and the subjects used walkie-talkies (Motorola Talk About 250) to communicate their sensations and answer questions while on the centrifuge. Figure 3.3 is a schematic of the centrifuge used for the Large N experiment.

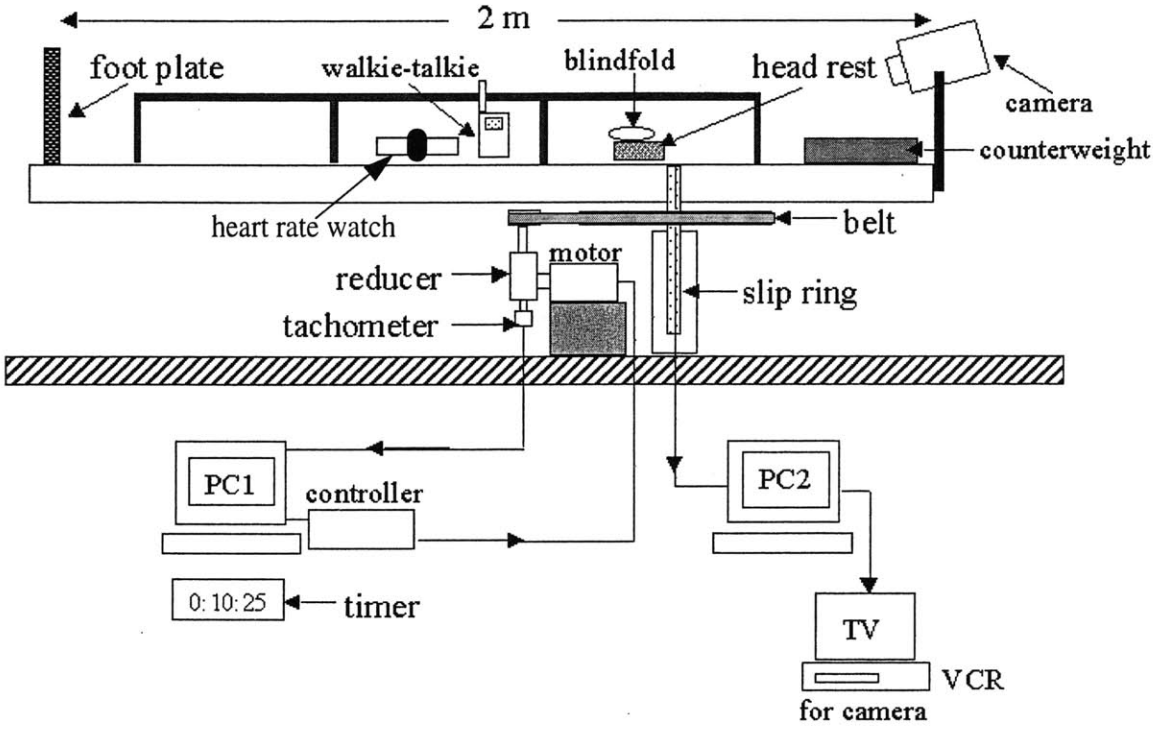

Figure 3.3 Schematic of Centrifuge for Large N Experiment

3.3.2 Heart Rate Monitor

The Acumen TZ-Max 100 heart rate monitor measured the heart rate during the experiment. This equipment included a data storage watch, a chest transmitter, and an adjustable elastic strap. Data heart rate was sampled every 5 seconds. The average of the heart rate was computed with a beat-to-beat measurement. The chest transmitter

was attached to the chest at the position of the heart level, just below the pectoral muscles. Aquasonic Electrode gel was spread on the electrodes of the transmitter to act as a couple medium and promote improved transmission of the heart signals to the chest transmitter.

3.4 Procedure

3.4.1 Pre-Experimental Briefing

Subjects were asked to abstain from consuming alcohol and caffeine 24 hours prior to the experiment. Before the experimental session, a consent form (Appendix A) was read and signed. All subjects underwent a medical examination for eye movements, eye dominance, and vestibular function by use of a Rhomberg test. Subjects were also asked to answer the following: weight, height, handedness, and activities that may affect vestibular function, such as flying, diving, or gymnastics. All subjects were informed about the nature and the purpose of the experiment as well as the risks involved.

After the subjects strapped on the Acumen heart rate monitor, they mounted the centrifuge such that their head was located on the center of rotation with their nose up. Final training for 90 degree yaw and pitch forward head movements was completed and the experimenters reviewed how to describe the illusory tilt motions. The subjects were given an ear bud for the walkie-talkie and instructed in using the walkie-talkie with volume level checks for both the subject's and experimenter's receiver. Attention was given to the location of motion sickness bag, and subjects were informed of the safety mechanisms of the centrifuge. The head movements in both the yaw and pitch planes were trained carefully to turn the head 90 degrees in 1 second. The blindfold was applied, and the subject was asked to ensure a dark environment. The centrifuge was covered with the canopy, then an experimenter walked the centrifuge around 1 revolution to ensure obstacle-free rotation for safety.

3.4.2 Protocol

Before the bed was ramped up the subjects had to answer questions concerning illusory tilt without making head movements, motion sickness and subjective orientation. The centrifuge then steadily ramped to 23 rpm in 25 seconds. While rotating in 23 rpm and after 30 seconds at constant rotation speed, the subjects were again asked the same questions prior to ramp up. Then head movements were made at the experimenter's cue. The subjects said, "stop" when the perceived motion stopped. Subjects had a 20 second interval between each head movement made to attain heart rate data and to permit the transient vestibular responses to die out. Subjects made 2 sets of yaw head movements where one set consisted of yaw head movements made to either the right or left. For example, the set of head movements made to the right entailed six yaw head movements (three of the six went from nose-up to right-ear-down and the other three were from right-ear-down to nose-up) for heart rate measurements and two more head movements for the interview session with the experimenters to report the direction and magnitude of perceived motion and subjective orientation (R,Q). These two head movements consisted of yaw from nose-up to right-ear-down, saying, "stop" and then the interview session to describe only the most recent head turn. Then the head is returned from right-ear-down to nose-up yaw, saying, "stop", and the interview session for that head turn. One set of head movements to the right is described in Figure 3.4. The same set is then done for yaw head movements to the left.

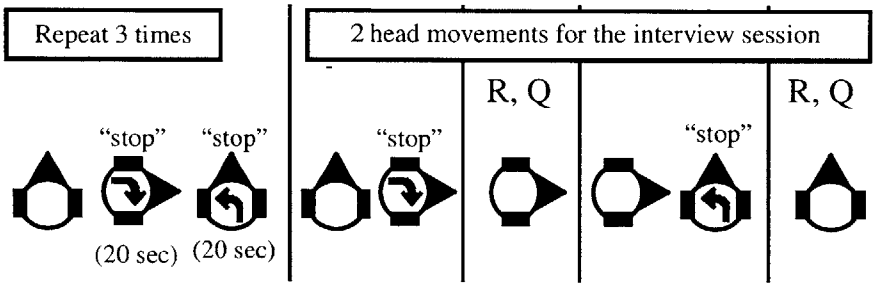

Figure 3.4 Set of Head Movements and Protocol for Yaw to the Right

After one set was completed, motion sickness, subjective orientation, and illusory tilt without head movements were reported.

When the motion sickness rating was below 3, the subject executed a pitch forward head movement from the baseline nose-up head position. Pilot experiments showed pitch head movements were very provocative. Additionally, the subject must use abdominal muscles to pitch the head forward while supine, which may elicit further pressure on the diaphragm to have a pronounced increase in motion sickness levels. Subjects were instructed to bring the chin to the chest. When the perceived motion dissipated, the subject said, "stop" and immediately pitched the head back onto the bed. Afterward, the subject had to report first the perceived motions for the pitch forward head movement and then for the pitch backward head movement. Finally, the subject was asked to report motion sickness rating, subjective orientation, and illusory tilt without a head movement.

The bed then ramped down linearly to rest in 25 seconds and the canopy was removed. The centrifuge was secured and follow-up questions below were asked while the subject remained on the centrifuge.

1) Did you feel a decrease in the strength of the sensations during one set of head movements, such as the set to the left or the right yaw head movements?

2) Did the strength of the sensations differ between the head movements made to the right or the left side?

3) Did you feel any other sensations while you were on the bed that you did not get to report? (Was the bed rotation smooth?)

Chapter 4.0

Large N Results

4.1 Heart Rate Results

The baseline reasonably shows no significant difference in heart rate before the centrifuge started rotating and after the experiment when the centrifuge had come to rest. However, during the 30 second ramp-up period average heart rate was significantly elevated from 70 bpm to 76 bpm ($F(5, 95)=6.87$, $p<0.001$). Approximately 15 seconds later, it had nearly resumed its baseline value (71.5 bpm).

All 20 participants made three sets of yaw head movements to each side. However, only 15 participants performed the pitch head movements because 5 participants attained a motion sickness level higher than the cutoff.

All head movement sets led to an increase in heart rate where pitch turns produced the most pronounced increase. Since 15 of the 20 subjects performed pitch head movements, two separate repeated measures ANOVAs were performed, for yaw and then for pitch. Results are shown in Table 4.1. No significant difference was found between clockwise (left-ear-down to nose-up and nose-up to right-ear-down) and counterclockwise (right-ear-down to nose-up and nose-up to left-ear-down) yaw head movements.

Table 4.1 Heart Rate Results

Phase	Ave. Heart Rate	Phase	Ave Heart Rate	Df	F	P-value
Baseline	71.5	Yaw Right	73.0	176	11.52	.004
Baseline	71.5	Yaw Left	75.7	16	16.94	.001
Yaw Right	73.0	Yaw Left	75.7	16	11.23	.004
Baseline	71.5	Pitch Up	79.1	10	21.89	.001

Table 4.1 Heart Rate Results

Phase	Ave. Heart Rate	Phase	Ave Heart Rate	Df	F	P-value
Baseline	71.5	Pitch Down	82.5	10	43.86	<.001
Pitch Up	79.1	Pitch Down	82.5	10	10.5	.009
YAW	74.0	PITCH	80.8	10	75.39	<.001

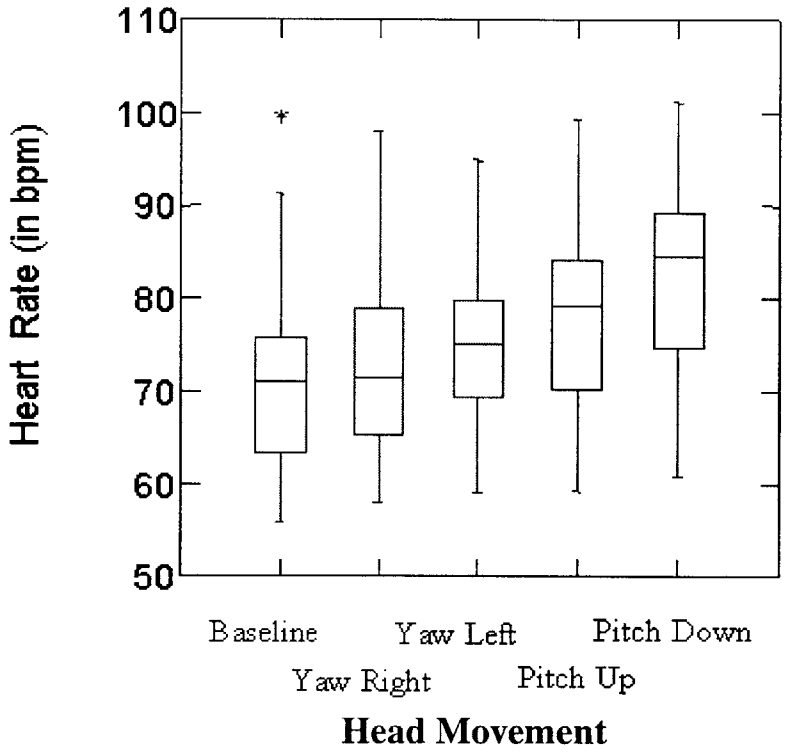

Figure 4.1 Heart Rate Box Plot of Heart Rate Distributions.

A box plot shows the heart rate distributions. The box comprises 50% of the values with their median at the center.

4.2 Illusory Body Tilt

Two measures were tabulated for subjective tilt experience: perceived motion and its temporal persistence. The data consisted of audiotape and written recordings of verbal

reports while participants were on the centrifuge. Ambiguous reports during the run were followed-up by demonstrations of perceived motion using a puppet after the experiment.

Based on a model of the semicircular canals, the directions of illusory tilt can be predicted for a given head movement. Since the centrifuge was rotating clockwise, a clockwise yaw head movement, left-ear-down to nose-up and nose-up to right-ear-down, would elicit a perceived body pitch backward simultaneously with a clockwise body roll. A counterclockwise yaw head movment, right-ear-down to nose-up and nose-up to left-ear-down, would produce a perceived body pitch forward and again a clockwise body roll. For a pitch forward head movement, whole body yaw right or clockwise and clockwise roll is predicted; and for a pitch backward head movement, a whole body yaw left or counterclockwise and clockwise roll is predicted.

Table 4.2 and Table 4.3 show a summary of the illusory tilt directions for yaw and pitch head movements respectively, compared to the predictions of the semicircular canal model. For yaw head movements, the majority of participants experienced the predicted pitch and roll. However, a few participants perceived illusory motion in the predicted plane but in the exact opposite direction. This was the case in 13% of all reported yaw head turns. Those participants were inconsistent, that is they did not always feel pitch and roll in the opposite direction to the predicted direction. Note that an asterick (*) is used to represent a sensation direction that is not a predicted motion by the canal model.

In the case of pitch head movements in 40% of the cases an additional body tilt in the direction of the head movements was reported. The canal model predicts only roll clockwise and yaw sensations; there should be no illusory tilt in the pitch direction, yet

a significant number of subjects perceived illusory pitch motions in the same direction as the pitch head movement for 9-10 seconds after the actual head turn was conducted.

Table 4.2 Reported Illusory Motion for Yaw Head Movements

Subjective Motion	Predicted	Opposite	Corresponding to Actual Turn	None
Pitch	76%	13%	-	11%
Roll	60%	13%	-	27%
Yaw	89% *	0%	11%	89%*

Note for the pitch head movement case, yaw and roll body motion is predicted while whole body pitch sensations are not predicted, therefore, not anticipated.

Table 4.3 Reported Illusory Motion for Pitch Head Movements.

Subjective Motion	Predicted	Opposite	Corresponding to Actual Turn	None
Pitch	60% *	0%	40%	60% *
Roll	53%	0%	-	47%
Yaw	43%	7%	-	50%

4.2.1 Magnitude of Illusory Body Tilt During Yaw Head Movements

Strength of illusory tilt was not different between yaw head movements to the left side and the right side. A right-ear-down to nose-up yaw head movement was significantly stronger than a nose-up to right-ear-down yaw ($t(1,19)=2.22$, $p<0.0389$). However, the left yaw magnitudes were not significantly different. Also, clockwise yaw were not significantly different from counterclockwise yaw head movements.

The absolute magnitude of illusory body tilt for the predicted and opposite direction for clockwise and counterclockwise yaw head movements are in Figure 4.2. 'N' stands for the number of subjects who perceived motion in the specific direction. The magnitudes are shown for the perceived pitch and roll direction. 3 of the 4 cases show a reduced strength of sensation for subjects who reported illusory tilt in the opposite direction compared to subjects who reported illusory tilt in the predicted direction.

Also, the fourth case has a sample size of only N=2, and therefore, is not a representative generalization. Between 3-5 subjects perceived motion in the opposite direction, whereas 12-13 subjects perceived completely predicted illusory tilt in the predicted direction. There is a more pronounced difference between predicted and opposite directions in the illusory pitch direction for both clockwise and counterclockwise yaw head movements.

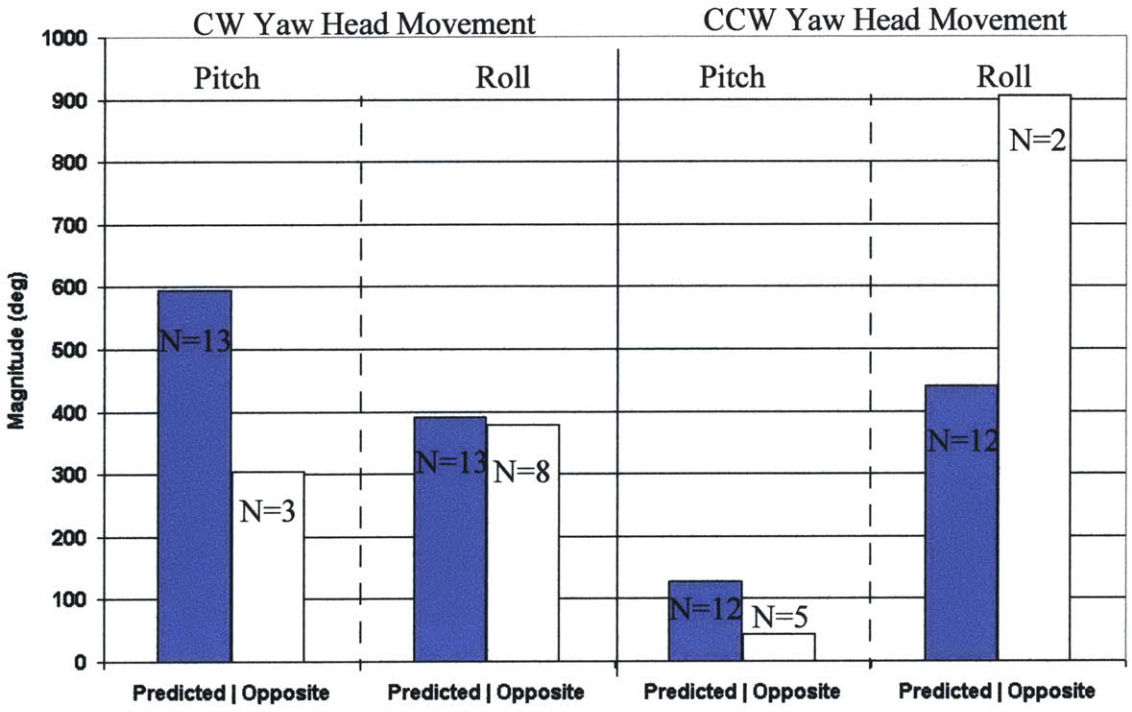

Figure 4.2 Absolute Magnitude of Perceived Motion for the Predicted and Opposite Direction

The magnitudes of perceived full body motion resulting from yaw head movements are depicted in Figure 4.3 to Figure 4.6. Because the stimulus for clockwise or counterclockwise yaw head movements elicit the same stimulus and same predicted directions of illusory body tilt, the plots are according to head movements of clockwise yaw in Figure 4.3. This figure shows the number of cases for which reports of pitch, roll and yaw occurred. Since the magnitude of the perceived motion varied between a set number degrees, such as in tilt, and revolutions, such as in tumbling and

roll, values represented in parenthesis indicate the average magnitude in degrees while the number of revolutions in the parenthesis is explicitly indicated. Positive values represent pitch down, roll clockwise, and yaw clockwise, respectively. The patterned bars denote the predicted direction of perceived motion made by the canal model.

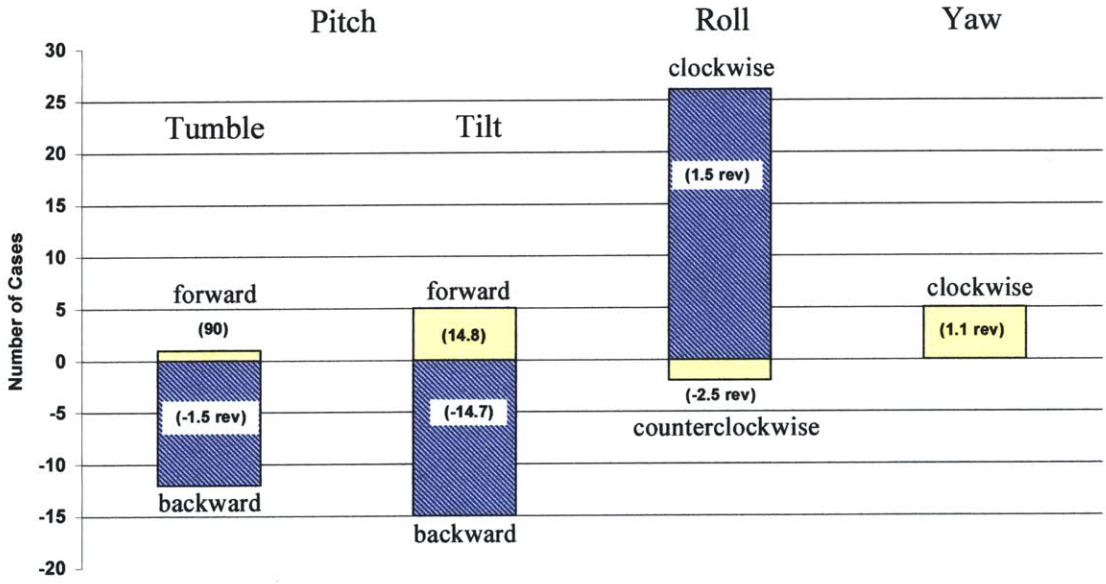

Figure 4.3 Cases of Perceived Motion for Clockwise Yaw Head Movements

Verbal reports revealed that 58% of the subjects felt yaw turns to the right side (first set of head movements) as less provocative than yaw turns to the left side (second set of head movements). The perceived motion caused by a pitch-forward head movement was more disturbing than that caused by pitch-backward turns, with the exception of one participant.

The next plot shows the number of cases of illusory tilt in the pitch, roll, and yaw planes for counterclockwise yaw head movements. The purpose to plot both the clockwise and counterclockwise yaw head movements were in the event of a yaw bias to the left or the right, particularly in relation to the centrifugal angular velocity vector. However, there was no significant difference between clockwise and counterclockwise yaw head movements.

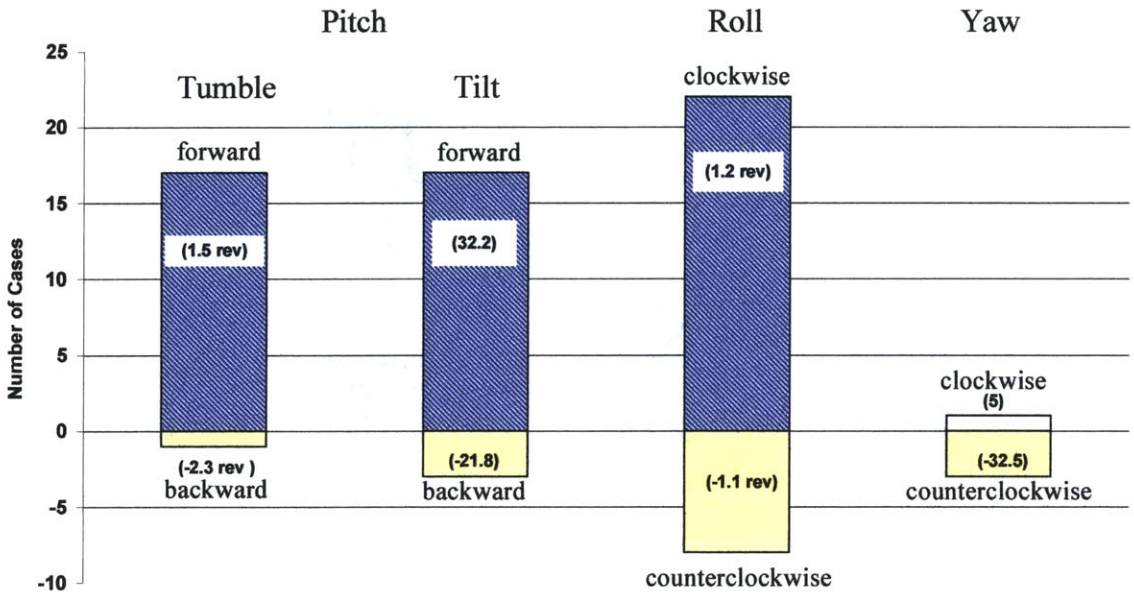

Figure 4.4 Cases of Perceived Motion for Counterclockwise Yaw Head Movements

Figure 4.6 illustrates the cases of perceived direction and magnitude for both ear down to nose up yaw head movements and nose up to ear down head movements. This plot was performed to examine the possible otolith contribution. There is no conclusive evidence of final otolith orientation contribution for the nose up-ear down plots.

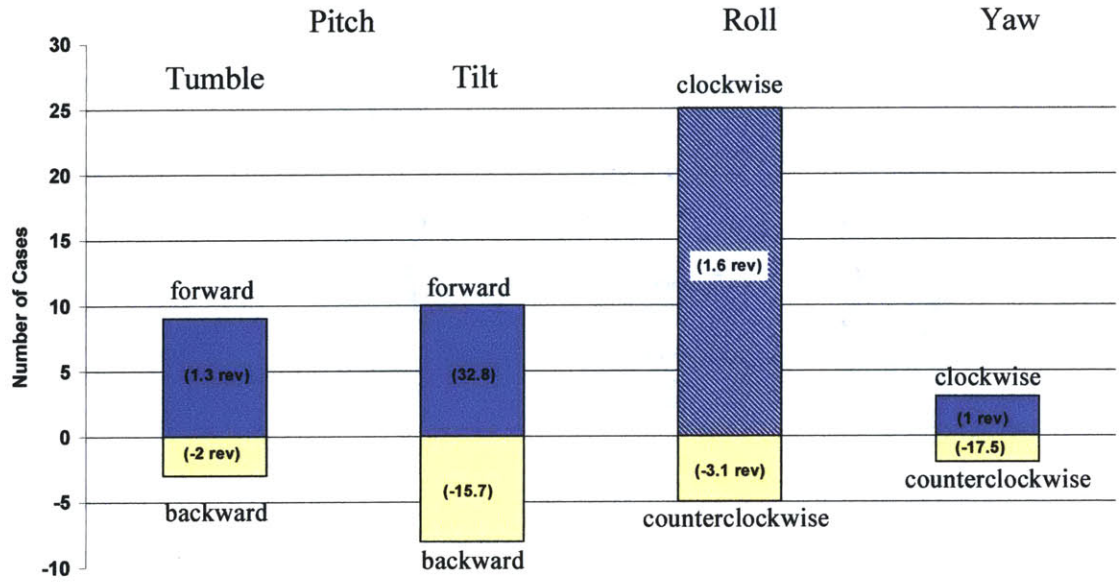

Figure 4.5 Cases of Perceived Motion for Nose-Up to Ear-Down Yaw Head Movements

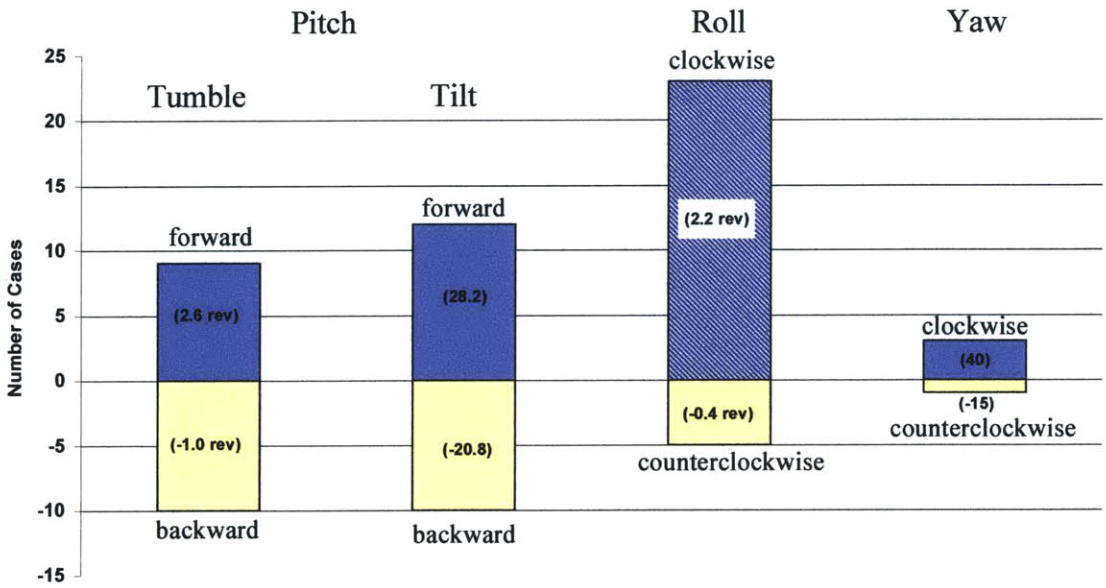

Figure 4.6 Cases of Perceived Motion for Ear Down and Nose Up Yaw

4.2.2 Magnitude of Illusory Body Tilt During Pitch Head Movements

15 participants performed pitch head movements. The predicted perceived motions for pitch forward head movements are a clockwise yaw to the right and a clockwise roll. Inversely, the predicted perceived motions for pitch backward head movements are yaw to the left and clockwise roll. The magnitude of their perceived tilt is shown in and Figure 4.8.

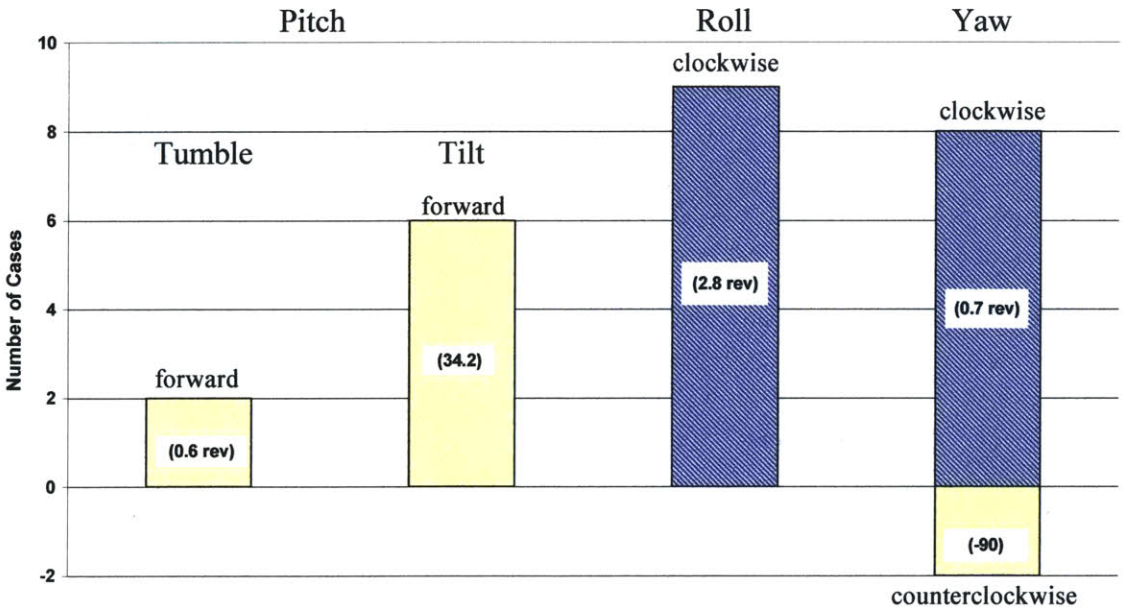

Figure 4.7 Cases of Perceived Motion for Pitch Forward Head Movements

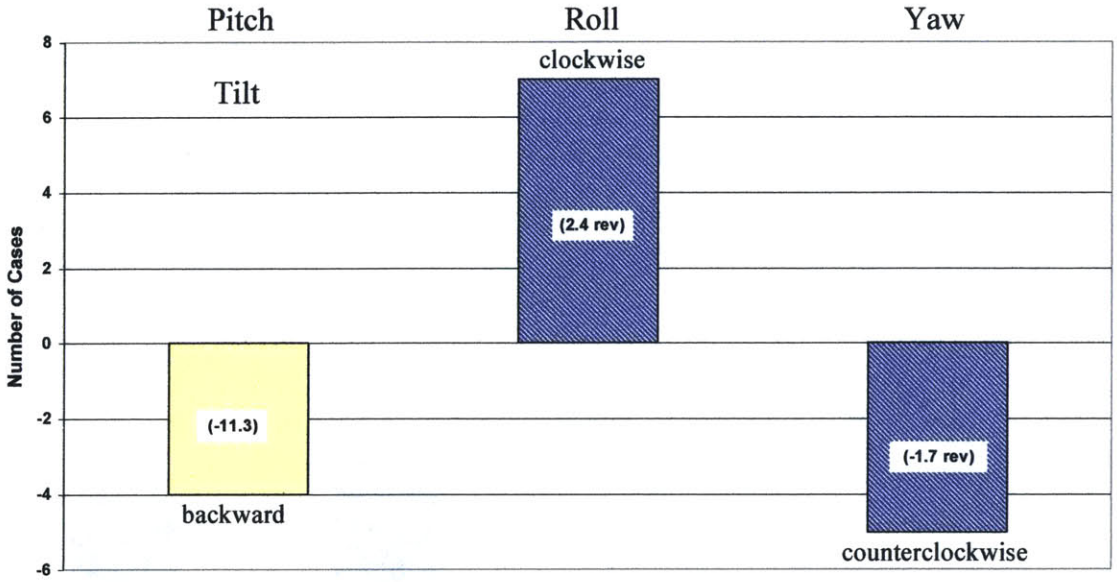

Figure 4.8 Cases of Perceived Motion for Pitch Backward Head Movements

The direction of illusory tilt was examined for a bias between predicted and opposite directions determined by handedness, eye dominance, and sports that may influence the vestibular system, such as flying, scuba diving, or gymnastics. Figure 4.9 shows the percent of subjects that experienced the predicted direction of illusory roll sensation for clockwise yaw head movements for right and left eye dominance. Handedness and sports were not studied since there were only four left-handed subjects and two subjects were involved in sports influence the vestibular system. Predicted perceived pitch sensations for clockwise and counterclockwise yaw and perceived roll motions for counterclockwise roll did not differ between right and left eye dominance (Appendix C).

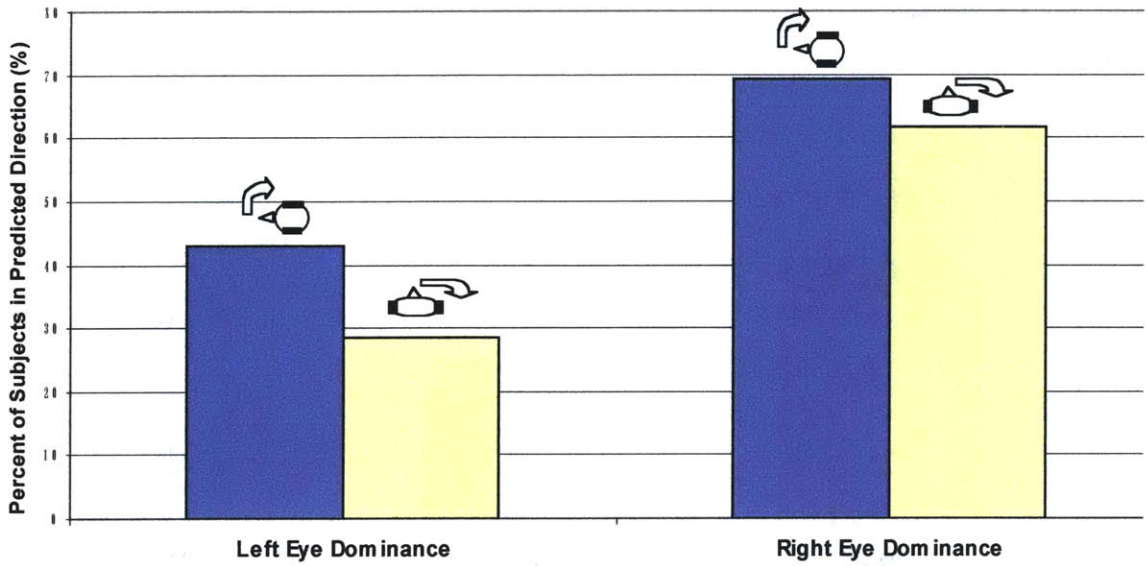

Figure 4.9 Percent of Subjects that Experienced Perceived Roll with Left and Right Eye Dominance for Clockwise Yaw Head Movement

4.2.3 Persistence of Illusory Body Tilt

According to a repeated measures ANOVA, the difference in persistence of illusory tilt between left and right sets of yaw head movements was significant where the persistence lasted longer for the left than right sets of yaw head movements. ($F(1,18)=7.015$, $p=0.018$). Also, head turns to nose-up produced longer lasting sensations than turns to ear-down ($F(1,18)= 6.066$, $p=0.026$). There was no significant difference between the persistence of clockwise versus counterclockwise yaw head movements. The average durations of illusory tilt are shown in Figure 4.10. Each set of bars are grouped according to yaw left, yaw right, and pitch head movements. The bar on the left side of the pair for yaw head movements is the head movement resulting in nose-up and the bar on the right of the pair is the head movement ending in the ear down position.

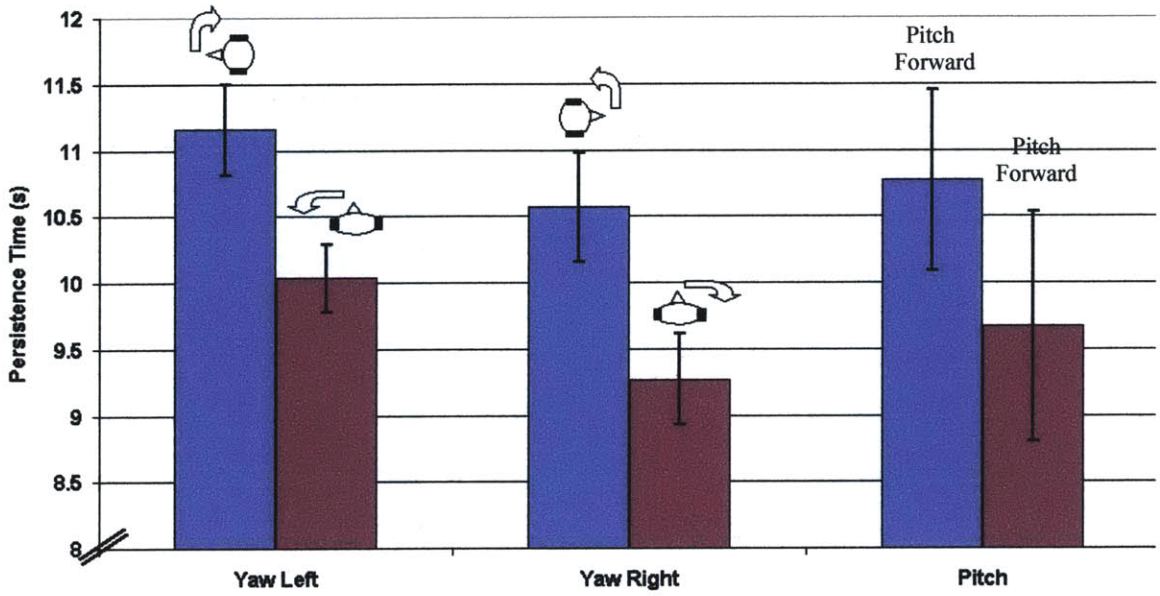

Figure 4.10 Persistence of Illusory Tilt

4.2.4 Perceived Orientation in the Room

45% of the participants did not report a specific orientation (where their feet were pointing in the room) during the experiment. 10% of the subjects felt a clear orientation, which was consistent during the whole experiment. The direction of this orientation was not related to the initial orientation of the centrifuge before it started rotating. 55% of the subjects felt oriented in the room at some point but changed where they felt their feet pointed. Out of this group 45% expressed difficulty indicating the direction.

Chapter 5.0

Large N Discussion

5.1 Heart Rate

A number of studies have attempted to correlate vestibular stimulation with autonomic responses. Results have been mixed. Although caloric stimulation of the vestibular system resulted in lower blood pressure in animal studies, it produced no significant changes in heart rate, blood pressure, muscle sympathetic nerve activity, or plasma norepinephrine in humans (Baggioni, Cost, and Kaufmann, 1998). On the other hand, low intensity electrical stimulation of the vestibular nerve provoked an increase in sympathetic discharge to the heart. One aim of our study was to assess vestibular stimulation by the angular cross-coupling, the disturbing and conflicting stimulus to the semicircular canals, and the conflict of the vestibular system with the otolith system, creating an increased response in autonomic cardiovascular control.

Semicircular canal stimulation has the potential for positive or negative influence on orthostatic intolerance. The carotid-cardiac baroreflex permits orthostatic tolerance. Anecdotal observations indicate that rotational head movements about the vertical axis of the body can induce orthostatic bradycardia and abnormally low blood pressure, hypotension, and through increased parasympathetic activity. Head movements in the yaw plane about the earth vertical with eye movements without fixation reduced baseline baroreflex responsiveness by 30 % (Convertino, 1998). Therefore, semicircular canal stimulation provides direct inhibitory effects on normal carotid-cardiac baroreflex response. It is possible that vestibular disturbances caused by adaptation to microgravity might contribute to post-spaceflight orthostatic hypotension by exacerbating already impaired carotid-cardiac baroreflex function. The benefit of artificial gravity in providing greater stimulation to prevent cardiovascular deconditioning brings with it the detrimental effects of increasing the vulnerability of astronauts to orthostatic side effects by inhibiting the carotid-cardiac baroreflex.

Although the Large N study demonstrated an increase in heart rate, the direct interaction with the baroreflex of the canals were not explored.

However, Pancratz, Bomar and Raddin (1995) propose a promising argument for cardiovascular conditioning using artificial gravity. They produced a mathematical model of the cardiovascular system that calculated the flow and pressure in 40 arterial and venous vascular segments and 10 peripheral capillary bed segments. The results of their simulation showed that space-based short-radius centrifugation in humans produced similar cardiovascular pressures as "those seen in the upright man at +1 Gz." (Pancratz, Bomar, and Raddin, 1995, p. 69). They also simulated short radius centrifugation on the earth 1-g environment and predicted that the only difference would be higher arterial and venous pressures at the hip segment. Therefore, intermittent exposure to short-radius centrifugation would provide a countermeasure suitable to act as a gravity agent in promoting orthostatic tolerance.

5.2 Illusory Tilt Differences

Although the majority of subjects felt the illusory tilt in the direction predicted by the semicircular canal model, there were a number of cases opposite from this direction and along an axis contrary to either predicted axes of illusory tilt. Approximately 11 % of subjects had sensations contrary to the predicted sensations, discounting the subjects that felt no illusory tilt in the predicted direction.

This directional anomaly was not a trend for any subject (i.e. there was not a complete inversion of the predicted directions for any subject). Rather, more generally, subjects perceived the predicted direction of illusory tilt for most of the head movements with the occasional exception of one unpredicted direction in only one of the two semicircular canal planes for illusory tilt during a yaw head movement. Dickman (1998) examined the structural locations of the roughly orthogonal semicircular canals in pigeons. There were significant deviations on the order of 5 to 20 degrees between complementary canals pairs in terms of structural relative location. Since "convergence in differing dynamic information from the afferents appears to be

important in determining the response sensitivity of these [semicircular canal] cells to head movement stimulation", (Dickman, 1998, p.7), unmatched convergence between bilateral canals due to local structural differences in a subject may help to explain the asymmetric nature of sensations for a subject.

A discrepancy between pitch and yaw head movements among subjects who did not feel the predicted direction. In yaw, 10-30% of subjects did not feel the predicted directions, while in pitch, the percentage of those subjects were higher, 40 %. Those who felt an unpredicted direction in yaw head turns were not correlated with subjects that felt the unpredicted direction in pitch head movements. This is perhaps due to the influence of the saccules in pitch. The saccules dominate perceived sensation much more in the z-plane, than the utricles in the x-y plane by a ratio of 3:1 (de Graaf, Bos, Tielemans, Rameckers, Rupert, Guedry, 1996). Since the otoliths play a more dominant role in pitch, it may mask more of the predicted semicircular canal directions. It is possible that the pitch head movement stimulates the proprioceptive muscles in the neck coupled with the vestibular signals of both the otolith and canals to produce this pronounced roll compared to in yaw head movements. The respective angles between head, neck and trunk corroborate an extant model of cross-multiplication of utricular, sacular, and neck receptor components (Mittelstaedt and Glasauer, 1993). In this model the neck receptor messages are first transformed into cosine and sine components and then are multiplied crosswise with the respective utricular and saccular angular messages before the products are summed. Because this relation is not additive but multiplicative, the pitch head movement elicits a stronger force on the neck muscles and the abdominal muscles in the trunk than a yaw head movement. Moreover, the saccular contribution compounds the sensation of tilt when stimulated by pitching the head up into the vertical z-plane. However, this postulate has a counter-argument by Hofstetter-Degen, Wetzig, and Von Baumgarten (1993) who conducted the effects of pure neck receptor stimulation on eye position, in which displacements of the eye signify vestibular stimulation. They found that the neck receptors do not contribute to a measureable extent to stimulating vestibular orientation when in microgravity. This is similar to other studies whereby the extent of

motion sickness cues and illusory body tilt is reduced at reduced gravity levels (DiZio, Lackner, 1991). A remarkable feature of the Coriolis, cross-coupling stimulation of the canals is that it is considerably less provocative under the weightlessness. This reduced sensation and reduced motion sickness symptoms in 0 g may be due to the reduced sensory conflict between the otolith organs and the semicircular canals. In a Coriolis, terrestrial environment, gravitational stimulation to the otolith organs would send an orientation signal to the body that conflicts with the semicircular canals, which sends a different body orientation when the head is turned. Whereas during centrifugation in 0 g, the otolith organs are no longer stimulated, and body orientation is only determined by the semicircular canals. This loss of conflict results in reduced motion sickness symptoms and less violent, disturbing motions. Only the illusory motions influenced by the semicircular canals are felt during a head turn. While spinning about the body z-axis at 0 g, the pitch head movement feels very gentle with little sense of spinning or head tilted associated with the movement. Apparently, the felt deviation of the head results in a perceived motion greater than the actual deviation of the head due to proprioceptive stimulation from muscles that oppose the movement (Lackner, 1993). Now if the proprioceptive neck muscles already do not contribute as greatly from Hofstetter-Degen, et al (1993) at reduced gravity, it is reasonable that the illusory sensations at 0 g are also considerably reduced.

5.3 Illusory Tilt Magnitude

Subjects reported perceived roll magnitude at least twice as high for pitch as yaw head movements. This may be due to the discrepancy in endolymph time constants for the individual canals. In the case of yaw head movements, only the pitch and roll canals are being stimulated, whose time constants are 6.1 seconds and 5.3 seconds respectively. These time constants are relatively close to one another when compared to the yaw canal, 10.2 seconds. Since the yaw canal's time constant is nearly twice as long, the yaw canal endolymph should repond twice as long to the same stimulus for either the pitch or roll canal, while resulting in the same magnitude of perceived motion. However, this was not found. In fact, the duration of the perceived illusory tilt

was approximately the same for yaw as pitch head movements, 10.26 seconds for yaw head movements and 10.76 seconds for pitch head movements. Additionally, the subjective sensation was twice as strong. These results are inconsistent with the known time constants of the effective canals. The difference between the Large N experiments and the experiments performed by Jones, et al (1964), who determined the canal time constants, was the body orientation with respect to the rotation axis. This implies an influence from both somatosensory cues and the otolith system.

In another experiment that studied tilt perception from linear acceleration by centrifugation (de Graaf, et al, 1998), subjects experienced larger tilt while oriented in the z-axis (39 deg) than in x- (27 deg) or y- (25 deg) axis. This corresponds to Large N data for all planes of tilt sensation. Consider the roll sensation for the Large N case. There was greater sensitivity along the x-direction (808.8 deg) where the final head position is nose-up than the y-direction (568.7 deg) where the final head position is ear-down. However, both were significantly less than the tilt sensations to pitch head movements in the z-direction (1008.3 deg).

The direction of centrifuge rotation compared to the quadrant the head is turned has an influence on the strength of illusory body motion. The results of Large N agree with a study by Reason and Graybiel (1969), whereby the larger strength of the illusory body tilt sensations were perceived by rotating the head in the plane that has the same sign as the constant velocity vector of the centrifuge. In both cases the head was held in the neutral "up" position during ramp up. Therefore, conducting the head turns in the direction opposite from the centrifuge rotational direction requires more work for the neck and shoulder muscles. The head is turned away from the direction of rotation. Reason and Graybiel's spinning chair rotated counterclockwise, and the magnitude estimates were significantly greater for roll head movements to the right ($p<0.01$). Similarly, for yaw head movements, the head movements to the left were significantly greater than the yaw head movements to the right as measured by the duration of the perceived motion. Verbal responses concur with stronger sensations felt on the left side for yaw head movements, although magnitude estimation data did not show a significant difference. Moreover, subjects in both studies reported returning the head to

the upright or nose-up position produced a stronger and more disturbing sensation than moving the head through the same angle to the shoulder or to an ear-down position. Perhaps the neck muscles and receptors play a more dominant roll in orientation to bring the head up against gravity and return it to the neutral position. Another possibility may be the effective pitch canal for both cases are being decelerated when the head is brought to the neutral position. This increased sensation may be explained by Guedry, Rupert, McGrath, and Oman, (1992), arguing that perceptual effects during deleration are much stronger. This also implies that the effective pitch canal may dominate the sensations in terms of heightened perception of sensations overall, not strictly in the perceived pitch direction, when pitch canal is decelerated.

Reason and Graybiel also used numerical estimates to represent the strength of sensations, although for their case, their basis for comparison was an estimation of loudness by a 1000 Hz tone at various sound pressure levels about 50 dB and then correlating that to perceived illusory magnitudes. However, we did not get similar results to repeated exposures to the head movements. Reason and Graybiel stated that nearly all of their 18 male subjects experienced diminished strength with 4 repeated runs, particularly between the second and third runs; whereas nearly all 20 of our subjects did not report any loss of strength in the sensations following 4 yaw head movements to the left or right.

In a study by Guedry, et al, (1992), perceptual effects during deceleration were much stronger than effects during acceleration for a similar experiment involving centrifugation about many axes of rotation, including the x-axis as in Large N. The stimulus was an angular velocity profile similar to that employed in centrifuge runs to train pilots. Descriptions during post-run discussion were aided by subjects moving a small manequin in space to illustrate the dynamics of their perceptions of linear and angular motion and position relative to the earth. Guedry's results are not supported by the Large N results. If that were the case, for all yaw head movements, illusory pitch sensations would dominate over the roll sensations. In the Large N study, pitch sensations are are not significantly different from roll sensations. This may be due to the overriding disturbing conflict of the cross-coupling of semicircular canals in two

planes instead of stimulating only one canal in the case of Guedry. Additionally, in Guedry's experiment, the otolith system concurred with the perceived sensations and there was no conflict, whereas in our study, the otolith system was conflicting with the semicircular canals.

De Graaf, et al, (1998), remarked that subjects consistently underestimated perceived illusory tilt during centrifugation. A perceived pitch tilt of 25 degrees while lying still during centrifugation of 1 g at the feet was lower than the true gravito-inertial force vector of 45 degrees. De Graaf speculated this underestimation was due to the unnatural method of stimulation by artificial gravity. The saccular influence in de Graaf's experiment (rotation about the vertical z-axis) was argued to mask the gravito-inertial force vector. For this to be true for our study, the utricles would also have to function similarly to the saccules in dominating the sensation from the gravito-inertial force vector. Another possibility is also cognizance of the true position of the body while riding the centrifuge, which may influence the perceived magnitude of tilt. A useful follow-up study would be to null out the motor noise and ramp up information and asked the perceived tilt question again while the subject was rotating. A priori knowledge would then help determine the masking influence of cognizance.

Lastly, a model has been developed by Grissett (1995) to characterize vestibular function and resulting vestibular-ocular reflex and perceptual responses. The model was particularly suited for six degrees of freedom, rotations along a number of different stimuli, off-vertical rotation, pendular rotation, non-pendular rotation, passive roll, linear and angular acceleration profiles. In particular the model characterizes otolith and canal interactions, such as the attenuation of linear input by angular input as shown by Clark and Graybiel's studies (1966). However, this model has not been validated by a large data set of vestibular responses from subjects. This Large N study could be used in conjunction with the model to more accurately predict subjective experiences based on the ideal semicircular canal model, to validate the model's algorithms, and possibly to account for large population differences in perceived illusory tilt.

Chapter 6.0

Regulator Feedback Control

6.1 Introduction

The short-radius centrifuge at the Man-Vehicle Lab was built in 1985 for research in artificial gravity (Diamandis, 1988). Prior experiments have studied the effect of artificial gravity on sleep patterns (Diamandis, 1988), how the 100 % gravity gradient changed cardiovascular pressure by measuring blood volume (Hastreiter, 1997), the rate of adaptation of arm trajectories under the influence of Coriolis forces (Tomassini, 1997). Recently, two experiments, the retention of Coriolis, vestibular adaptation and the Large N study (Section 2.2) that examined the perceived illusory tilt and heart rate changes to head turns during centrifugation, were performed. Thus far, all experiments involve very little motion by the subject, and time-varying centrifuge speed control was not needed. Therefore, a constant torque output, in terms of a constant controller voltage, was used to maintain a constant angular velocity of the centrifuge. The rotational speed control of the centrifuge was open loop and manually driven with a Controller Browning Focus 2. Within the controller there exists a feedback check on the angular velocity that is supposed to maintain a +/- 1/2 % accuracy.

In the current retention of adaptation study, one of the primary measures was vertical eye nystagmus to head turns while on the centrifuge. An anomalous nystagmus can occur in response to a velocity disturbance in the centrifuge constant velocity profile while the subject is lying still. Angular accelerations as low as 0.5 $^{o}/s^{2}$ to 0.8 $^{o}/s^{2}$ (Groen and Jongkees, 1948) would be detected, eliciting an undesired nystagmus. Therefore, it is crucial to know whether disturbances as large as 0.5 $^{o}/s^{2}$ were affecting the velocity profile and when they occurred. Additionally, control of the centrifuge velocity is currently determined by the performance of the controller. Controller documentation states that motor velocity is maintained within +/- 1/2 % accuracy. However, the motor was designed for industrial purposes at a higher rpm and lower

moment of inertia. It is not certain that the true angular velocity accuracy coincides with controller documentation. Therefore, accurate tachometer measurements and a controller independent PID (proporional-integral-derivative) feedback are desirable for consistent velocity control. Further, a feedback velocity control would open the possibility for active motion on the centrifuge.

Active disturbances, such as when an object or the subject was to displace its distance from the axis of rotation on the centrifuge during the experiment or during exercise experiments on the centrifuge, would shift the moment of inertia. If the centrifuge were controlled with open loop constant voltage output, then the torque applied to the centrifuge would not be able to compensate for this change in moment of inertia and the angular velocity of the centrifuge would be compromised. Automatic feedback control of the centrifuge rotation would significantly enhance the elegance, robustness, and credibility of the experiment. With automatic feedback control, the subject would receive the desired stimulus in a highly controlled environment that can compensate for external disturbances and is measurable.

Before automatic feedback control can be considered, the centrifuge must first be automated and equipped with an accurate, low noise tachometer. Then regulator control must be implemented to achieve high accuracy maintenance of constant angular velocity. Then it is fully possible to conduct disturbance experiments of changing mass distribution on the centrifuge. To conduct controlled experiments, the centrifuge must be controlled by a feedback system.

6.2 Requirements

The initial impetus for a feedback control was to remove the slight velocity changes in the centrifuge that a subject may sense, eliciting an undesired nystagmus. It was crucial to eliminate all velocity changes of 1% peak to peak. Any velocity change greater than this threshold would be sensed and produce the undesired nystagmus.

Following many pilots and an experiment not influenced by nystagmus, it was determined that the open loop control of the centrifuge produced a slight rocking

motion or a periodic kick. However, the motion, though subjectively experienced, did not produce a nystagmus. A general requirement was then set to have an automatic regulator control to the centrifuge for robustness and experimental credibility. Design requirements such as response time of the feedback and steady state error were not determined.

Chapter 7.0

Regulator Control Equipment

7.1 Equipment

The conditions of the centrifuge and the controller equipment prior to my thesis work is described. The centrifuge was operational, including some level of experimental equipment onboard. Watson angular rate sensors and ISCAN eye recording equipment were installed on the centrifuge and connected to the data acquisition equipment through a slip ring at the axis of rotation. The centrifuge was driven by a Browning 1 hp motor, powered by 90 VDC/120 VAC and 10 Amps, and was controlled by a Browning LWS Series LW Focus 2 controller box. The block diagram for the controller is in Figure 7.1. It had an internal speed control, which depended on the back emf of the motor. The comand is filtered by a time lag that is adjustable by a potentiometer between 2 sec and 40 sec. Currently, it is set to 2 sec. This motor was probably designed for industrial applications where motor speed changes were relatively slow, and this 2 second delay is a safety feature that acts as a buffer against high acceleration changes to the centrifuge's large moment of inertia. However, this severely limits the time response of the PID control.

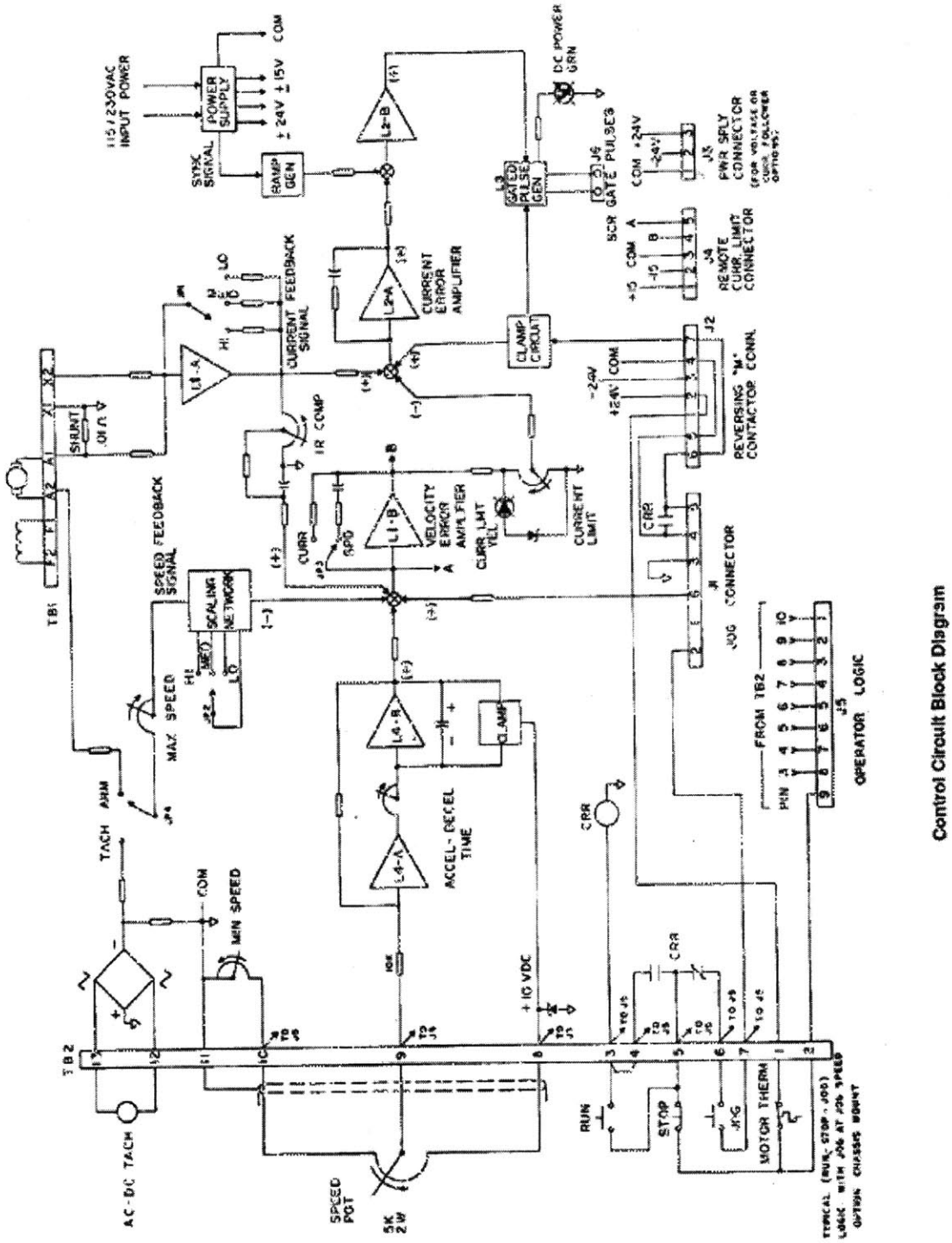

Figure 7.1 Controller Block Diagram (User's guide for Focus 2, p. 25)

The centrifuge was controlled manually by a dial that had settings in terms of voltage, not angular rate. A pencil mark was placed at the desired location of 23 rpm; this translates to 1 g longitudinally at the foot of the centrifuge for a person of height 5'6. The motor shaft speed is then reduced by 10:1 at the worm gear. A belt attached the gear box to the centrifuge. At the shaft of the gear box was an inverted dc motor that acted as a tachometer. It had not been connected by any data acquisition equipment at the time, so its performance on accuracy of shaft speed measurement was not known.

Data acquisition equipment consisted of a National Instruments PCI-6024E data acquisition card, and E-machine computer, a National Instruments SC2050 analog to digital converter, and a Keithley MB39 voltage to current isolator. The computer's ground and the controller's ground differed by 100 volts. Since the data acquisition card would be connected to the controller, a voltage isolation unit was in place consisting of a 250 ohm resistor and a Keithley MB39 voltage to current isolater. Although maximum output voltage from the data acquisition card was 10 volts, it was experimentally determined that the voltage isolation unit limited the voltage to 6.6 volts between the data acquisition card and the controller box.

7.2 Automatic Control

To attain greater fidelity in controlling the speed profile, automatic control was implemented using LabView's Write One sub.vi program.

This sub.vi was used to produce a LabView program for the current experiment (Figure 7.2). The control profile for this experiment needed to ramp linearly the bed from rest up to 23 rpm in a set period of time, and then, at the experimenter's discretion, to ramp the bed down to rest. The logic of the program sends a voltage value to the analog output channel that was connected to the controller. This performs an immediate, untimed update to the specified channel. To run continuous analog output to the controller, this update was put into a "while" loop that configures the channel group and hardware at the first loop and then with subsequent iterations only writes a value to the specified channel. Also, in the loop is a timer to constantly send a

discrete voltage at set time intervals. The user inputs were the setpoint, which is the desired bed speed, time to ramp up and down, scan rate, device number and channel number. Additionally, there was a virtual button with which to ramp the bed down from the setpoint to 0 rpm. The program determined what voltage increments needed to be made depending on the desired setpoint and the time between each loop. The logic for the ramp compared the desired bed speed to the current one. As long as the bed speed was less than the setpoint, as extrapolated by the control voltage and the voltage relationship to bed speed, the program continually incremented until the desired voltage is reached. A linear relation between control voltage and bed velocity between rest and the operating setpoint was assumed. Then the logic of the program sends this setpoint voltage to the bed until the "Ramp Down" button is depressed. At this point, the program logic sends the control voltage increment below the prior value until the control voltage reaches 0 volts. The LabView program diagram is in Appendix D.

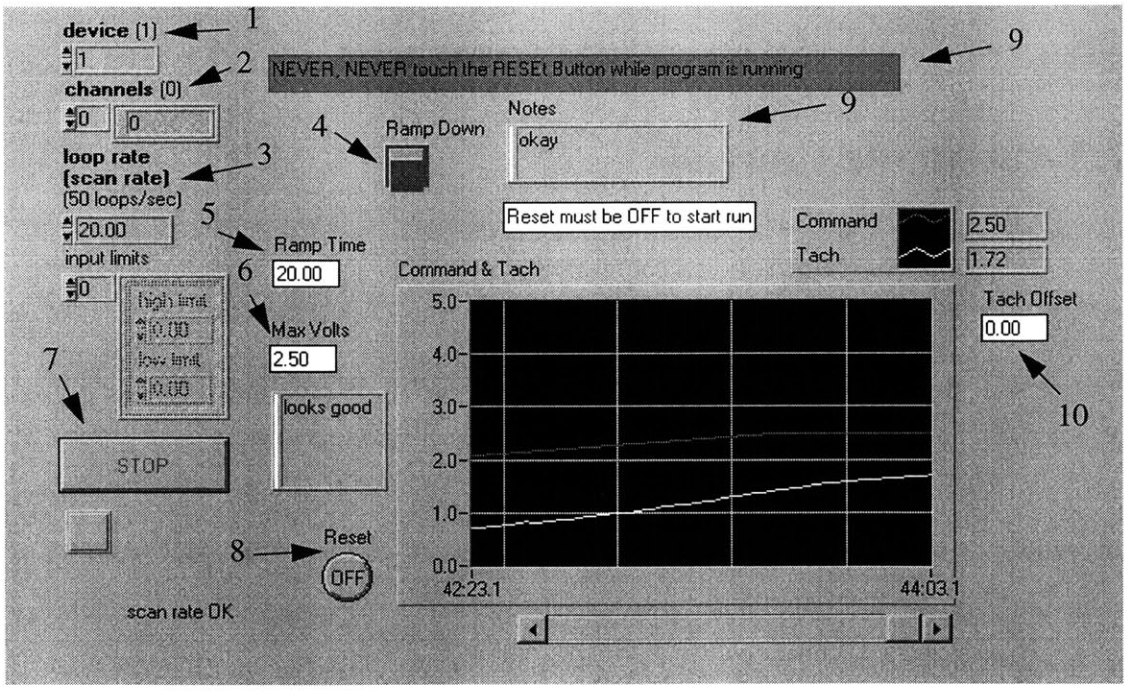

Figure 7.2 User Interface for Automatic Control of Centrifuge

Figure 7.2 describes the user interface for automatic control of the centrifuge. 1) specified devices that matches data acquisition card, 2) user specified channels which read in tachometer analog input, 3) scan rate for restrieving analog input, 4) ramp down button -- when depressed, the output profile to the controller ramps down from the Max Volts to 0, 5) user specified ramp time in seconds, 6) user specified desired voltage for constant angular velocity, 7) stop button -- when depressed, the program stops running, 8) reset button as a safety mechanism sets the control voltage to 0, 10) user input tach offset. The tachometer is temperature sensitive and a reading of the initial offset can correct for these changes. The program provides for immediate adjustments after input from the tachometer is examined before running any experiments.

When the program is started, the user is asked to input a filename. During the course of the program run, a 2-column text file is written. The first one is voltage command to the centrifuge and the second column is the tachometer input.

The profile LabView program was used by a number of different researchers; therefore, a couple of safeguards needed to be implemented for user ease and in the event of any careless mistakes. Within the logic, there was a check to make sure the output voltage did not exceed 4 volts, which approximately correlated to 26.39 rpm. If the user inputs a value higher than 4 volts, the setpoint is automatically assigned to be 0 volts, and a text box appears that warns the user that the setpoint is dangerously high.

Automatic control to the bed was kept in units of voltage when displaying the output to the screen and writing to the text file. During the calibration of control voltage to rpm of centrifuge velocity, at any given measurement the exact rpm would change by up to 2 rpm. This is probably due to a number of human and instrumental errors. Open loop control voltage to the controller would result in an angular velocity change of 0.5 rpm to 1 rpm per run. Also, the measured angular velocity depended on the increment size. Three measurements of rpm of the centrifuge using a stopwatch and the passage of 10 revolutions would give an error of 0.5 rpm. This led to three values of the slope and y-

intercept. From 0 rpm to 23 rpm, the equation for the voltage relation to rpm is in Equation (7.1).

$$rpm = 7.9125 \cdot volts - 5.4688 \tag{7.1}$$

However, if the scale is lowered and increments taken in smaller steps of 0.25 volts, from a voltage of 3.25 rpm to 3.75 the rpm to voltage relation is Equation (7.2).

$$rpm = 7.61925 \cdot volts - 5.02712 \tag{7.2}$$

then if the increments are made smaller by 0.1 volts, and taken from 3.3 volts to 3.7 volts, the equation for the voltage to rpm is Equation (7.3).

$$rpm = 8.085 \cdot volts - 5.9485 \tag{7.3}$$

Note that the above measurements of rpm were taken by a stopwatch and the passage of 10 revolutions. Further calibration equations are worked out in Section 7.4.1 and 7.5.3 for the new tachometer equipment of the encoder and accelerometer, respectively.

7.3 Tachometer Development

The inverted dc motor signal was read into LabView using the Acquire 1 Scan.vi program. The Acquire 1 Scan.vi uses three basic programs, AI Config.vi, AI Start.vi, AI Single Scan.vi. The logic in the program starts at AI Config where it configures the hardware and allocates a buffer for a buffered analog input operation for the specified channel. It is in AI Config where the taskID is set. Also, it configures the coupling for the channel and the input configuration, which is differential for this case. AI Start initiates a buffered analog input operation that sets the scan rate and trigger conditions (hardware) and then starts the acquisition of data. AI Single Scan reads one scan of data directly from the data acquisition board at its specified input channel. To read the analog input continuously, these subprograms were combined into one that was in a while loop whose timed intervals were 50 ms. The tachometer data was very poor (Figure 7.3). For a constant control voltage of 3.5 volts that correlated to 21.64 rpm

(calculated by a stopwatch), the speed that the tachometer read ranged between 13.2824 rpm and 41.0194 rpm. In other words the noise range of the inverted dc motor voltage output was between 4.668 volts to 7.251 volts. This produced an accuracy of 28.2 %.

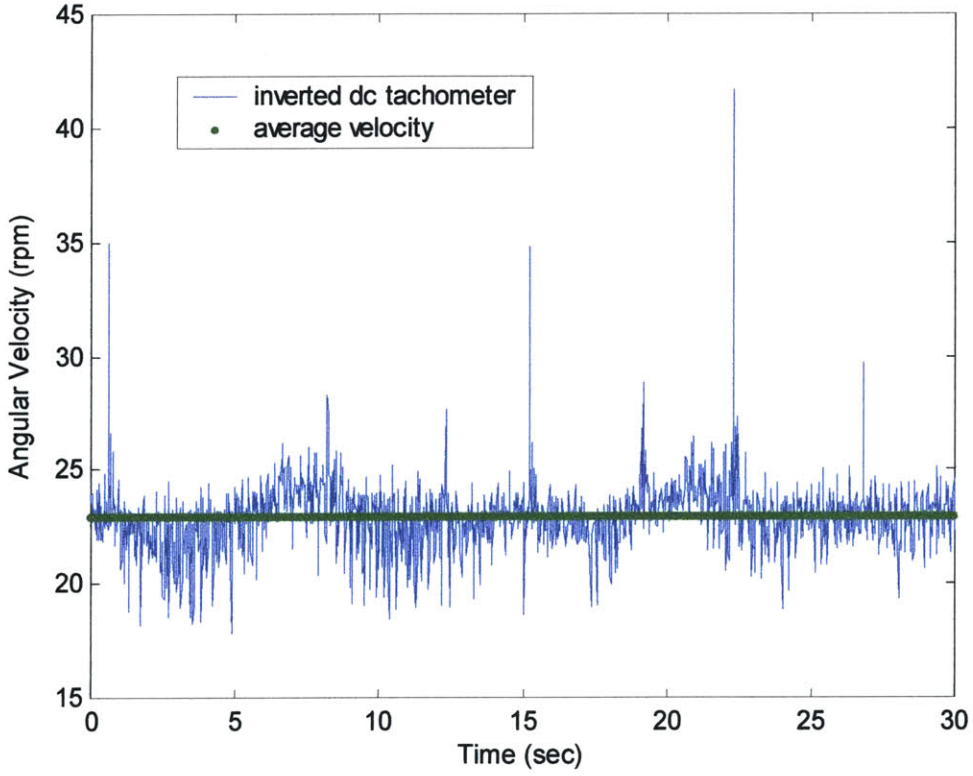

Figure 7.3 Inverted DC Motor as a Tachometer for Control Voltage of 3.58 volts

In fact, during the inverted dc motor tachometer measurements, from a control voltage of 1 volt to 3.75 volts, with 0.25 volt step increments, the slope between the step sizes were calculated and plotted. Instead of the slopes being relatively flat, the slope values behaved like the square root of the input voltage. It was primarily for this reason that it seemed reasonable to output the true voltage until a reliable tachometer was installed, in the event of equipment errors in the inverted dc motor. It was postulated that perhaps the square root behavior of the reading is not necessarily from actual angular velocity but from instrumental errors in the inverted dc motor.

After examining a number of different designs for a tachometer, two primary instruments were chosen: an optical encoder and an accelerometer would be installed. A hall or magnetic sensor was disregarded due to the tachometers close proximity to the motor. Photoelectric sensors were also unfavorable. Any detector needed to be attached directly on the worm gear shaft. A separate stand would need to be built to attach any two-part detectors, and errors in location and isolation from the rotating bed would cause a number of difficult problems. Potentiometers were a possible solution, however, any errors that resulted per rotation of the shaft would be compounded for more rotations and the error would linearly escalate. Also, a potentiometer measures position and is not designed to measure angular rate. Its output required differentiation. Encoders were already recognized for taking measurements from rotating shafts. Therefore, an optical encoder was appropriate, as it functioned like a photoelectric sensor but had both instruments fully encased and a shaft attachment that made installation more practical. The accelerometer appeared favorable because of its low g operating range, high resolution, and ease of procurement. Additionally, the accelerometer had adjustable signal amplification and temperature compensation.

7.4 Optical Encoder

The Hewlett-Packard HEDS-5700, a panel mount optical encoder has a resolution of 256 counts per revolution and requires a 5-volt power supply that is supplied by the computer. It has an operating temperature range of -20 to 85 degrees Celsius. Its complete technical description is included in Appendix J. Whereas the inverted dc motor required some effort to rotate the shaft, the encoder shaft has a starting torque of only 0.47 oz in.

7.4.1 Tachometer Installation

The optical encoder replaced the inverted dc motor and was attached at the worm gear shaft. The shaft coupling needed to be slightly modified for the encoder's smaller shaft diameter, from a 3/4" to a 1/4", but it mounted to the same angled apparatus that held the inverted dc motor in place. The output of the encoder is digital and therefore, the

pin allocation needed to be modified. The optical encoder was calibrated by rotating the centrifuge by hand exactly 10 revolutions and counting the number of ticks. The correlation was 699 counts equaled one revolution. The calibrated units of encoder output to rpm is the in Equation (7.4). The encoder is scaled by the gear ratio between one revolution of the centrifuge and one revolution of the gear reducer, resulting in a factor of 0.09868.

$$rpm = 0.09868 \cdot encoder - 0.308742 \tag{7.4}$$

7.4.2 Optical Encoder in LabView

LabView required a different set of programs to process digital input from counters like the optical encoder called counter programs (Appendix E). Frequency, pulse width, period and counting pulse measurements are a set of predefined programs already in LabView for counter data acquisition. For this tachometer application, the fastest running program and the lowest noise was the period measurement program. The logic for the program counts the rising edges of each pulse using an STC-based device, PCI-6024E compatible. The counter increments the event count every time a pulse comes into its source input where each edge is counted as the rising edge for each pulse. The current value of the counter is read when the counter completes or an error occurs. Inputs to the encoder program are the device and counter number, and loop delay. The program outputs the count number, period and pulse, assuming a 50% duty cycle, and plots the frequency or inverse of the period. The encoder data possessed intermittent spikes that were neither periodic nor velocity dependent. The source was attributed to program bugs rather than equipment issues. It was assumed that software would filter the spikes. The program nulled the spike anomalies by comparing the current value to the value before the previous one. The current value, due to the large inertia of the bed, could not increase by a large amount in only 50 ms, so the threshold of 20 added to the average input value would remove all the unreasonable spikes that are a result of encoder noise and not actual centrifuge velocity. If a spike was found, the program would then null the value. This was quite effective and removed of the large magnitude spikes. During a run of the program for five minutes, only 2-3 spikes would be counted. The top figure of Figure 7.4

exemplifies a typical spike that has been nulled out, and the lower figure is a zoomed in view of the encoder response to constant voltage control. The data had an accuracy of 0.83 rpm standard deviation and a peak-to-peak spread of 2.58 rpm about the median and had a periodic fluctuation that matched the rotation of the bed. This is probably due to an imbalance in the ball bearing attachment of the centrifuge to the connecting shaft.

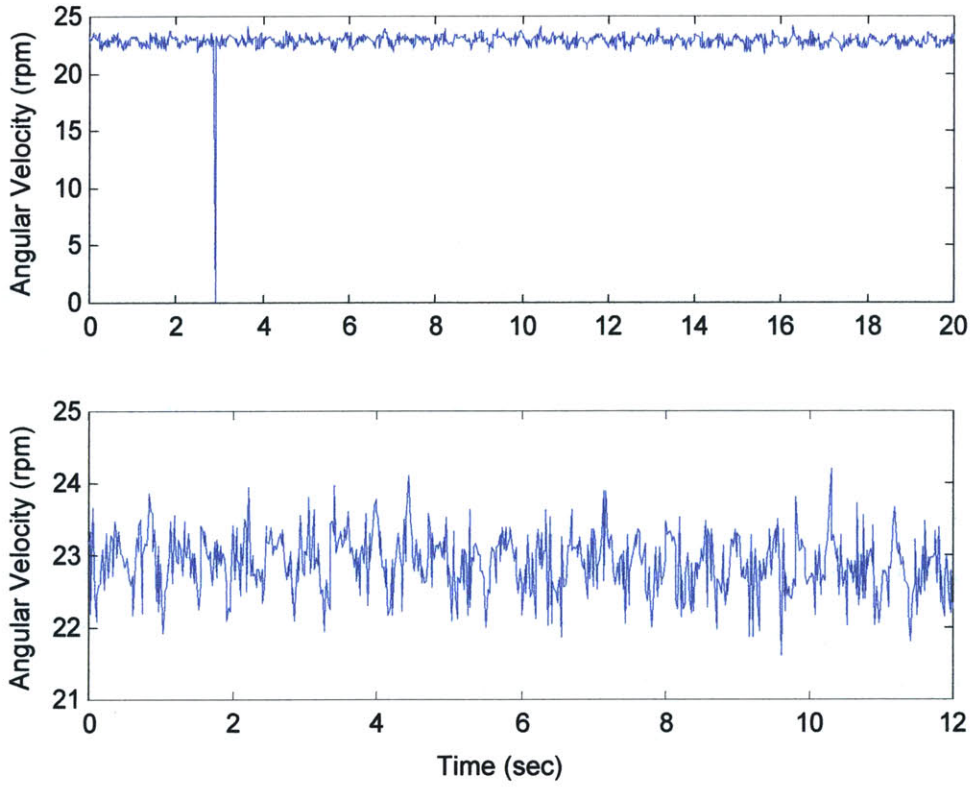

Figure 7.4 Optic Encoder Tachometer for Control at 22.85 rpm

A difficulty with this program was at very low speeds and at rest, the program's period measurements had pulse widths of longer and longer durations. This introduced a number of spikes and noise that force the program to automatically stop. This problem is presumed to be cause by encoder logic problems. Possibly a bug in the internal programs that read in the digital data, normally meant to read measurements between 1

kHz and 10 MHz, explodes at such low count rates. A couple of logic patches were made to send these values straight to 0. This limited the encoder functionality to measure a minimum of 3 rpm.

7.5 Accelerometer Development

The ADXL105 accelerometer from Analog Devices is a high accuracy +/- 1 g to +/- 5 g single axis *i*mems accelerometer with analog output. Its minimum resolution is 2 mg with a 10 kHz bandwidth, and has a typical noise floor of 225 μg/(sqrt(Hz)). There is an on-board temperature sensor, compensator, and an uncommitted amplifier. The temperature sensor on the accelerometer permits on-board processing to correct for temperature dependent accelerometer fluctuations. The temperature sensor was not used in the installation due to the limited number of operational connections in the slip ring. The accelerometer's temperature operating range is 0 degrees to 70 degrees Celsius. The accelerometer's output is nominally 250 mV/g. The specification information on the ADXL105 is in Appendix J.

7.5.1 Accelerometer Installation

The accelerometer is attached on the underside of the bed near the footplate. The accelerometer's single axis is aligned radially outward from the bed to reduce the effect of offset errors in the measurement. If the accelerometer were aligned tangentially, in order to measure angular velocity, the signal would have to be integrated. Since accelerometers tend to have an offset bias, this offset error would increase with each continual integration.

The accelerometer is located 12.5 inches from the foot of bed and along the center 18 inches from the either side. It is attached to Plexiglas that is then bolted to the aluminum underside. The power and the analog output signal are sent to the top of the bed and strung along the bed's right side to the connector strip on-board. Through the slip ring, the power supply uses the 5 volts that also powers the angular accelerometers, and the analog signal gets sent through twisted telephone cable to the data acquisition equipment. On-board processing amplifies the signal response to scale

the output by a factor of 3. Then signal is sent through a 10 Hz low pass filter. The accelerometer was calibrated by pointing the accelerometer perpendicular to the floor. 1 g was equal to -1.52413 volts. The offset is found by inverting the accelerometer; the resulting signal is -3.04826 volts. The initial tachometer reading, unloaded, is -2.297 volts. Therefore, the g to accelerometer output relation is in Equation (7.5). The relation between angular velocity (rpm) and g is in Equation (7.6). The radius of the location of the accelerometer is r = 1.82 meters. Therefore, the resultant rpm to g relation is in Equation (7.7).

$$g = (accel + 2.297) - 0.018524 \tag{7.5}$$

$$rpm = \sqrt{\frac{g \cdot 9.8}{r}} \tag{7.6}$$

$$rpm = 9.549297\sqrt{g \cdot 5.384615} \tag{7.7}$$

7.5.2 LabView for the Accelerometer

The accelerometer used the LabView AI Sample Channel.vi program (Appendix F). The update or loop rate can be much higher than the optical encoder and is not restricted by counter buffers. The input signal is at a much lower voltage, and the accelerometer is not as sensitive to slight changes in velocity. An example of the typical data from the centrifuge at 23 rpm is shown in Figure 7.5. Also, the velocity fluctuates about 0.35 rpm from the median with a standard devation of 0.1183 rpm. However, the periodic fluctuations are not as pronounced with the accelerometer as the encoder. The noise for the accelerometer is of smaller spread but larger magnitude and behaves more like isolated incidences of noise, in the other hand the encoder has a larger spread of noise where incidences of spikes are not as common. One reason for this is more frequency filtering is performed for the accelerometer on-board before it gets sent to the data acquisition equipment, whereas the encoder signal only checks for large magnitude spikes after the signal has pass through the data acquisition board. One source of noise that affects the accelerometer but not the encoder is the cross-axis sway of the centrifuge as it rotates. If the centrifuge is not completely balanced on its rotational bearing, as it rotates, the foot of the bed will have an oscillatory vertical displacement whose frequency is equal to the angular velocity. The accelerometer

would no longer be perpendicular to gravity and the accelerometer would sense an increased or decreased g, as the foot of the bed tilts up and down with the bed's vertical sway. In general, the disturbances at the foot of the bed should be damped out by its large moment of inertia. Therefore, the optical encoder is more susceptible to irregularities in the belt and vibrations than the accelerometer.

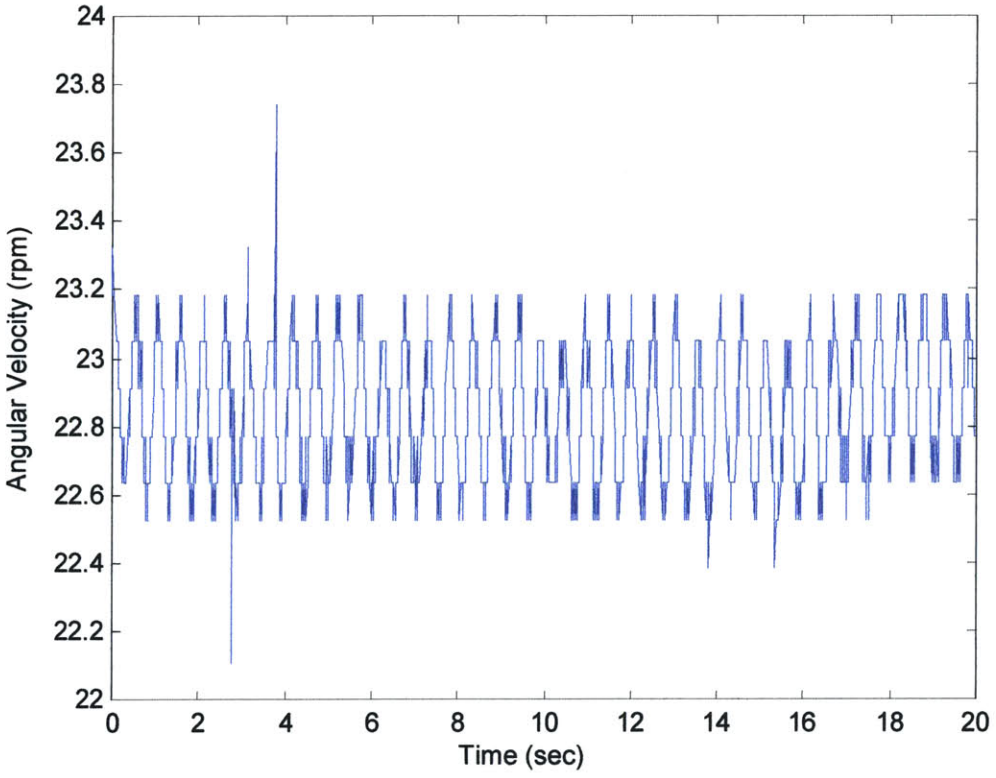

Figure 7.5 Accelerometer Tachometer Output from Control Voltage of 3.58 volts

Chapter 8.0

PID Development

8.1 Feedback Control Loop

Once the centrifuge was equipped with both automatic control and an accurate tachometer, a feedback control scheme was then implemented for automatically monitoring and finely adjusting the bed speed to maintain regulator control. This feedback control scheme would account for active adjustments made to the center of mass of the centrifuge and would continually monitor and maintain a set speed. For experimental purposes, robust control of centrifuge angular velocity is crucial for credible results. In order to implement feedback control for the centrifuge, a transfer function was developed for the system, tools were used to simulate the open loop transfer function behavior of the PID-plant system in Matlab, and finally, a LabView PID program was made to fully implement regulator control of the centrifuge.

8.1.1 Centrifuge Transfer Function

A transfer function of the centrifuge was first determined by the physics of the system. Then the time constants of the system were determined by its step response. An equation of motion for the centrifuge plant system can be characterized by a motor whose shaft has a very large moment of inertia. In this way, an approximate equation for the motor was needed. Equations that describe the behavior of a motor are typically determined by its speed-torque curve (Savant, 1964), Figure 8.1.

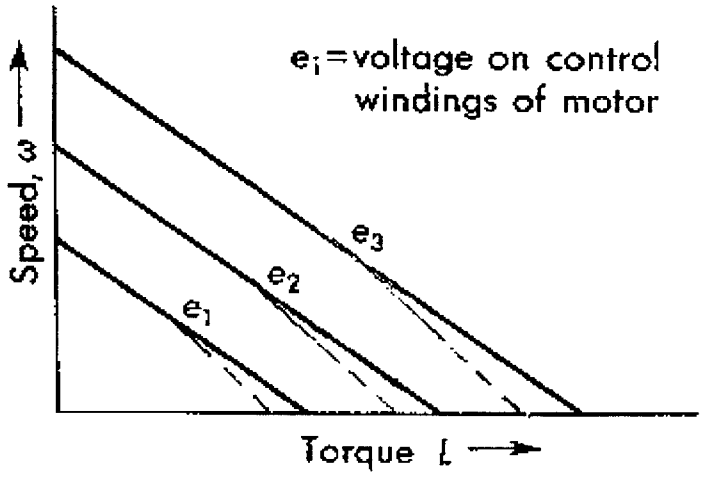

Figure 8.1 A Generic Motor Speed-Torque Curve (Savant, 1964, p. 10)

Unfortunately, the rated speed-torque curve given by the User's Guide was inappropriate for this application, as it did not account for the large moment of inertia of the bed. Generally, speed-torque curves are linearized and are expressed by Equation (8.1)

$$L = a\omega + b \tag{8.1}$$

where L is the torque delivered by the motor, ω is the angular velocity of the motor shaft and a, b are constants. For a typical motor, a is constant and negative. The b is depends on the control voltage. At $\omega = 0$, the straight line speed-torque curve intersects the horizontal torque, L, axis and gives values that then plot a stall torque vs voltage curve as in Figure 8.2.

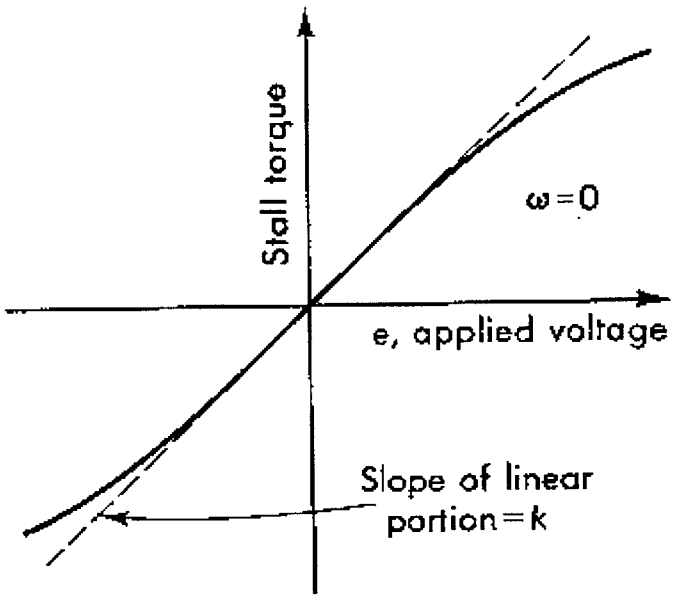

Figure 8.2 Typical Linearized Stall-Torque Curve (Savant, 1964, p. 11)

The slope of this curve is k. The linearized equation for this stall torque curve is Equation (8.2).

$$L_o = ke \tag{8.2}$$

where e is the voltage applied to the motor and L_0 is the stall torque at $\omega=0$. Then we solved for b, for $\omega=0$,

$$b = L_o = ke \tag{8.3}$$

When L does not equal 0, the equation for the motor is Equation (8.4)

$$L + mw = ke \tag{8.4}$$

where L is the torque delivered by the motor, e is the applied voltage and ω is the motor velocity. Now, L, the motor torque, drives the inertial load of the bed. Therefore, $L = J\, d\omega/dt$ where J is the centrifuge moment of inertia. It is assumed that the back emf and friction of the motor is taken into account by the intermediary Browning controller, and we are primarily concerned with torque control by the command voltage. We have the differential equation for the motor-centrifuge system Eq. (8.5),

$$J\frac{d\omega}{dt} + m\omega = ke \tag{8.5}$$

where e is the voltage applied at the motor terminals.

Now the differential equation for the motor is obtained, the Laplace transform is: Jsω+mω=ke. With a little algebra the transfer function for the centrifuge is Eq. (8.6).

$$\frac{\omega}{e} = \frac{\frac{k}{m}}{\left(\frac{J}{m}s + 1\right)} \tag{8.6}$$

Now the time constant J/m and the gain, k/m is determined by the step response of the centrifuge. Because we were only concerned with the regulator control of the centrifuge, the system was linearized about its nominal operating point, not the entire velocity profile. A step occurred about 1 % of its operating point to determine the time constants for regulating the velocity. Therefore, since its operating point was 23 rpm, to correlate to 1 g for a 5'6 person, then a step input of 2.3 rpm; in other words, the centrifuge operated at 21.85 rpm and then a stepped up 2.3 rpm to have an angular velocity of 24.15 rpm. At the time, only the optical encoder was installed on the centrifuge. Therefore, the data presented is from the encoder tachometer, Figure 8.3.

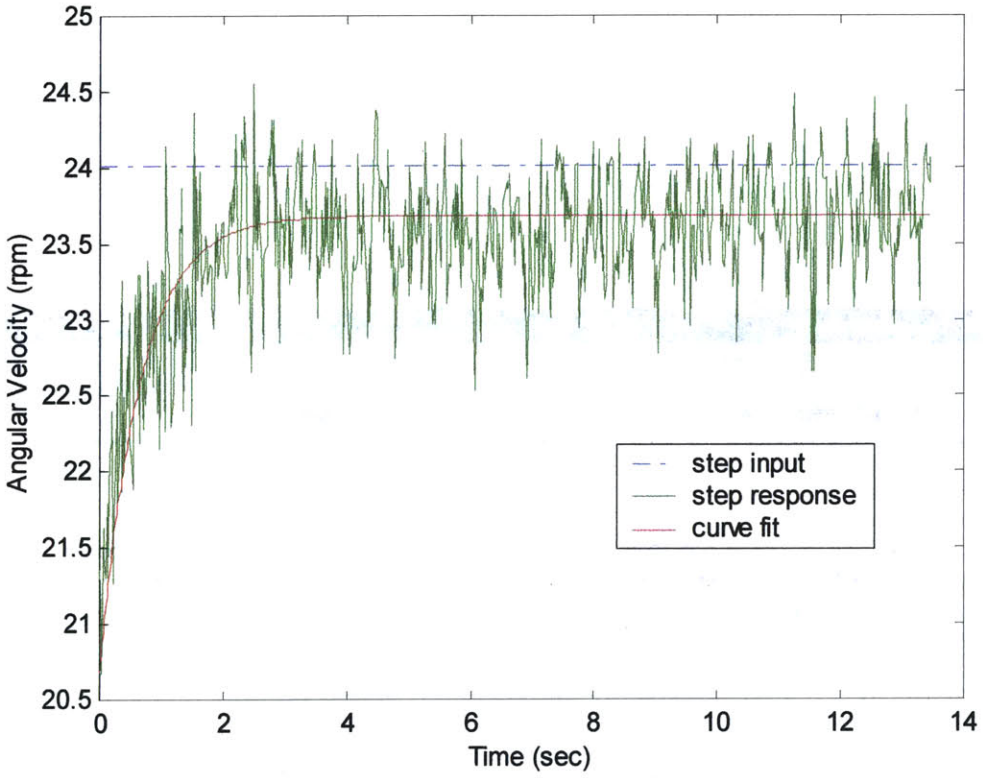

Figure 8.3 Curve fit to 1% Operating Point Step Response

Although the data appeared quite noisy, it was most likely a first order response with perhaps a slight overshoot. Therefore, we needed to determine the time constant, $\tau = J/m$. This was determined in two ways. The curve fit of $y = C(1-\exp(-t/\tau))$ as shown automatically gives τ. The more classical method for determining tau is the time at the curve where the speed would be 1-1/e of its final value. The final value was determined by taking the average of the steady state tachometer data. This was then .6321*(2.402678) = 1.517 rpm. The time at this value was 1.95 seconds. The curve fit τ is 1.9 seconds. Both methods were in good agreement.

Now that a transfer function for the centrifuge behavior was developed, a PID was implemented. It was difficult to determine the transfer function of the behavior of the tachometers, the optical encoder and the accelerometer. The primary concern was if

there was any significant lead or lag in the response of the tachometers. Additional filters were added onto both tachometer signals before entering the data acquisition equipment. A set of capacitors and resistors low-pass filter all the frequencies below approximately 2 Hz. Since the bed response was almost 2 seconds, the transducer response of the tachometers was negligible. The feedback block diagrams in Figure 8.4 were used in determining an appropriate theoretical feedback control system.

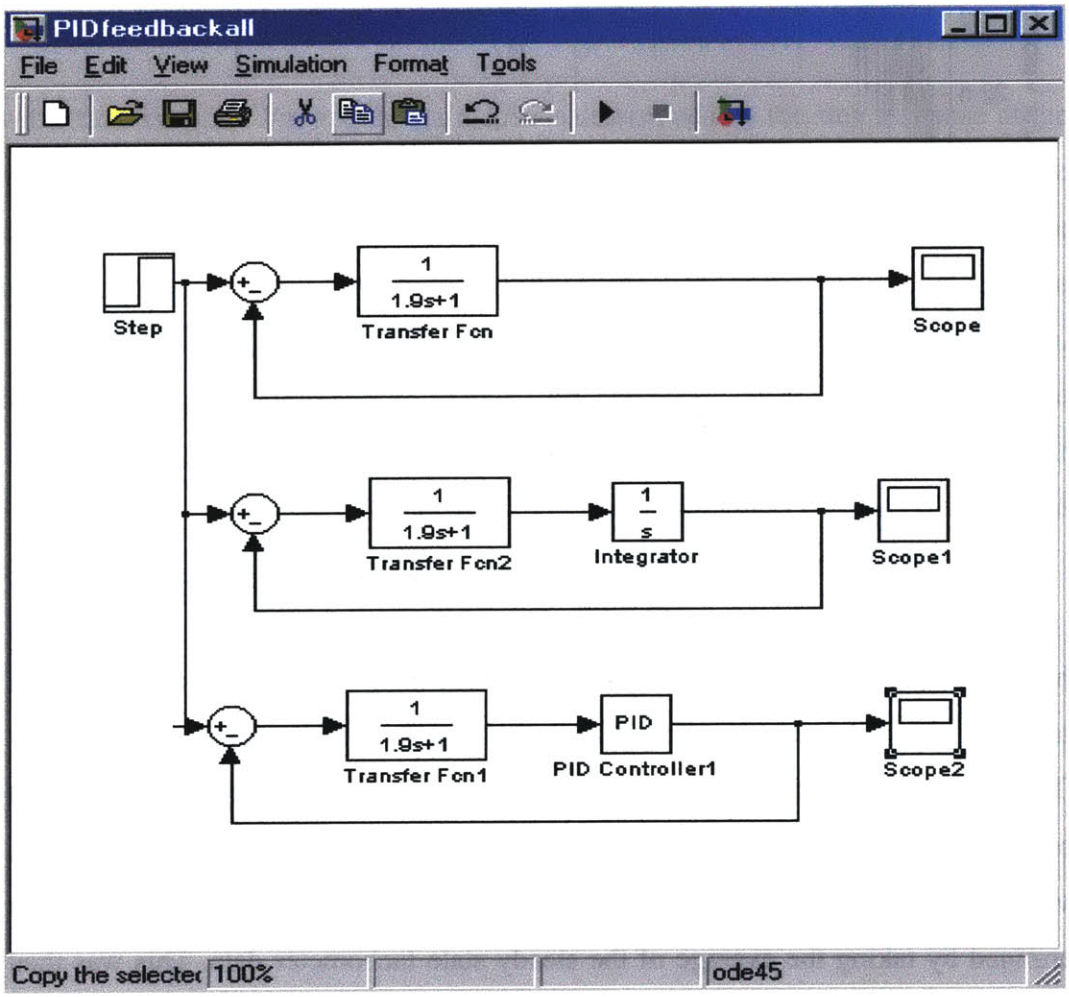

Figure 8.4 Feedback Block Diagrams

8.1.2 Gain and Integrator Time Constant

The characteristic equation for the open loop response is 1+GH = 0. This was used for the root locus plots and the final feedback system, GH/(1+GH) = ω/e, was used in a

simulink simulation to predict potential values for gain K, the integral time constant, Ti, and the derivative time constant, Td. The initial feedback response where H is unity and G is the plant reponse is in Figure 8.5. Schwarzenback and Gill (1984) first recommend a pole at the root locus origin to eliminated the steady state error (Figure 8.6).

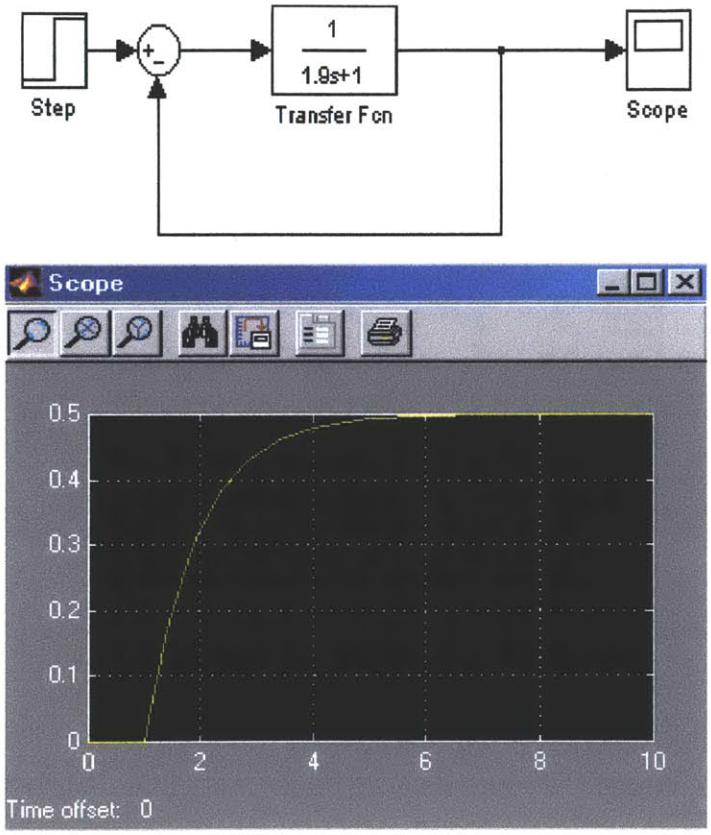

Figure 8.5 System Response with a Steady-State Error of 50 %.

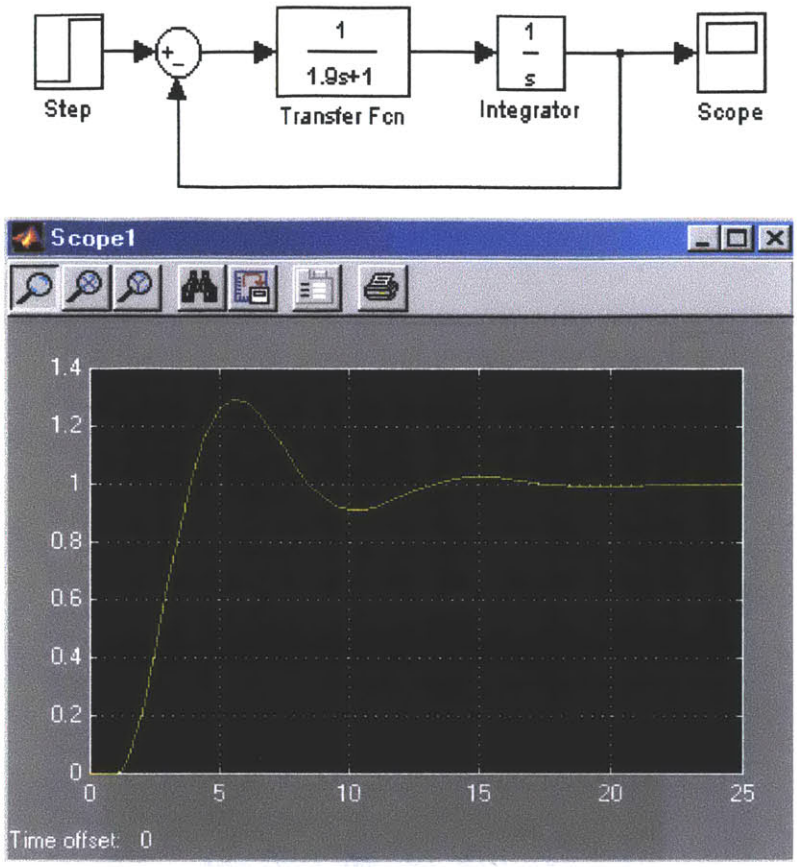

Figure 8.6 Feedback Response After Addition of Integrator

Since noise was an issue and velocity drift errors were more of a concern than high frequency velocity errors, Td was assumed to be near zero. Then the PID was developed for K and Ti. As there was no defined method with which to pick the gain K and integral time constant Ti (Schwarzenbach, et al, 1984), these constants were empirically determined by trial values of K first, then Ti in joint root locus and step response plots. As values of K and Ti were adjusted, the zeros would either pull the system further toward the real axis away from the imaginary axis reduces a periodic response. As these zeros moved around the complex plane, the step response to the closed loop system would develop peak overshoots or slower rise times. K and Ti were maximized to reduce peak overshoot while attaining a fast rise time, and keeping the zeros as far as possible from the right half plane for maximal stability. Plots of ranges

of K, Ti, and Td are in Appendix G. After Ti and K were varied and optimized, the derivative time constant Td was also studied. Any value of Td greater than zero pulled the zeros and the system response toward the imaginary axis, increasing periodic oscillations. It became apparent, however, that for quickest response time and stability, Td is most ideally 0. The response of the maximized response K and Ti were then run through Simulink to examine the response for any missed peak overshoot. The final ideal gain K and Ti were 1.5 and 1 sec., respectively for a tau of 1.9 sec. and were 1.6 and 1.1 sec., respectively for a tau of 1.95 seconds. Primarily, K was chosen to achieve the lowest possible rise time, 1.18-2.25 sec., while minimizing the percent overshoot, 1.47 %. Another factor was considered were the closed loop zeros. The higher the gain, the closer the zeros approach the real axis, which is desired. However, the limiting factor in the feedback response was ultimately the 2 sec. delayed response in the Browning controller box.

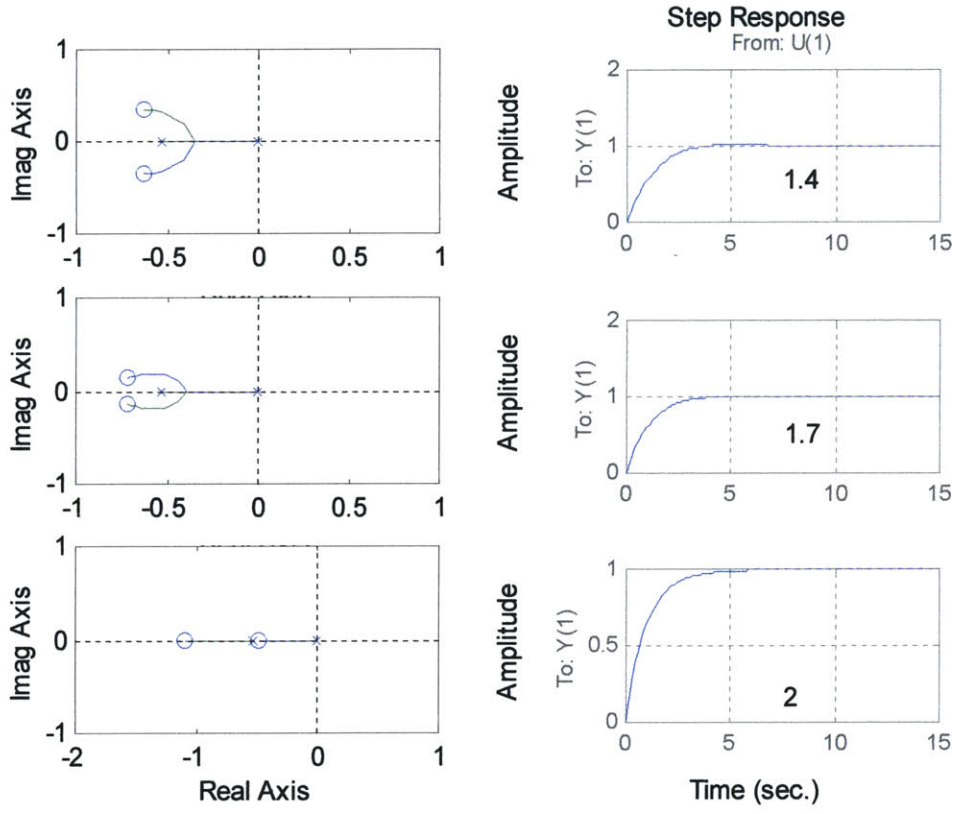

Figure 8.7 Root Locus and Feedback Step Response for Different Value of K, Ti=1 sec.

Since feedback control design is dependent upon the desired resultant response of the feedback system, two methods were approached to determine the two maximal sets of integrator time constant and gain. The first method used the classical theory of aiming for highest rise time with a maximum of 10 percent overshoot. Because the transfer function did not have any roots significantly far from the dominant roots, all poles were considered. After iterations with Matlab trials and observations, the ideal K and Ti were 1.5 sec. and 1.823 sec., respectively. This resulted in the root locus plot of the open loop poles in Figure 8.8 and the closed feedback step response in Figure 8.9. The rise time for this sytem is calculated by the time difference for the system to reach 10% to 90% of the steady state value.

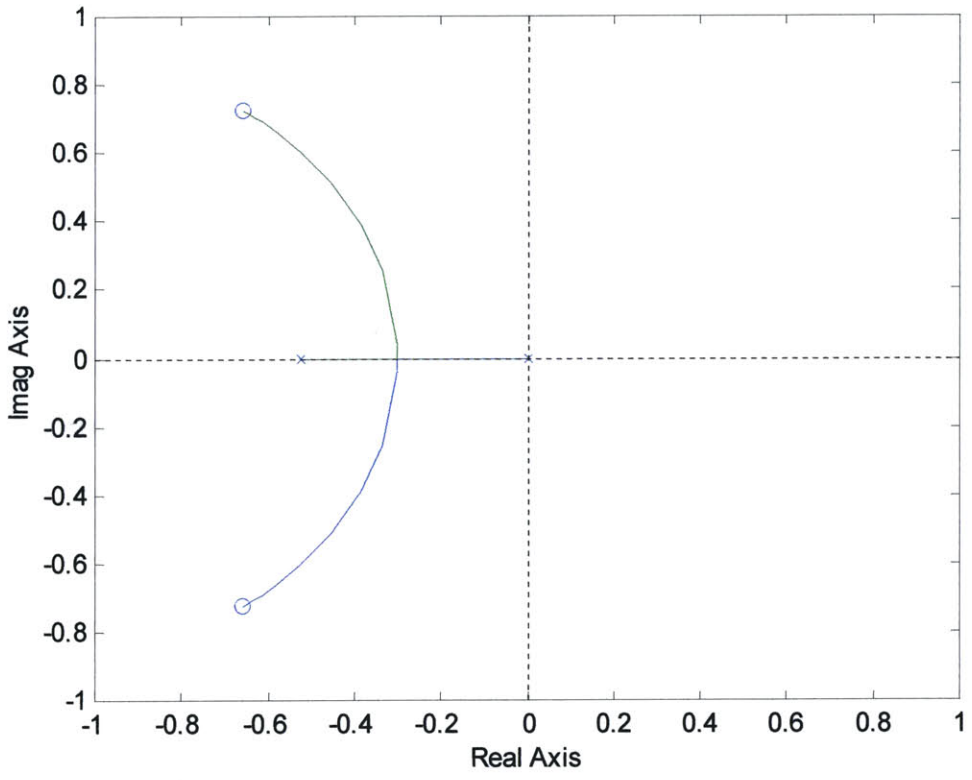

Figure 8.8 Root Locus Plot of Open Loop Poles for K=1.5, Ti=1.823 sec

As is shown, the gain sufficiently pulls the pole response further into the left half plane by the zeros. This extension into the left half plane, further ensures greater stability. Although the zeros also pull the system response further into the imaginary axis, permitting greater periodic response, hence the overshoot of 10 %.

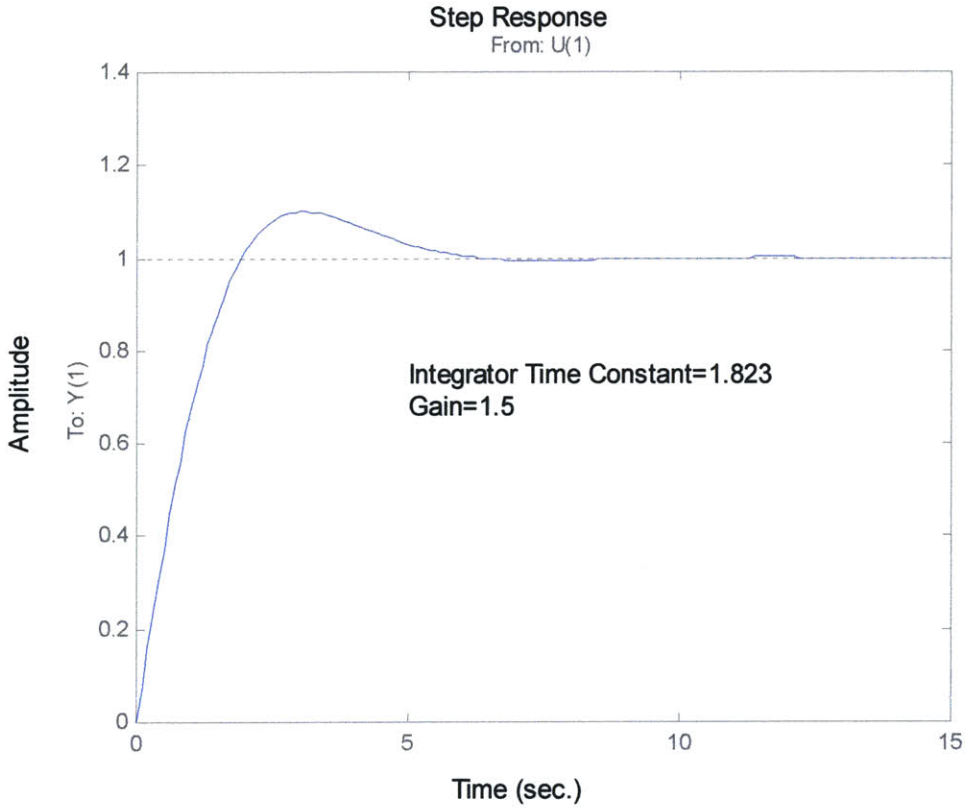

Figure 8.9 Feedback Step Response for K=1.5 and Ti=1.823 sec

This rise time is 1.08 seconds. For this case the natural undamped frequency, the damping ratio, and the system poles were found using Matlab. Here, the damping ratio is nearly the desirable 0.7, also the ideal closed loop system characteristic (Savant, p. 14).

$\omega n = 0.9814$ rad/s damping ratio = 0.6704 system poles = -0.6579 +/- 0.7282i

The other method used computer iterations of trial and error to minimize overshoot while maximizing rise time as described. This value was found at K=1.5 and Ti = 1 sec. The root locus is plotted in Figure 8.10, and the time domain step response for this closed loop system is in Figure 8.11.

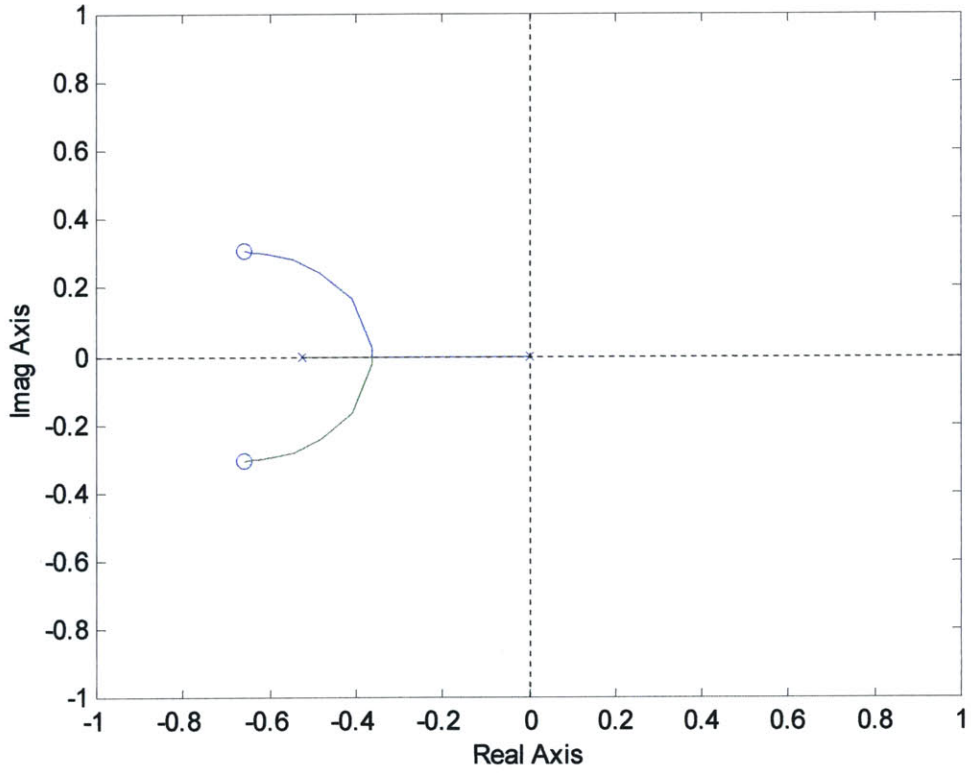

Figure 8.10 Root Locus Plot for Open Loop Poles at K=1.5, Ti=1 sec

With this response the zeros were not as far into the imaginary axis, yet were the same distance from the imaginary axis along the real axis. This maintained stability and reduced the periodic overshoot, but limited the time response of the closed loop system.

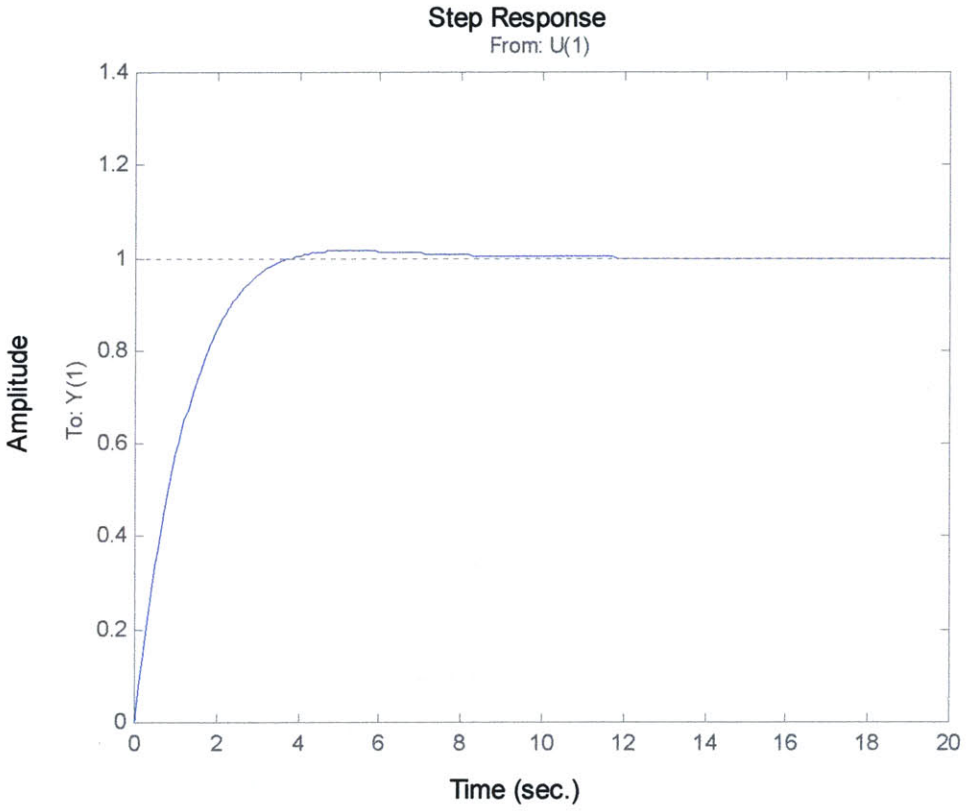

Figure 8.11 Feedback Step Response for K=1, Ti=1 sec.

This response had an overshoot of 1.47 % and had no 2nd overshoot. This rise time was 2.23 sec. Likewise, the natural undamped frequency, damping ratio, and system poles were found. The system poles were exactly the same on the real axis as for when K=1.5 and Ti=1.823 sec.

$\omega n = 0.7255$ rad/s damping ratio = 0.9068 system poles = 0.6579 +/- 0.3058i

By this time, both optical encoder and accelerometer were installed to implement PID control in LabView. It became apparent, however, that it was not possible to neglect the response of the tachometer and processing speed. The PID constants, while relatively comparable for the accelerometer, were very different for the optical encoder.

The PID LabView program for the optical encoder required a little finesse to work around the problem of spikes when the period went to infinity as the angular velocity of the centrifuge approached 0 volts. As mentioned before, the optical encoder at rest was very noisy and unreliable. In fact, the logic of the program was such that an open loop control directed the bed speed up to the desired setpoint. At this point, the PID control was turned on and remained on only during the regulator control. Control reverted back to open loop for the ramp down profile. At this point, PID K and Ti needed to be iterated until the system stabilized with minimum setpoint error. This occurred at K=0.5 and Ti=0.1 sec. The logic in the LabView PID sub-program calls for explanation. Unlike the logic in Matlab for PID, LabView PID used the gain K and multiplied that by Ti, so the effective integrator time constant was in fact K*Ti in LabView. This made Ti equal to 0.05 sec, even smaller and further from the proposed Ti=1 sec. The tachometer data of the PID feedback as measured by the optical encoder is in Figure 8.12. The peak to peak velocity fluctuations for optical encoder regulator feedback were 0.9 rpm. The encoder data, though improved, shows an obvious periodicity that matched the centrifuge rotation. The velocity fluctuations caused by the uneven bearing attachement could not be eleviated by the feedback control even at the slower speed of 10 rpm. The PID encoder control was unable to compensate for the 2 second time delay by the controller.

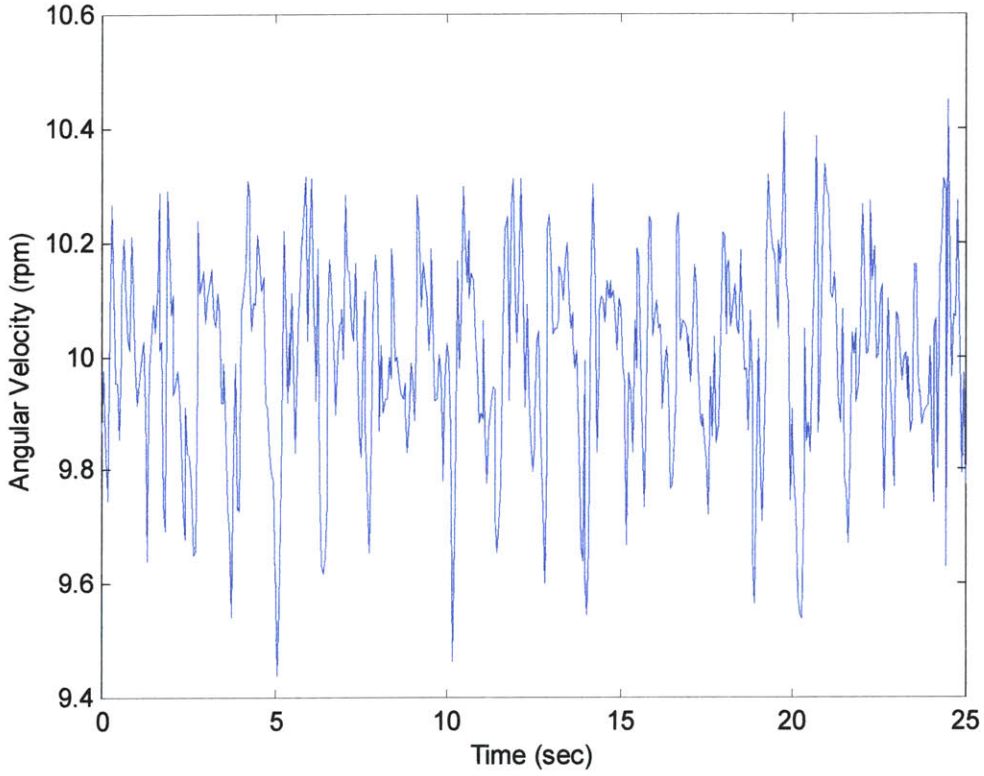

Figure 8.12 Encoder Feedback

Then the LabView PID program for the accelerometer was implemented. The accelerometer scans were possible at any speed, and therefore, did not require sequenced logic like the encoder case. The accelerometer PID permitted a higher gain K than the simulation predicted. Although the loop was closed and the system was stable at K=1.5 and Ti=1 sec., iterations led the optimized system to a gain K = 15 and a Ti=0.07 seconds. Recall, in LabView, Ti is related to the theoretical Ti by K, so actually, the recommended Ti of 1 sec. is about equal to the LabView Ti, Ti*K=1.05 seconds. The tachometer data for accelerometer feedback is in Figure 8.13. The peak to peak velocity fluctuations for accelerometer regulator feedback were 0.8 rpm. Again, the periodic fluctuations are evident, and the bearing-induced velocity disturbance can be located at each lower bound. Although the gain was high and

therefore responds more quickly to the irregularity, the PID accelerometer was unable to correct for the uneven bearing.

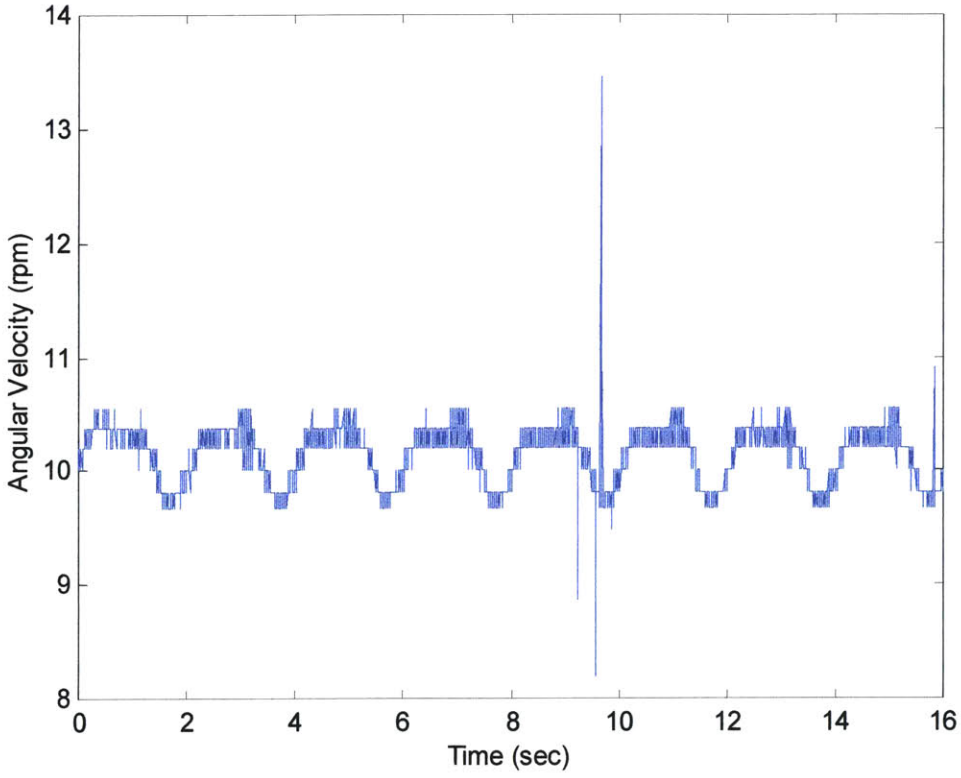

Figure 8.13 Feedback Control with Accelerometer, K=15, Ti=0.7sec

Chapter 9.0

PID Analysis

9.1 Control Analysis

This section will describe the performance analysis of the optical encoder and accelerometer for both the open loop control and the regulator closed feedback control. In light of the initial tachometer, the inverted dc motor, the progression of improved velocity measurements is discussed, the counter measurement of the optical encoder, the analog input of the accelerometer, and finally the digital to analog converter of the optical encoder measurement.

9.1.1 Open Loop Control

The initial inverted dc motor tachometer possessed a great deal of noise in the upper register of analog input. Although the velocity change for an average angular velocity measurement (ω) of 21.46 rpm was $\Delta\omega$=8.6 rpm, the maximum velocity measurement was three times higher than the minimum velocity measurement. The inverted dc motor measured velocity fluctuations of 40.23 % without filtering. It was observed that the actual centrifuge velocity did not vary by this amount. This called for an improved tachometer.

For open loop control, an input control voltage of 3.58 volts drove the centrifuge for an ideal angular velocity of 23 rpm. However, it was soon recognized that the true angular velocity of the centrifuge for a given trial deviated by about 0.5 rpm. The optical encoder used counter period measurements for angular velocity. For an average velocity of 22.16 rpm at a control voltage of 3.58 volts, the measurements ranged from 20.98 rpm to 23.48 rpm. This resulted in a measured velocity accuracy of 11.26 %. Whereas the accelerometer measurements ranged from 21.93 rpm to 23.71 rpm for the same control voltage to produce an average velocity of 22.85 rpm. Here, the measured accuracy is 7.76 %.

The accelerometer open loop accuracy was better than the optical encoder accuracy for several reasons. First, the optical encoder measurement was filtered only by eliminating any anomalous spikes, that is then replaced by the null value. There was more high frequency filtering to the accelerometer measurements. All the filtering was performed before the analog signal was measured from LabView and followed the recommendations of the Analog Devices data sheets. Additionally, as described the accelerometer had the advantage of being isolated from much of the higher frequency vibrations by being attached at the foot of the centrifuge. This resulted in a marked increase of accuracy compared to the optical encoder. Moreover, the LabView optical encoder analog input tools were not designed for real-time angular velocity measurements of high resolution. Attempts were made to maximize the update rate, but buffer capacity limits and limitations in configuring the counter reduced the update rate to at best 10 scans/second.

9.1.2 Closed Loop Control

The encoder feedback control loop improved performance by 10 % from the open loop case. The encoder measurements ranged from 9.45 rpm to 10.46 rpm about an average velocity of 10 rpm, the desired setpoint. The improved accuracy with the encoder feedback was 10.1 % of the setpoint value. This included a low-pass filter of 2 Hz at the data acquisition board.

Again, the accelerometer feedback had improved performance over the open loop and the closed loop encoder. The range for a setpoint of 14.60 rpm was 14.30 rpm to 14.93 rpm. The low-pass 2 Hz filter was also used for the closed loop accelerometer. The accuracy for the closed loop accelerometer was reduced to 4.39 %, an improvement of 43.3 %. The ability to ascertain the desired angular velocity was successful with the feedback control. It became evident that the feedback control could only reduce the magnitude of velocity oscillations, as shown by the improved accelerometer feedback performance over the encoder feedback performance. However, due to the controller response delay of 2 seconds, tighter response of the feedback had little effect. An increased gain resulted in an unstable system.

In open loop control, a desired angular velocity set by fixed control voltage produced an error from the setpoint by 0.5 rpm, whereas with feedback regulator control, steady state errors were on the order of 0.0001 rpm.

9.2 Step Response

The step response for the open loop system is in Figure 9.1. The step input was a magnitude of 1.771 rpm, which deviated from the desired 2.3 rpm set by 23 %. The final steady state value was a change of 2.4 rpm to 23.7 rpm. At any given run, the open loop voltage control resulted in an angular velocity may range within 0.5-1 rpm. The actual desired step input was 2.3 rpm. The actual step error between the setpoint, the control input, and the steady state value was within this open loop error.

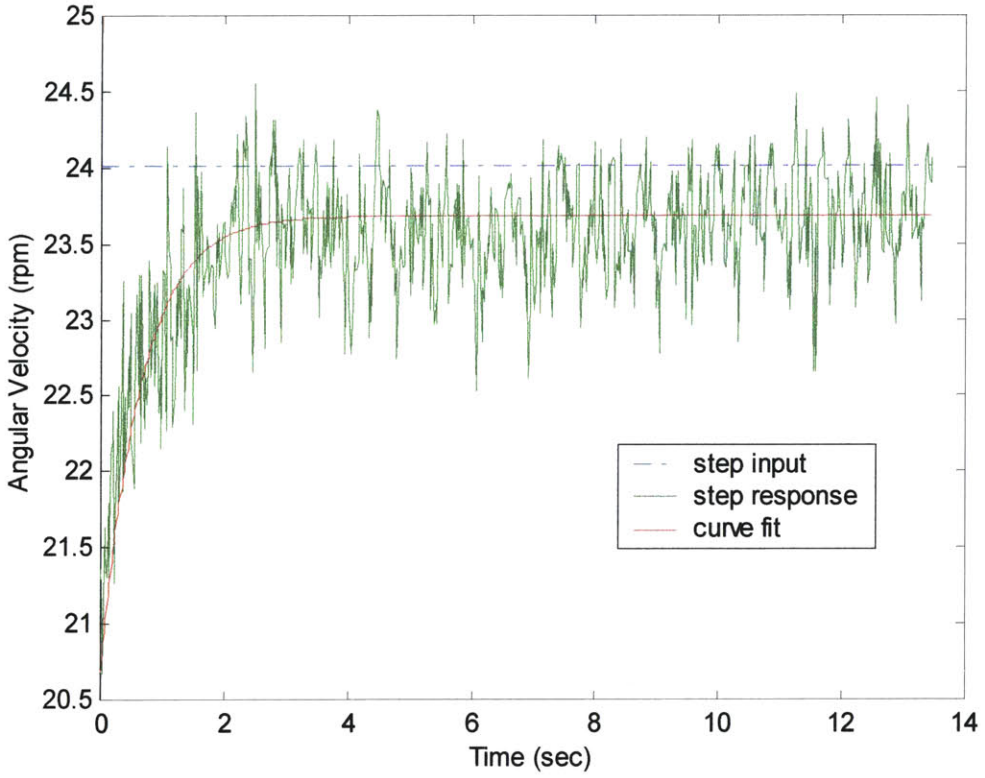

Figure 9.1 Open Loop Step Response

With the feedback control, the step response is shown in Figure 9.2. The desired setpoint, resultant input step, and recorded angular velocity were more agreeable. The desired step input was from 21.85 rpm to 24.15 rpm. The measured mean angular velocity as measured by the accelerometer was 21.8466 rpm to 24.1386 rpm. The step error was 0.35 % and the steady state error was 0.04 %.

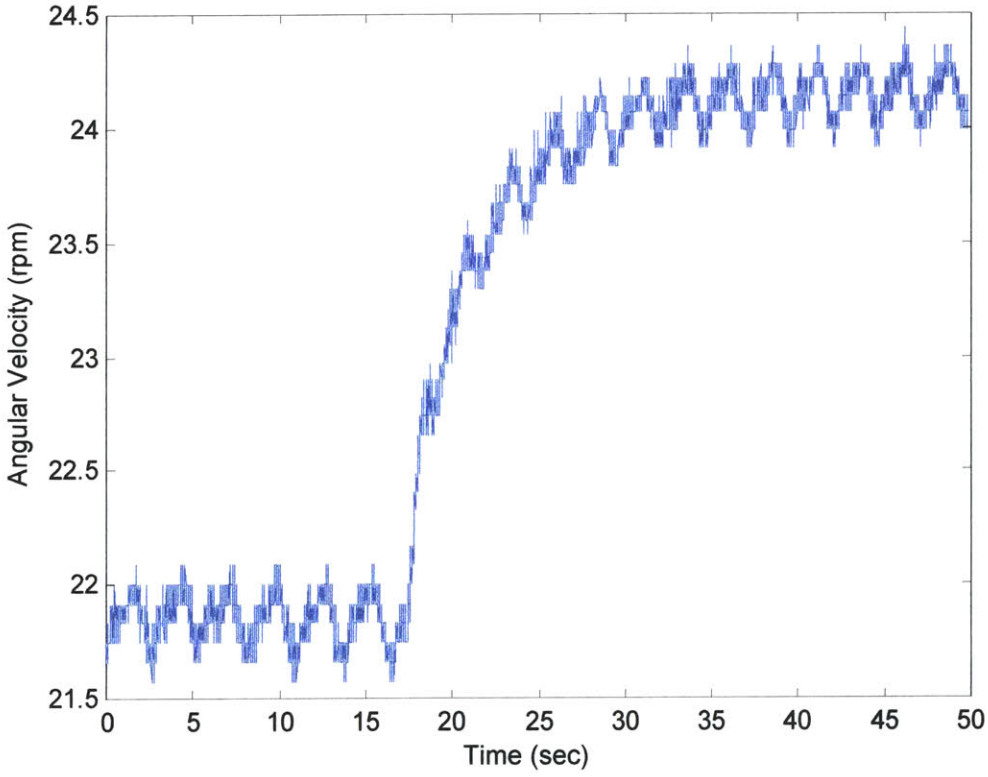

Figure 9.2 Feedback Step Response

An exponential curve fit of the feedback response was performed. The response, though in block diagram form is second order. It looks like for 1% velocity changes about the operating point, the behavior is linear. Therefore, a curve fit of A(1-exp(-t/ τ)) would suffice. Using the same process as described in Section 8.1.1, the time constant τ was found to be 3.2 sec (Equation (9.1)). This is 32.5 % longer than the

open loop response time . The response time may be considerably longer, however, the accuracy of reaching the steady state response is acceptable.

$$y = 2.3\left(1 - e^{\frac{-t}{\tau}}\right) \tag{9.1}$$

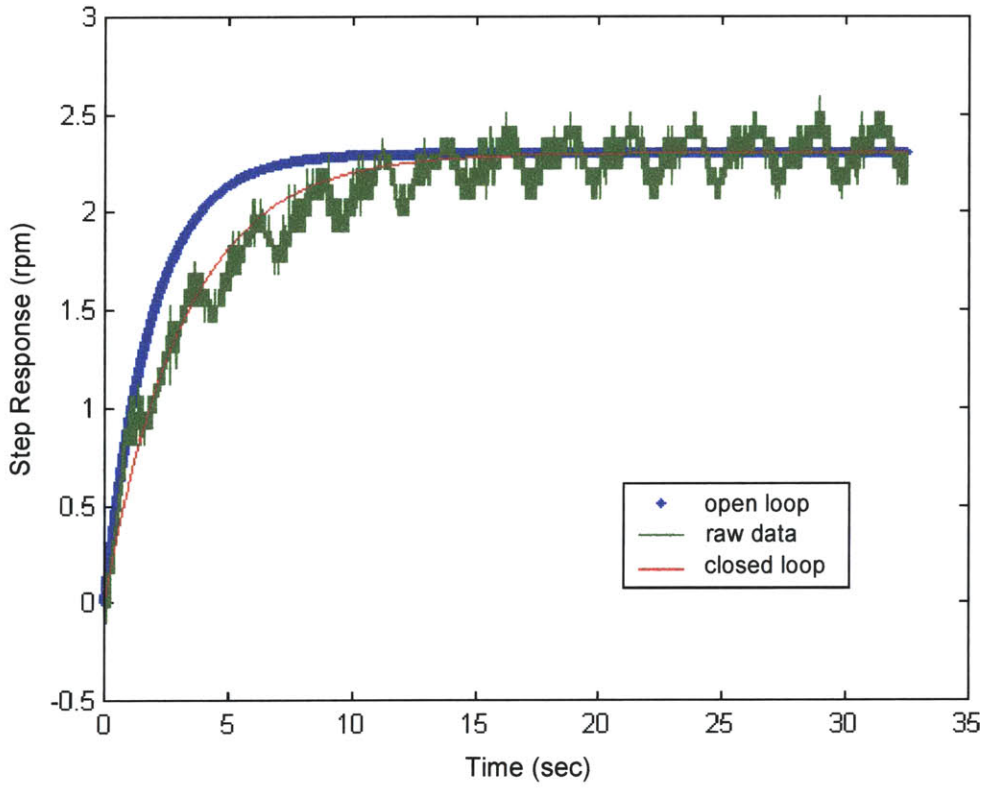

Figure 9.3 Curve Fit to the Closed Loop Step Response and the Open Loop Curve Fit

9.3 Open and Closed Loop Standard Deviation

The standard deviation, root mean square, and mean values were calculated for both the accelerometer and optical encoder for open and closed loop control (Barlow, 1989). The methods used to calculate these values are in Equations (9.2), (9.3), and (9.4).

$$\text{mean} = \frac{1}{N}\sum_{i}^{N} x_i \tag{9.2}$$

$$s = \sqrt{\frac{\sum_{i}(x_i - \bar{x})^2}{N-1}} \tag{9.3}$$

$$\text{root mean square} = \sqrt{\frac{\sum_{i} x_i^2}{N}} \tag{9.4}$$

Tachometer	Mean	Std Dev	% Deviation from Mean	RMS
Encoder (Open)	22.853 rpm	0.8267 rpm	7.235 %	22.867 rpm
Accelerometer (Open)	22.845 rpm	0.1962 rpm	1.718 %	22.846 rpm
Encoder (Closed)	9.9952 rpm	0.1732 rpm	3.466 %	9.9967 rpm
Accelerometer (Closed)	14.596 rpm	0.1183 rpm	1.621 %	14.5965 rpm
Analog Encoder (Open*)	10.7257 rpm	0.0722 rpm	1.346 %	10.7259 rpm
Accelerometer (Open*)	10.7274 rpm	0.3681 rpm	6.863 %	10.7336 rpm

Table 9.1 Accuracy Performance of Open and Closed Loop Tachometers

The data is expressed in Table 9.1. The percent deviation from the mean value was also determined. It was calculated by the 2 standard deviation lengths over the mean divided by the mean. The improvement of accuracy by use of closed loop control opposed to open loop control was a disappointingly -5.65 % for accelerometer measurements but was much higher for optical encoder measurement; a 52.1 % improvement for the maintaining the angular velocity response to the desired setpoint. This larger improvement by the encoder can be attributed to the relatively higher deviations from the mean value for the open loop case. It is worth emphasizing that the use of feedback control has closed the steady state error down to 0.0001 rpm at least for both the encoder and accelerometer.

It can been seen in Table 9.1 that the accelerometer compared to the encoder generally performed better. The closed loop control did converge the standard deviations closer

to zero. A closed loop effectively did not produce significant advantages to reducing velocity fluctuations down to a level of 1.5 % for the case of accelerometer measurements. This may be limited by the feedback response time being in inhibited by the 2 sec response delay of the controller.

Moreover, the best performance was seen by the analog encoder with open loop control. It was noteworthy that the last two entries, the analog encoder and the accelerometer for the same run (*). The analog encoder refers to the current configuration of the encoder, in which the output of the encoder was processed into an analog signal and was then similarly read into LabView like the accelerometer. The difference in this case was the standard deviation for the analog encoder was considerably reduced. However, this may not be due to true angular velocity representation but to a great deal of high and low frequency on-board filtering when converting from the digital to analog signal.

9.4 Recommendations for Future Work

For a marked improvement in the feedback response of the centrifuge, direct torque control of the motor is recommended. The controller, although suited with a number of excellent safety mechanisms, severely limits the ability to control the angular velocity of the centrifuge. Without the controller, safety mechanisms would need to be installed, but direct torque control would permit the experimenter to have full control of the speed profile of the bed without unavoidable response lags.

The potential for an optical encoder to accurately and precisely measure the angular velocity of the centrifuge was not fully realized in this work. Counter software prevented data rate scans at a rate high enough to be used for a PID. LabView Real-Time for Windows a tool that mitigate this issue, where a devoted processor is used exclusively for data acquisition and hardware control. In this way, other operations like mouse movement and file writing do not require processor speed during centrifuge operation. Also, improved counter algorithms where the counter is not intialized at each loop would enhance the speed of the program considerably.

One primary recommendation to remove the periodic disturbances to the centrifuge is to dismantle the centrifuge, clean the bearings, and reassemble the centrifuge with particular attention to the attaching the bed balanced onto the bearing. Currently, the bed is attached to the bed so unevenly, the centrifuge cannot be adequately balanced. This leads to vertical displacements at the foot of the centrifuge as well as periodic velocity disturbances. Conducting a rebalance of the bed on the bearing would eliminate the periodic angular velocity fluctuations that the feedback control loop is unable to remedy. Especially if experiments where squats exercises would be performed, not balancing the bed on the bearing would result in larger vertical sway displacements of the foot of the bed.

Because there are currently two functional tachometers on the centrifuge, it would be useful to integrate the velocity measurements of each to produce a more accurate reading with higher fidelity. An algorithm for using both readings would need to be developed in LabView. Resolving the two tachometer measurements into one angular velocity measurement, though requiring some computations, would complement each other. The accelerometer is more suitable for low frequency fluctuations while the optical encoder is better suited to higher frequency velocity measurements.

Chapter 10.0

Conclusion

My work on the artificial gravity project was unique in that both an experiment and technical equipment upgrades were performed. Hopefully both will further the prospect of artificial gravity as a suitable and realistically implementable countermeasure.

The Large N study meant to answer the question whether the perceptions of illusory tilt caused by head movements while rotating are not completely predicted by the idealized semicircular canal model. The results show that the canal model, though accurate for a majority of the population, still do not represent all illusory tilt sensations for the entire population. About 12 % of subjects felt illusory tilt in an unpredicted plane while up to 60% of subjects felt a compensatory illusory tilt in the same, unpredicted plane as the pitch head movement. It is speculated that this deviation from the predicted canal model may be explained by structural canal asymmetries and therefore, asymmetric afferent firing responses that become confused during the coriolis cross-coupling stimulus.

Although feedback control of the short-radius centrifuge was not able to lower the angular velocity peak-to-peak fluctuations by 1 %, direct torque control, without the 2 sec response delay, would remedy this issue. However, with the current tachometer equipment and LabView feedback control of the centrifuge, the feedback response still improved the open loop system by 96% compared to the initial tachometer and controller design.

References

1 http://www.hq.nasa.gov/office/nsp/hedsroad.htm, May, 2000.

2 Young, L. R., "Artificial Gravity Considerations for a Mars Exploration Mission," Annals of the New York Academy of Sciences, Vol. 871, May 1999, pp. 367-378.

3 Landauer, J. A., and Burke, T. J., "A Proposed Cause for and Prevention of Bone and Muscle Wasting in Microgravity," Aviation, Space, and Environmental Medicine, Vol. 69. No. 7, July 1998, pp. 699-702.

4 Riley, D. A., Ellis, S., Slocum, F. R., Sedlack, F.R., Bain, J.L., Krippendorf, B. B., Lehman, C. T., Macias, M. Y., Thompson, J. L., Vijayan, K., "In-flight and Post-flight Changes of Skeletal Muscles of SLS-1 and SLS-2 Spaceflown Rats," Journal of Applied Physiology, Vol. 81, No. 1. July 1996, pp. 133-144.

5 Tipton, C. M., Sebastian, L. A., "Dobutamine as a Countermeasure for Reduced Exercise Performance of Rats Exposed to Simulated Microgravity," Journal of Applied Physiology, Vol. 82, No. 5, May 1997, pp. 1607-1615.

6 Oman, C. M., "Sensory Conflict in Motion Sickness: An Observer Theory Approach," In NASA, Ames Research Center, Spatial Displays and Spatial Instruments, p. 15, N90-22918 16-54.

7 Bucky, J. C. Jr., "Preparing for Mars: The Physiologic and Medical Challenges," European Journal of Medical Research, Vol. 4, 1999, pp. 353-356.

8 Wimalawansa, S. M., Chapa, M. T., Wei, J. N., Westlund, K. N., Quast, M. J., Wimalawansa, S. J., "Reversal of Weightlessness-Induced Musculoskeletal Losses with Adrogens - Quantification by MRI," Journal of Applied Physiology, Vol. 86, No. 6, June 1999, pp. 1841-1846.

9 Purdy, R. E., Duckles, S. P., Krause, D. N., Rubera, K. M., Sara, D., "Effect of Simulated Microgravity on Vascular Contractility," Journal of Applied Physiology, Vol. 85, No. 4, Oct. 1998, pp. 1307-1315.

10 Watenpaugh, D. E., Smith, M. L., "Human Cardiovascular Acclimation to Microgravity," Annual International Gravitational Physiology Meeting, 19th, Rome, Italy, May 31-June 5, 1998, Proceedings, A99-28501 07-51, Journal of Gravitational Physiology, (1077-9248), Vol. 5, No. 1, July 1998, pp. P-15 to P-18.

11 Tallarida, G., Peruzzi, G., Castrucci, F., Raimondi, G., Legramante, J. M., Cassarino, S., Jellamo, F., Di Nardo, P., "Dynamic and Static Exercises in the Countermeasure Programmes for Musculo-Skeletal and Cardiovascular Deconditioning in Space," International Union of Physiological Sciences Commission on Gravitational Physiology, Annual Meeting, 12th, Leningrad, USSR, Oct. 14-18, 1990, Physiologist, Supplement , Vol. 34, No. 1, Feb. 1991, p. S-114-S-117.

12 Snow, L. Dale., "Dextroamphetamine: a Pharmacologic Countermeasure for Space Motion Sickness and Orthostatic Dysfunction," In Louisiana Tech Univ., National Aeronautics and Space Administration (NASA)/American Society for Engineering Education (ASEE) Summer Faculty Fellowship Program, 1995, p 23-1 - 23-13,

NASA Technical Report N96-34217 12-99.

13 Pecaut, M. J., Simske, S. J., Fleshner, M., Zimmerman, R. J., "The Effects of Spaceflight and Insulin-like Growth Factor-1 on the T-cell and Macrophage Populations," Space Technology & Applications International Forum - Conference on Applications of Thermophysics in Microgravity, 1st and Conference on Commercial Development of Space, 2nd, Albuquerque, NM, Jan. 26-30, 1997, Proceedings, Pt. 2 (A97-26032 06-12), Woodbury, NY, AIP Press, AIP Conference Proceedings, No. 387, 1997, pp. 907-913.

14 Chapes, S. K., Forsman, A. D., Simske, S. J., Bateman, T. A., Zimmerman, R. J., "Effects of Space Flight and IGF-1 on Immune Function," Life Sciences: Microgravity Research I; Proceedings of the F1.1, F1.2, F1.3 Symposia of COSPAR Scientific Commission F, 32nd COSPAR Scientific Assembly, Nagoya, Japan, July12-19, 1998. A00-12304 01-51, Advances in Space Research (0273-1177), Vol. 23, No. 12, 1999, pp. 1955-1964.

15 "Biological Bases of Space Radiation Risk", 12th Man in Space Symposium: The Future of Humans in Space, NASA Technical Report 19980024368.

16 Ohnishi, T., Wang, X., Fukuda, S., Takahashi, A., Ohnishi, K., Nagaoka, S., "Induction of p53-Dependent Signal Transduction by Low Dose Radiations or Space Environment," IAF, International Astronautical Congress, 49th, Melbourne, Australia, Sept. 28-Oct. 2, 1998.

17 Cowings, P., "Autogenic Feedback Training Experiment: A Preventative Method for Space Motion Sickness," In NASA, Marshall Space Flight Center, Spacelab J Experiment Descriptions, pp. 227-248. N94-13732 02-29.

18 Dickman, D. J., "Otolith-Canal Convergence in Vestibular Nuclei Neurons," NASA Technical Report 19980031512.

19 Burton, R.R., and Meeker, L.J., "Physiologic Validation of a Short-Arm Centrifuge for Space Application," Aviation, Space and Environmental Medicine, June, 1992. pp. 476-481.

20 Lackner, J. R., DiZio, P., "Sensory Motor Coordination in an Artificial Gravity Environment," Journal of Gravitational Physiology, Vol (4) 2, 1997, pp. p-9-p-12.

21 Benson, A. J., Guedry, F. E., Parker, D. E., and Reschke, M. F. "Microgravity Vestibular Investigations: Perception of Self-Orientation and Self-Motion," Journal of Vestibular Research, Vol. 7, No. 6, 1997, pp. 453-457.

22 Young, L. R., "Perception of the Body in Space: Mechanisms," Chapter 22 of Handbook of Physiology: The Nervous System III, Williams & Wilkins, Bethesda, 1977, pp. 1023-1066.

23 Peters, Richard. "Dynamics of the Vestibular System and their Relation to Motion Perception, Spatial Disorientation, and Illusions," 1969, NASA CR-1309, Technical Report No. 168-1.

24 Pancratz, D. J., Bomar, J. B. Jr., Raddin, J. H. Jr., "Modeling Platform Dynamics and Physiological Response to Short Arm Centrifugation." AL/CF-TR-1994-0025, N95-

20457.

25 Lyne, L., "Artificial Gravity: Adaptation to Head Turns During Short-Radius Centrifugation Using Subjective Methods," M.S. Thesis, MIT, 2000.

26 Sienko, K., "Artificial Gravity: Adaptation of the Vestibular-Ocular Reflex to Head Movements During Short-Radius Centrifugation," M.S. Thesis, MIT, 2000.

27 Ernsting, J., Nicholson, A., Rainford, D., Aviation Medicine, 3rd Edition, Linacre House, Oxford, 1999, pp. 419-446.

28 Meiry, J. L., "The Vestibular System and Human Dynamic Space Orientation," Sc.D. Thesis, MIT, 1965.

29 Van Egmond, A. A. J., Groen, J. J., and Jongkees, L. B. W., "The Mechanics of the Semicircular Canals," Journal of Physiology, Vol 110, 1949, pp. 1-17.

30 Groen, J. J., "Problems of the Semicircular Canals from a Mechanico-Physiological Point of View," Acta Oto-Laryngology, Supplement, Vol. 163, 1960, pp. 59-67.

31 Jones, G. M., Barry, W., and Kowalsky, N., "Dynamics of the Semicircular Canals Compared in Yaw, Pitch and Roll," Aerospace Medicine, Vol. 35, No. 10, October 1964, pp. 984-989.

32 Graybiel, A., "Space Missions Involving the Generation of Artificial Gravity," Environmental Biology and Medicine, 1973, Vol. 2, pp. 91-138.

33 Berthoz, A., Grandt, T., Dichgans, J., Probst, T., Bruzek, W., and Vieville, T. "European Vestibular Experiments on the Spacelab-1 Mission: 5. Contribution of the Otoliths to the Vertical Vestibulo-ocular Reflex." Experimental Brain Reserach, Vol. 64, 1986, pp. 272-278.

34 Diamandis, P., "The Artificial Gravity Sleeper: A Deconditioning Countermeasure for Long Duration Space Habitation," M.S. Thesis, MIT, February, 1988.

35 Biaggioni, I., Cost, F., and Kaufmann, H., "Vestibular Influences on Autonomic Cardiovascular Control in Humans," Journal of Vestibular Research, Vol. 8, No. 1, 1998, pp. 35-41.

36 Convertino, V., "Interaction of Semicircular Canal Stimulation with Carotid Baroreceptor Reflex Control of Heart Rate," Journal of Vestibular Research, Vol. 8, No. 1, 1998, pp. 43-49.

37 de Graaf, B., Bos, J. E., Tielemans, W., Rameckers, F., Rupert, A. H., and Guedry, F. E., "Otolith Contributions to Ocular Torsion and Spatial Orientation During Acceleration." NAMRL 96-3, NASA Technical Report 19970021712.

38 Mittelstaedt, H. and Glasauer, S. "Crucial Effects of Weightlessness on Human Orientation." Journal of Vestibular Research, Vol. 3, 1993, pp. 307-314.

39 Hofstetter-Degen, K., Wetzig, J., and Von Baumgarten, R. J. "Oculovestibular Interactions Under Microgravity," Journal of Clinical Investigation, Vol. 71, 1993, pp. 749-756.

40 Dizio, P., Lackner, J. R., "Motion Sickness Susceptibility in Parabolic Flight and

Velocity Storage Activity," Aviation, Space, and Environmental Medicine, Vol. 62, April 1991, pp. 300-307.

41 Lackner, J., "Orientation and Movement in Unusual Force Environments," Psychological Science, Vol. 4, No. 3, May 1993, pp.134-142.

42 Reason, J. T. and Graybiel, ., "Magnitude Estimations of Coriolis Sensations". NASA-CR-106389, N69-41174.

43 Guedry, F. E., Rupert, A. H., McGrath, B. J., Oman, C. M. "The Dynamics of Spatial Orientation During Complex and Changing Linear and Angular Acceleration." Journal of Vestibular Research, Vol. 2, 1992, pp. 259-283.

44 de Graaf, B, Bos, J. E., Goen E., Tielemans, W., Rameckers, F., Clark, J.B., Mead, A.M. and Guedry, F. E. "Otolith Responses During Centrifugation Along Three Axes of Orientation," NAMRL-1402, NASA Technical Report 1998-223934.

45 Grissett, J. D. Mathematical Model for Interaction of Canals and Otoliths in Perception of Orientation, Translation, and Rotation. NASA NAMRL Special Report 93-5, NASA Technical Report N95-16151.

46 Clark B., Graybiel A., "Factors Contributing to the Delay in the Perception of the Oculogravic Illusion," American Journal of Psychology, 1966, Vol. 79, pp. 377-388.

47 Hastreiter, D., "Artificial Gravity as a Countermeasure to Spaceflight Deconditioning: The Cardiovascular Response to a Force Gradient," S.M. Thesis, MIT, June, 1997.

48 Tomassini, A. M., "The Effect of Coriolis Forces on Performance of Two-Handed Tasks," S.M. Thesis, MIT, 1997.

49 Groen, J. J. and Jongkees, L. B. W., "The Threshold of Angular Acceleration Perception." Journal of Physiology, Vol. 107, 1948, pp. 1-7.

50 Savant, C. J. Jr., Control System Design, McGraw-Hill, New York, 1964, pp. 9-15, 95-96.

51 Schwarzenbach, J. and Gill, K. F., System Modelling and Control, 2nd Edition. London, Edward Arnold, 1984. pp. 152-189.

52 Barlow, R.J., Statistics: A Guide to the Use of Statistical Methods in Physical Sciences, John Wiley & Sons, New York, 1989, pp. 7-11.

Appendix A

Experimental Consent and Medical Consent Form

MASSACHUSETTS INSTITUTE OF TECHNOLOGY
MAN-VEHICLE LAB
CONSENT FORM

I have been asked to participate in a study on adaptation to movement in a rotating environment. I understand that participation is voluntary, and that I may end my participation at any time for any reason. I understand that I should not participate in this study if I have any heart or respiratory conditions, if I have medical conditions, which could be triggered if I develop motion sickness, if I am taking prescribed antidepressants or barbiturates, or if there is the possibility that I may be pregnant. I agree not to consume any alcoholic beverages the day of testing and to avoid caffeine.

My participation as a subject on the MIT Artificial Gravity Simulator (AGS) involves either testing of equipment or actual experimental trials. Prior to rotation, I will be oriented to the AGS and all monitoring equipment. During rotation I have to make 24 head movements; right ear down (4*), right ear up (4*), left ear down (4*), left ear up (4*), head up (4*) and head down (4*). I will answer the following questions after each head movement:

Q: What did you experience?
Q: Are you tilted? head up or down?
Q: Do you feel other body motions?
Q: Where are your feet pointing?
Q: Motion sickness grade?

My rotation on the AGS will not exceed the following parameters:

- onset rate of no greater than 1 rpm/s
- G level at my feet no greater than 1.5 G
- time of rotation not exceeding 20 minutes
- the bed rotates at 23 revolutions per minute
- the head will move at approximately a speed of .25 meters per second.

I understand these are well within the safe limits for short-radius rotation. I can end rotation at any time by pressing the stop button, the use of which has been demonstrated to me.
I understand that during rotation I may feel a headache or pressure in my legs caused by a fluid shift in the body due to centrifugation. I may also feel nausea or motion sickness, especially as a result of the required head movements.
I understand that serious injury could result form falling off the AGS while it is rotating. I will be loosely restrained at around the abdomen. The restraint is equipped with quick release latches making it possible to escape quickly, if necessary. If I sit up, these latches will be released. In addition, the AGS is equipped with side railings similar to those on a hospital stretcher.
I will be continuously monitored by at least one experimenter in the same room.The investigator checks me during the experiment through a video camera mounted on the AGS.
In the unlikely event of physical injury resulting from participation in this research, I understand that medical treatment will be available from the MIT Medical Department, and that my insurance carrier may be billed for the cost of such treatment. I further understand that making such medical treatment available does not imply such an injury is the investigator's fault. (Further information may be obtained by calling the Institute's Insurance and Legal Affairs Office at 253-2822.)
I understand that I may also contact the Chairman of the Committee on the Use of Humans as Experimental Subjects, H. Walter Jones, Jr. M.D. (E23-389, 253-6787), if I feel I have been treated unfairly as a subject.
I have been informed as to the nature and purpose of this experiment as well as the risks involved. I agree to participate in the experiment.

Subject _____ Date _____

Experimenter _____ Date _____

Medical Consent Form

The subject confirms not to have one of the following problems or diseases:

- Frequent or severe headache
- Dizziness or fainting spells
- Paralysis
- Epilepsy
- Disturbances in consciousness
- Loss of control of nervous system functions
- Neuritis
- Loss of memory or amnesia
- Ear, nose or throat trouble
- Hearing loss
- Chronic or frequent colds
- Head injury
- Asthma
- Shortness of breath
- Pain or pressure in the chest
- Medication (check for sedatives, anti-dizziness, anti-depressants; birth prevention medication is allowed)
- Substance dependence or abuse (includes alcohol, and drugs like sedatives, anxiolytics cocaine, marijuana, opioides, amphetamines, hallucinogens or other psychoactive drugs or chemicals)
- Diagnosis of psychosis, bipolar disorder or severe personality disorders
- Heart problems (check for Angina pectoris, coronary heart disease, congenital heart disease, myocardial infarction in the past, cardiac valve replacement, pacemaker
- High or low blood pressure
- Recent loss or gain of weight
- Moderate car, train, sea or air sickness
- Thyroid trouble

Questions:

1) Handedness:
2) Sleep quality recent weeks before experiment:
3) Have you ever had an ear infection? When?
4) What kind of sports do you do? (flying, diving) please list all
5) Dominant: Right/ Left Eye (please ask if you don't know)
1) Vision: glasses/ lenses/ non
   Prescription: left: Right:

Subject's name:
Birthdate:
Height:
Weight:
Signature

Date:

Appendix B

Large N Questionaire

Communicating the direction and magnitude of illusory or perceived motions accurately is crucial to successful data collection. A conventional language was developed and explained to subjects for the experiment.

To describe perceived illusory tilt in response to head movements made in the rotating environment, motions to describe the 3-axis space are described below. They were requested to accompany the description of the perceived direction with a magnitude estimation in degrees or revolutions.

For Pitch: Tumbling forward or backward for a constantly increasing angular motion

Tilt head up or head down for a fixed angular displacement

For Roll: Feet to the right or left

For Yaw: Spinning to the right or left

To describe perceived pitch tilt without making head movements in response to the increased gravito-inertial force detected by the otolith system, they were asked, "Are you tilted right now?" and were instructed to respond with, "no", "head up", or "head down" with a degree estimation.

To describe orientation in the room, subjects were asked the question, "Where are your feet pointed?" and they could answer anywhere in the room where their anchoring orientation points were the four sides of the room, described by their defining characteristics, "Hallway, Blackboard, Moon, or You (experimenters)". We were careful to inform them that it was equally possible for them not to feel oriented at all.

To describe their state of motion sickness, a motion sickness self assessment score of 0 to 20 was used, where 0 meant "I feel fine" and 20 meant "I have to vomit". These self perceived assessments were communicated verbally.

Appendix C

Eye Dominance Plots for Roll and Pitch

The plots below are for left eye dominant subjects (N=7) and right eye dominant subjects (N=13).

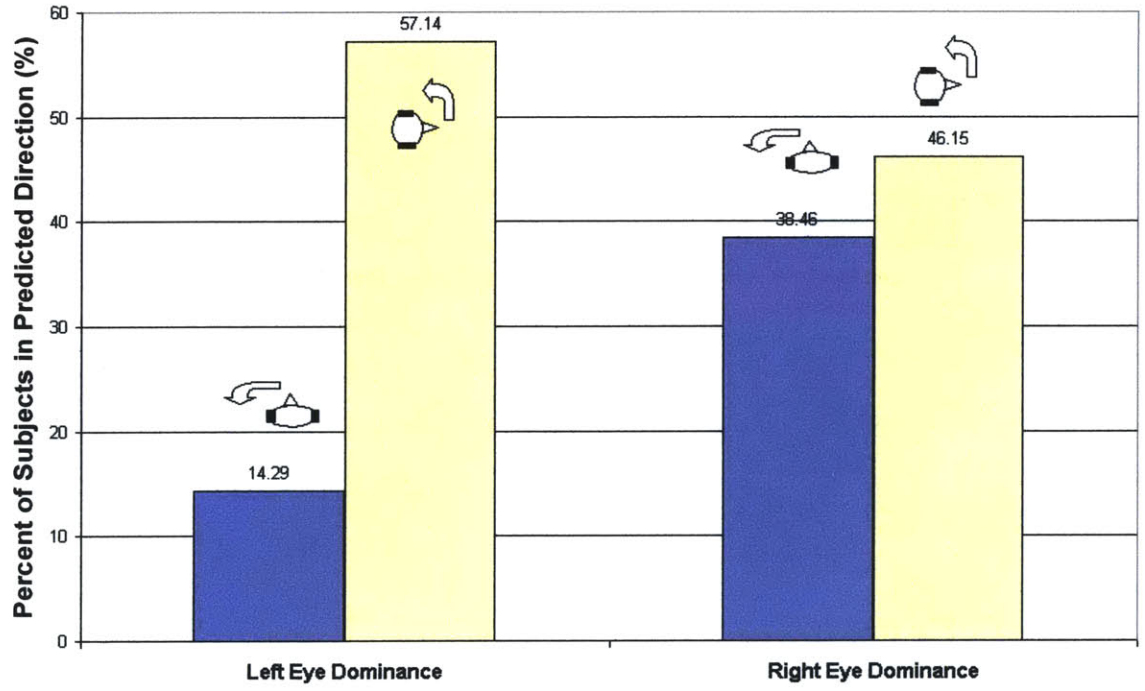

The figure above shows the percent of subjects with the predicted roll direction for counterclockwise head movements between subjects with left eye dominance and subjects with right eye dominance.

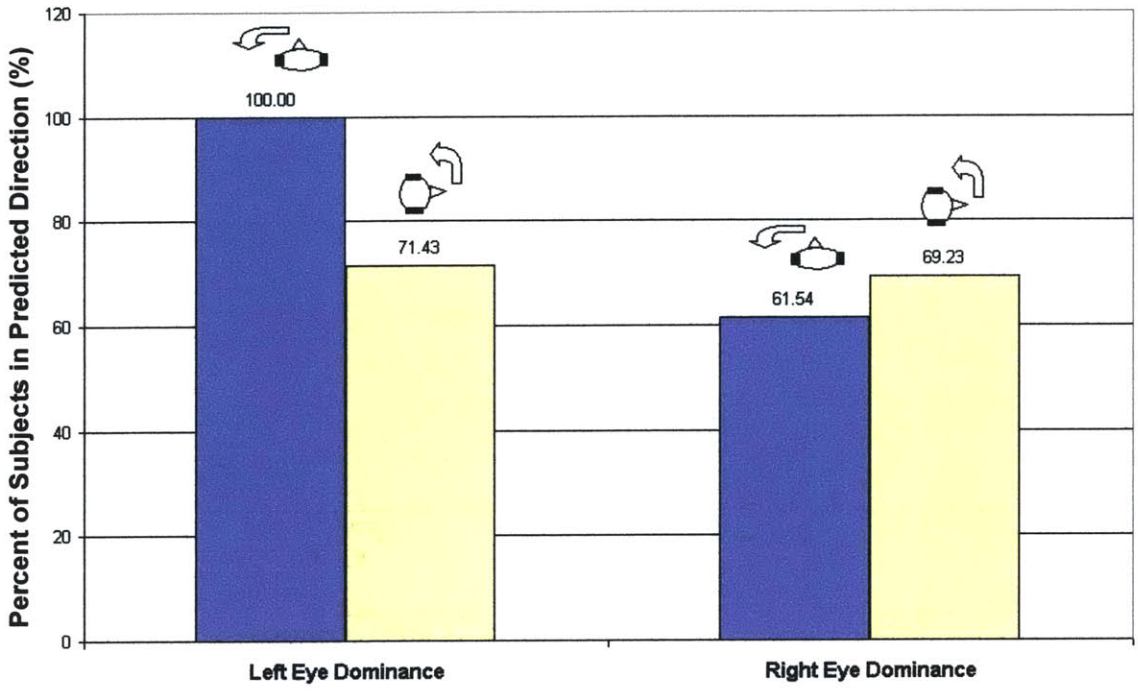

This figure shows the percent of predicted pitch directions for counterclockwise head movements between subjects with left eye dominance and subjects with right eye dominance.

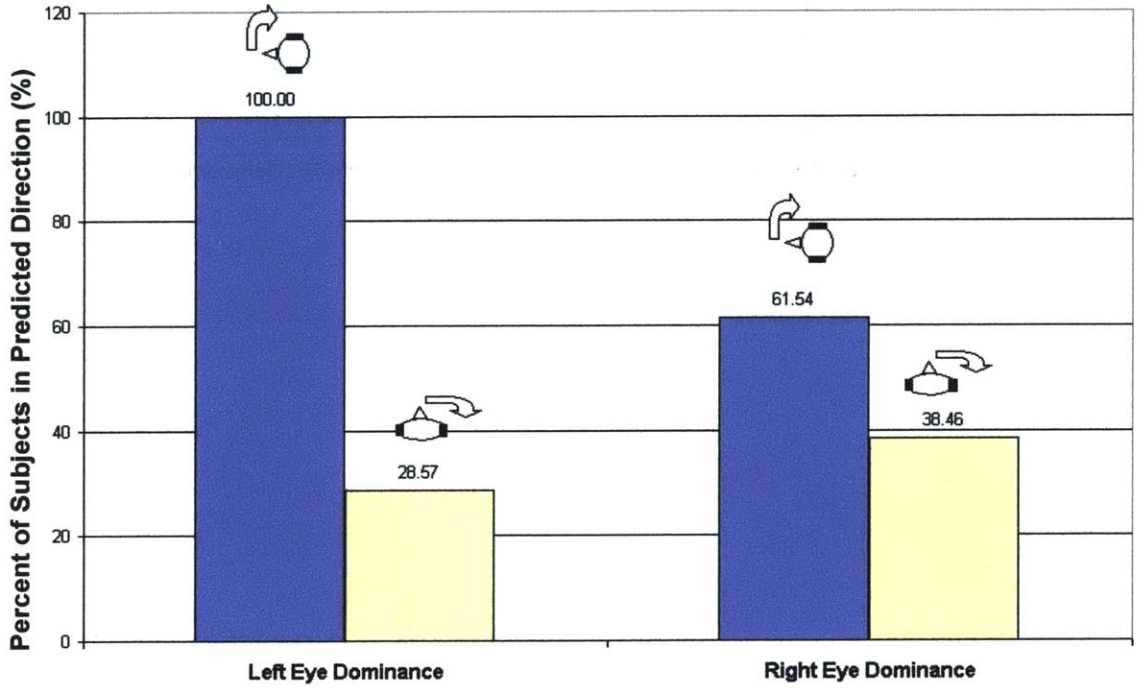

This figure shows the percent of subjects with predicted pitch direction for clockwise head movements between subjects with left eye dominance and subjects with right eye dominance.

Appendix D

LabView Diagram: Automatic Control with Tachometer Analog Input

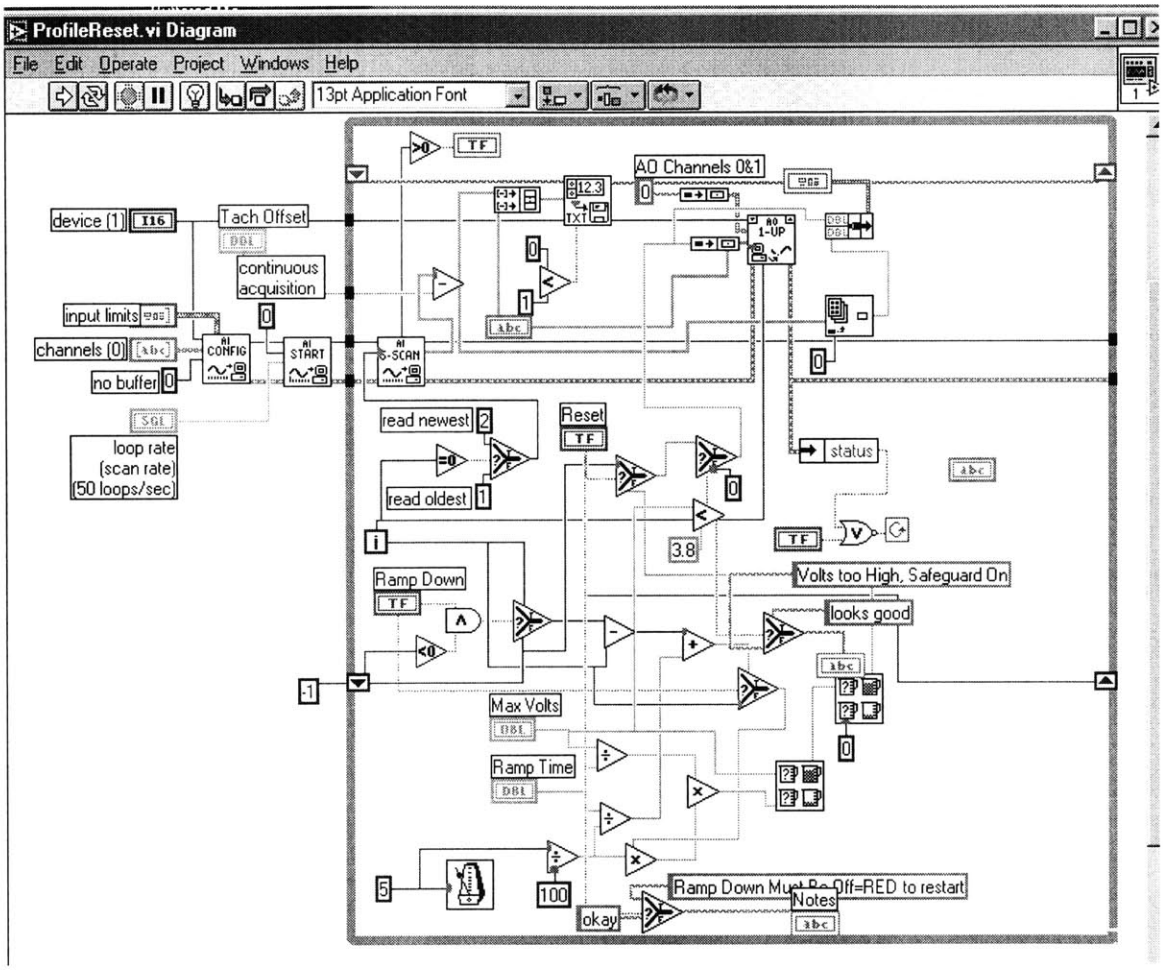

Appendix E

Encoder Open Loop LabView Program

Encoder Open Loop User Interface

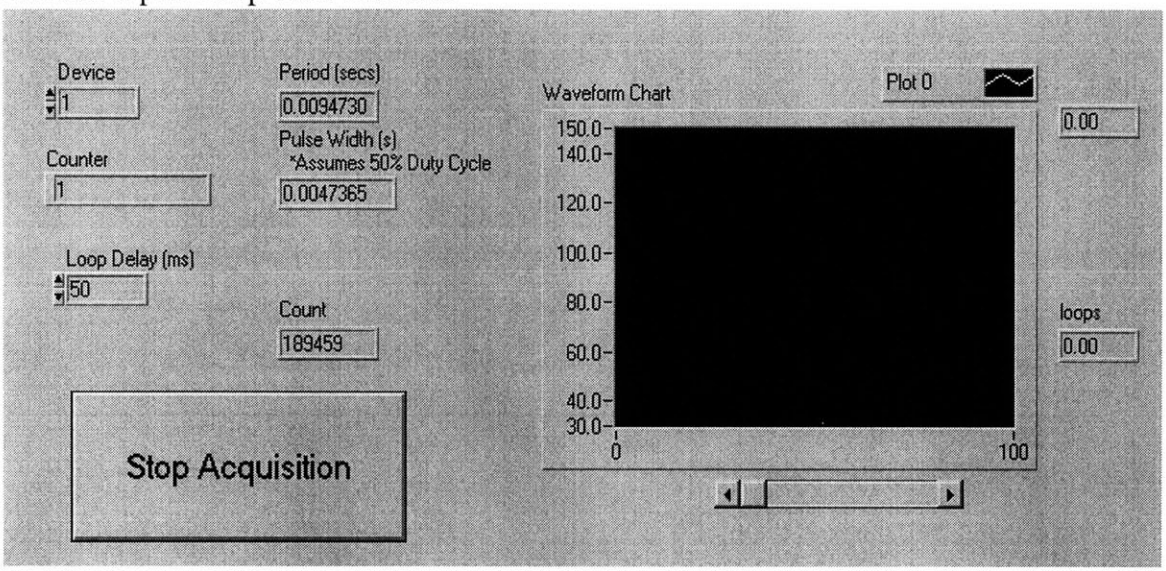

Encoder Open Loop Diagram: the logic for this diagram sends spikes not to null but to the

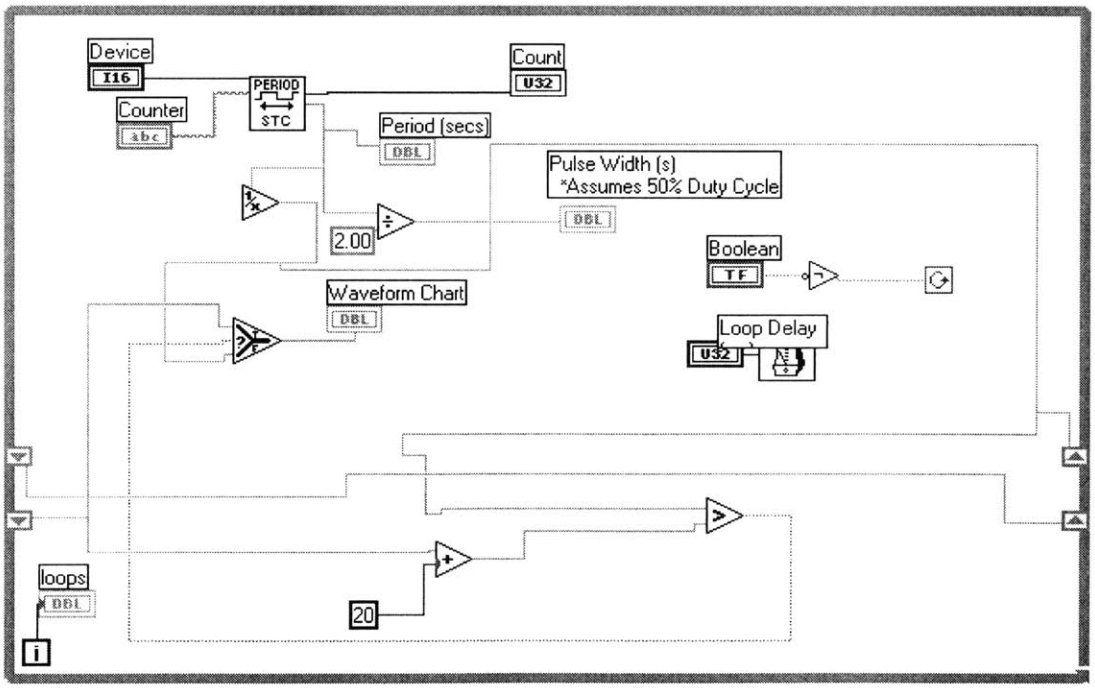

value before the last one. This diagram provides the potential for feedback input.

Appendix F

Accelerometer Open Loop LabView Program

Accelerometer Open Loop User Interface

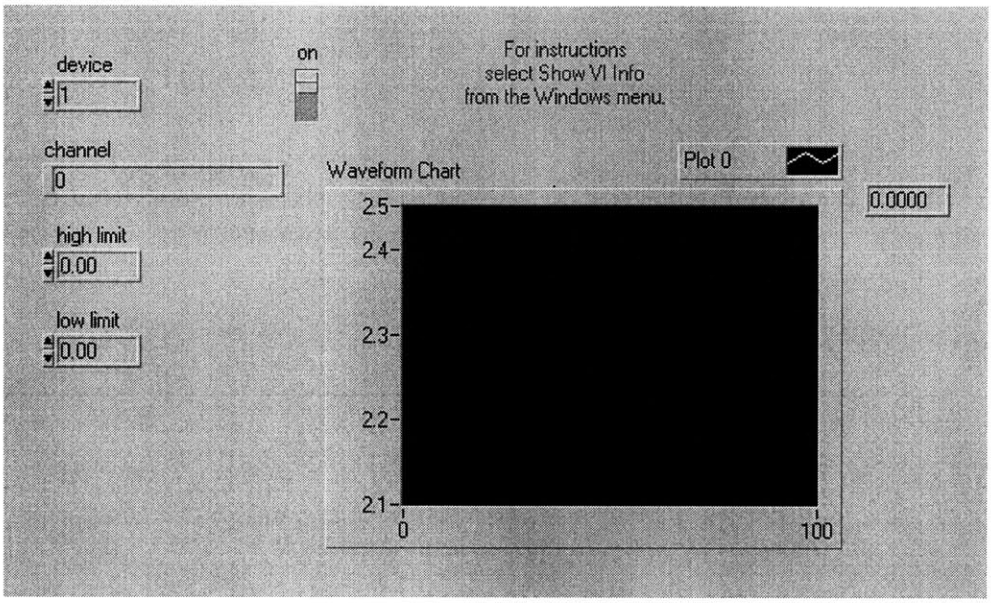

Accelerometer Open Loop Diagram

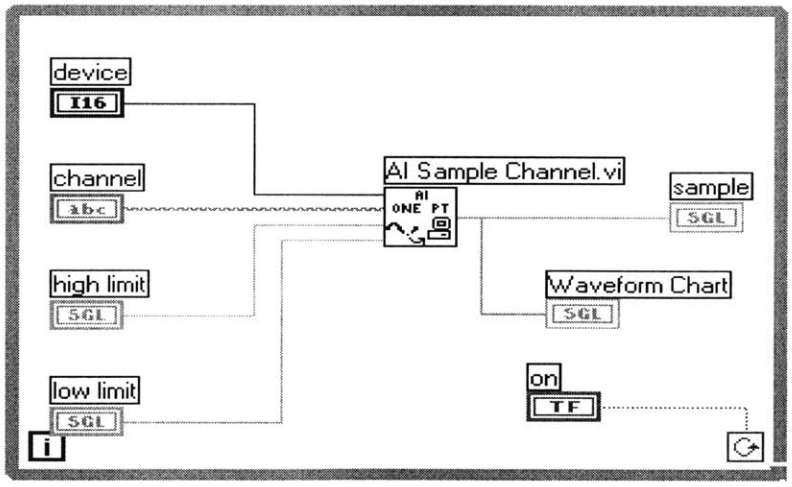

Appendix G

Optimizing K and Ti

Determining K by varying its values and looking at the root locus and feedback step response. The numbers in the step response plot represent the calculated gain K.

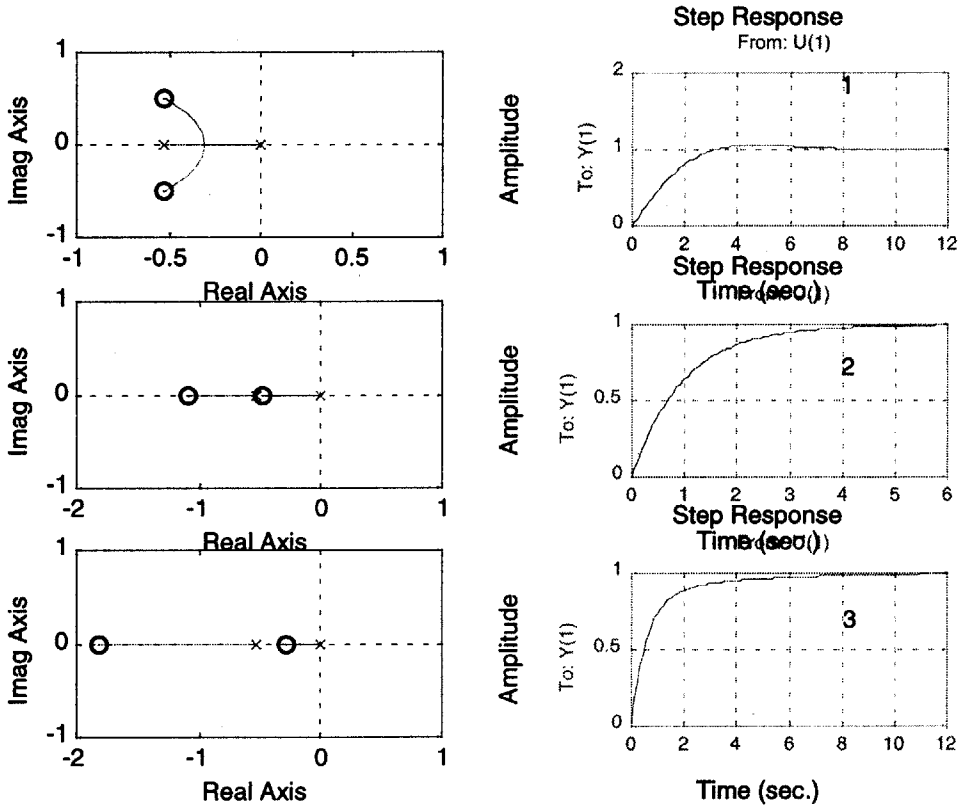

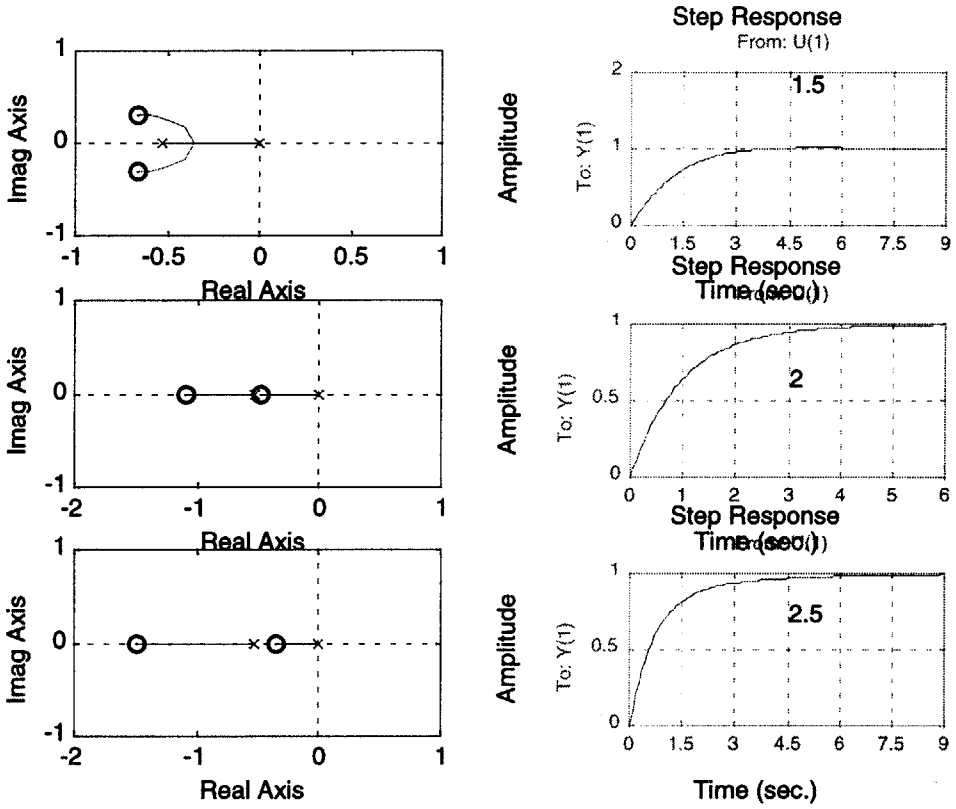
Imag Axis
Real Axis
Step Response
From: U(1)
To: Y(1)
Amplitude
1.5
2
2.5
Time (sec.)

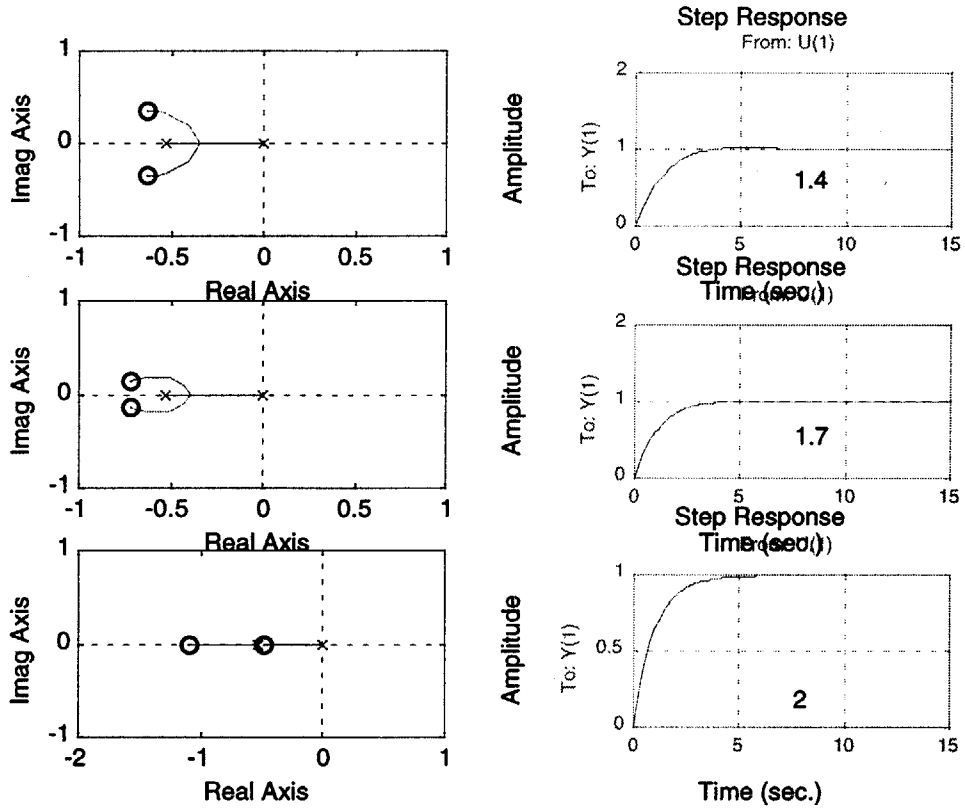

Once K was determined to be 1.5, then trial values for Ti were performed and plotted similarly. Now the values in the step response are the values of Ti, where K=1.5.

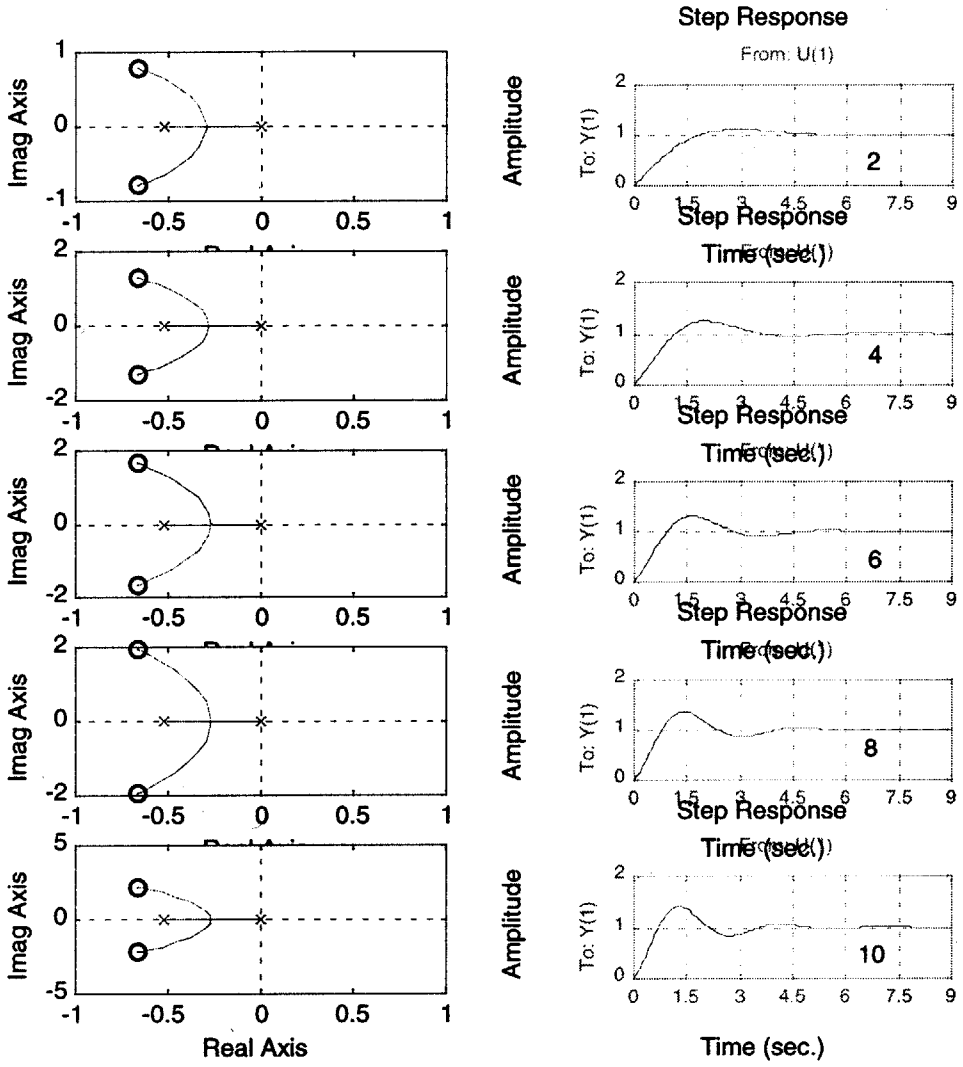
Step Response
From: U(1)
Imag Axis
Amplitude
To: Y(1)
2
4
6
8
10
Time (sec.)
Real Axis

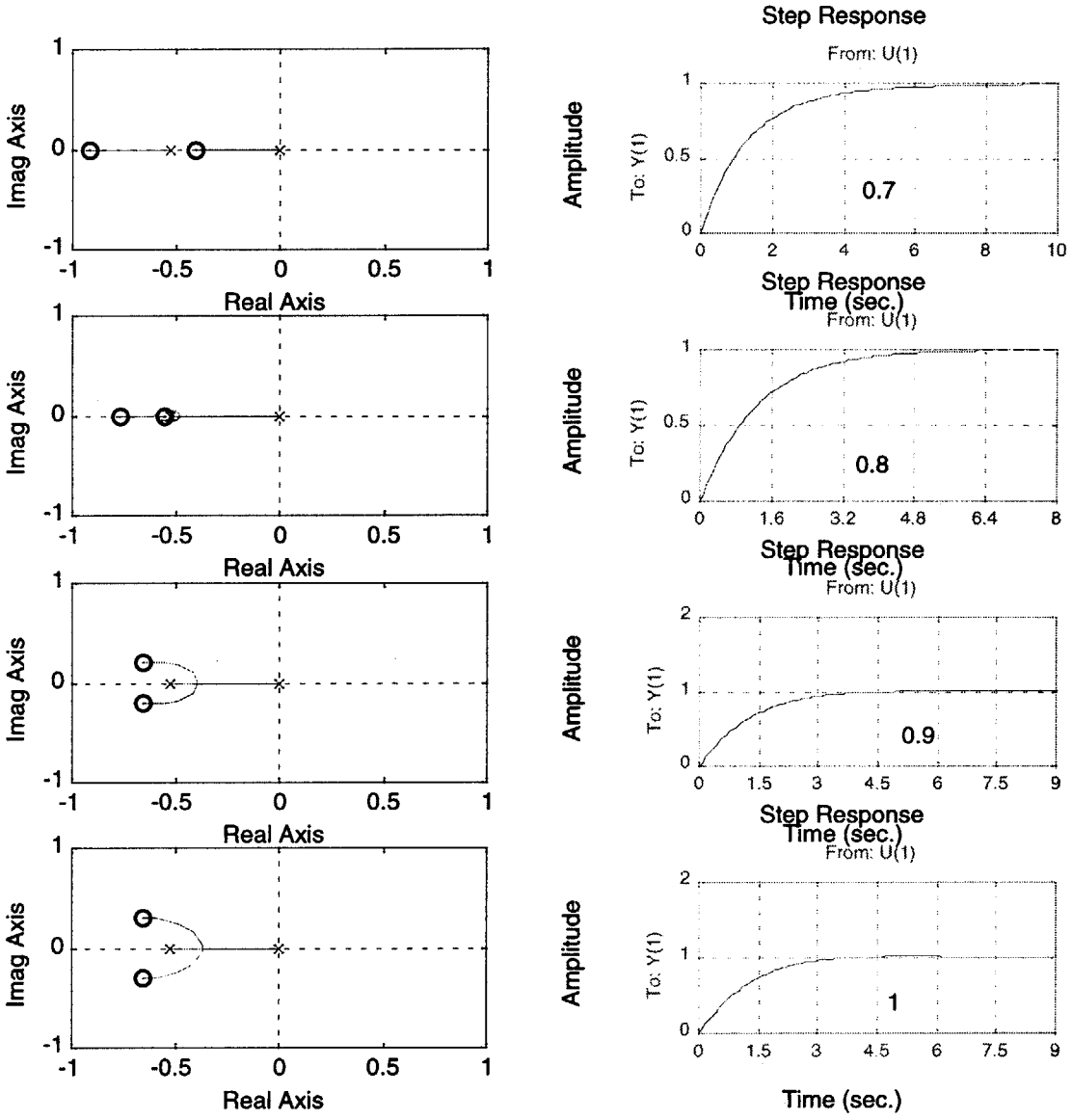
Imag Axis
Real Axis
Step Response
From: U(1)
To: Y(1)
Amplitude
0.7
0.8
0.9
1
Time (sec.)

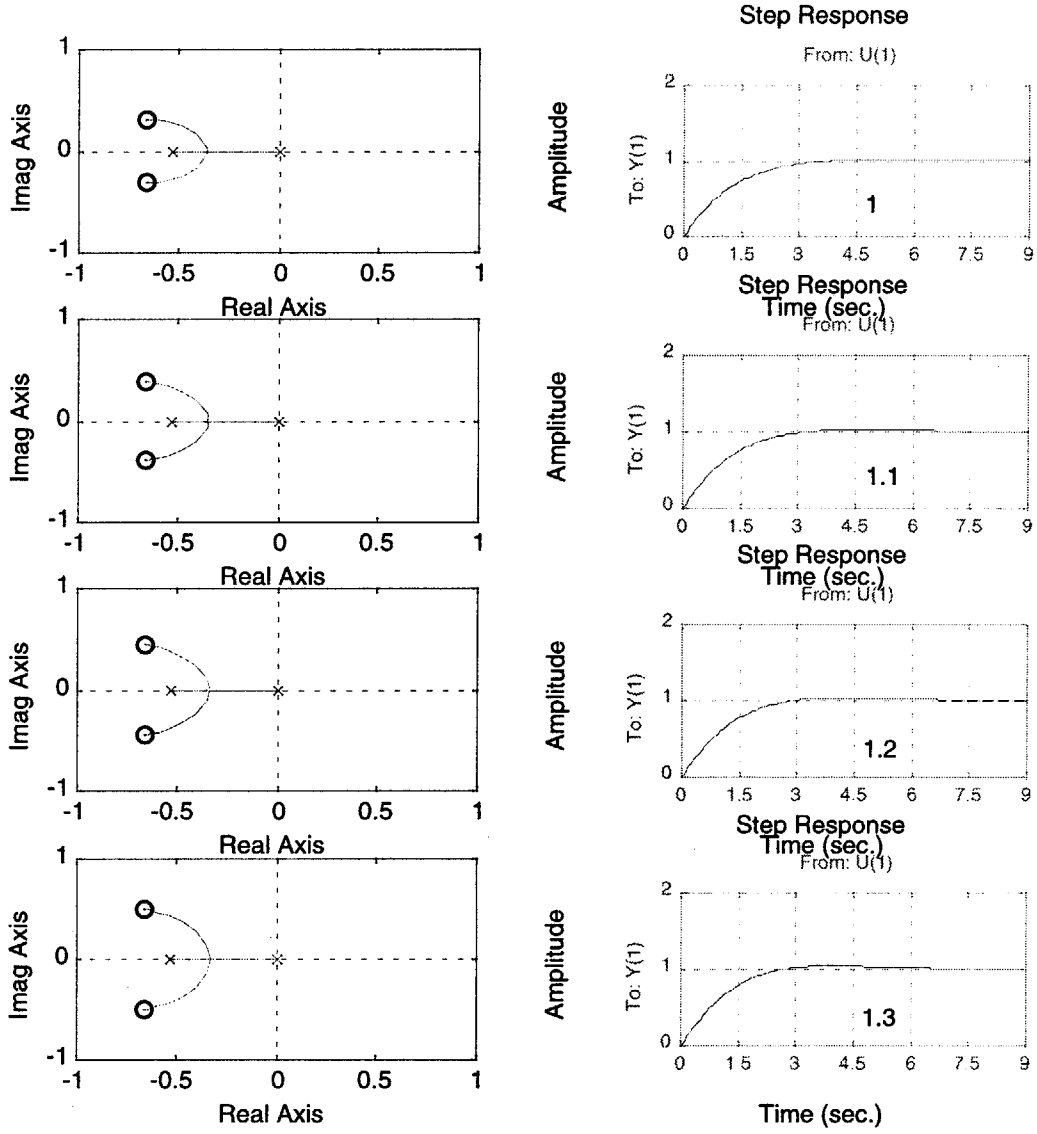

Then although it was assumed that Td, the time constant for derivative control would be 0. This was verified by looking at different values of Td. Indeed, the best response was for when Td=0.

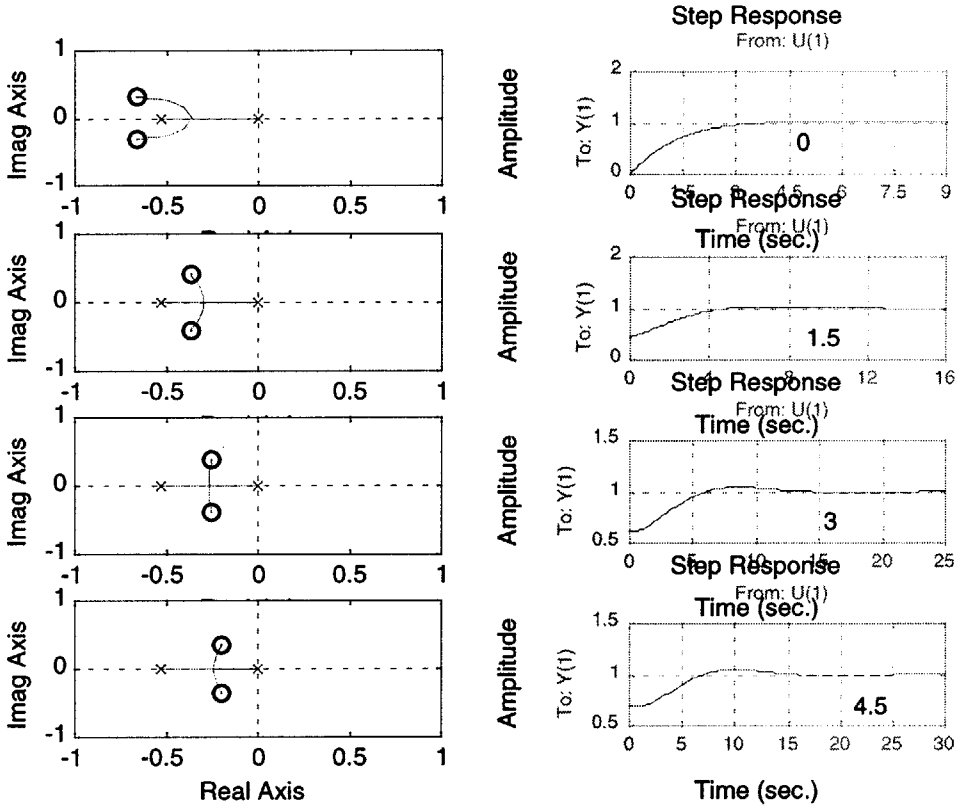
Imag Axis
Real Axis
Step Response
From: U(1)
To: Y(1)
Amplitude
Time (sec.)
0
1.5
3
4.5

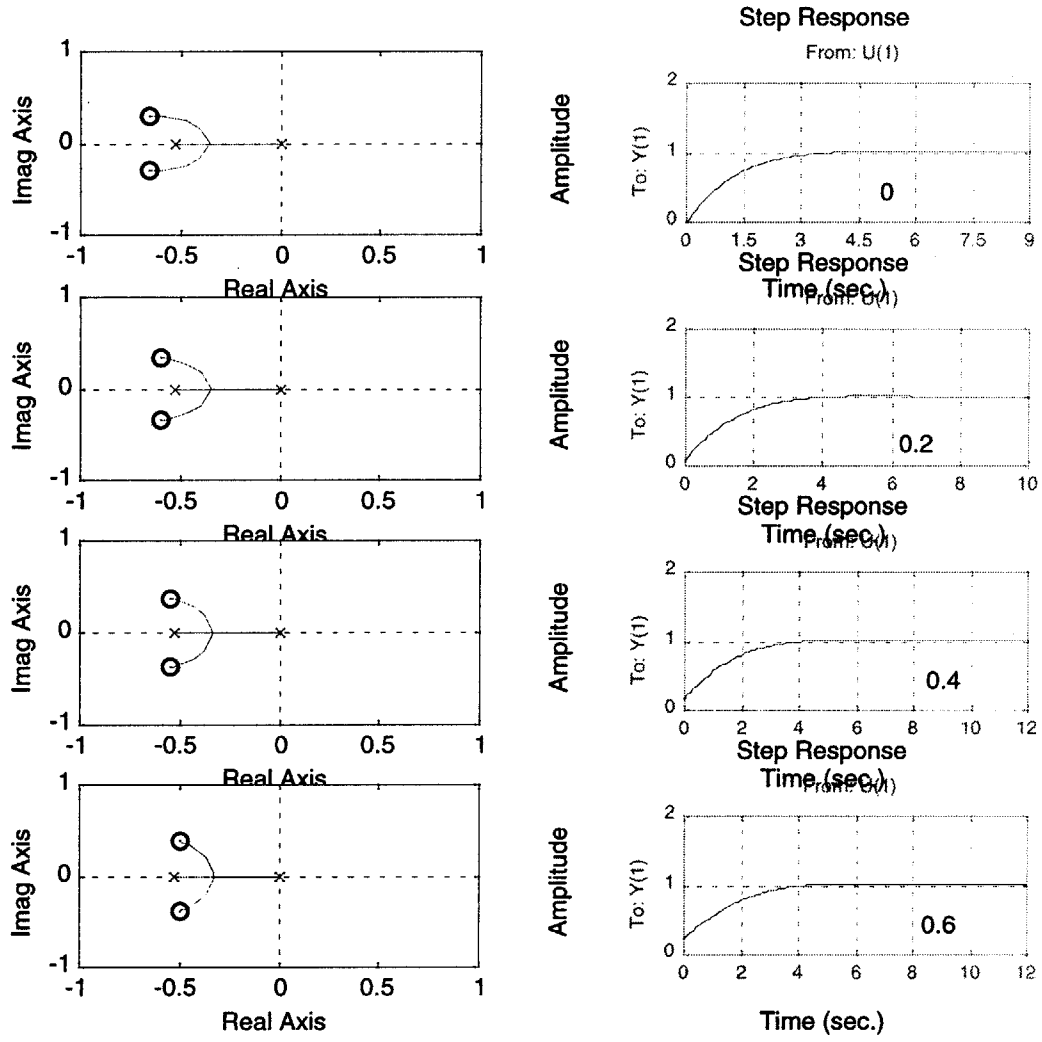
Step Response
From: U(1)
Imag Axis
Real Axis
Amplitude
To: Y(1)
0
0.2
0.4
0.6
Step Response
Time (sec.)
Time (sec.)

Appendix H

Encoder Feedback LabView Programs

Encoder Feedback Interface

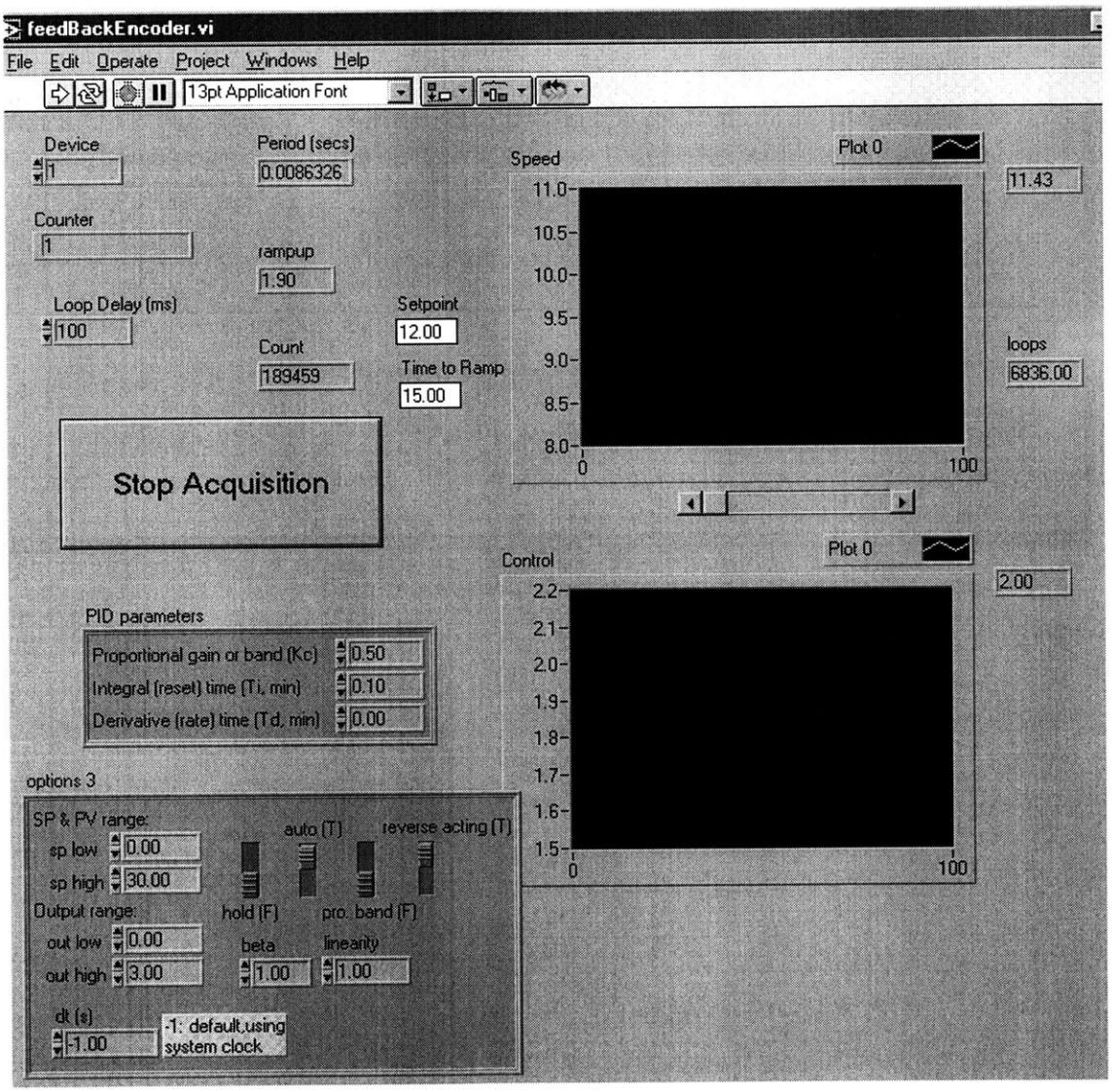

Feedback Encoder Diagrams: Algorithms

In order to not use the PID until the centrifuge was already rotating, sequence frames were used instead of the normal while loop.

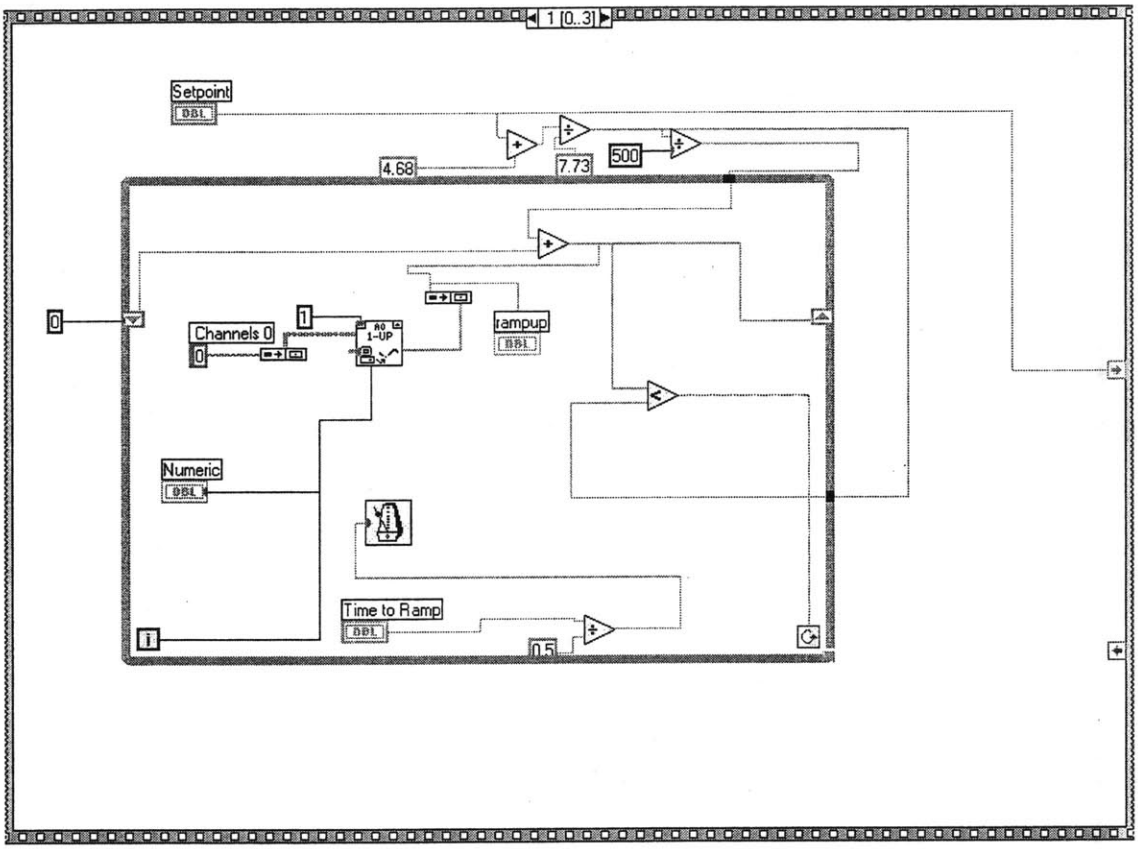
1 [0..3]
Setpoint
DBL
4.68
7.73
500
0
Channels 0
0
1
AO
1-UP
rampup
DBL
Numeric
DBL
Time to Ramp
DBL
0.5
i

Sequence 2:

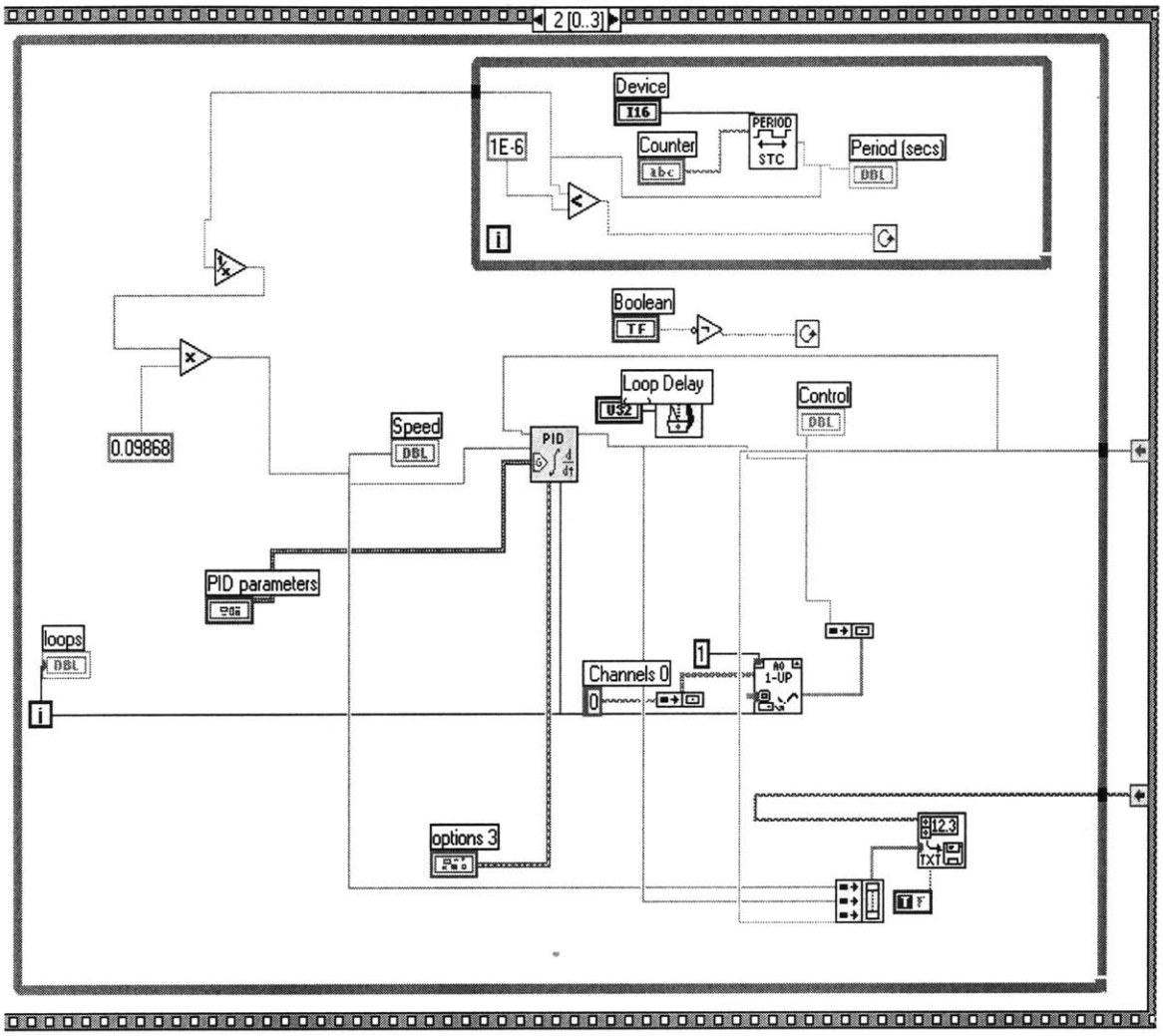
2 [0..3]
Device
I16
1E-6
Counter
PERIOD
STC
Period (secs)
DBL
i
Boolean
TF
Loop Delay
U32
Control
DBL
0.09868
Speed
DBL
PID
PID parameters
loops
DBL
i
Channels 0
0
1
AO
1-UP
options 3
12.3
TXT

Sequence 3:

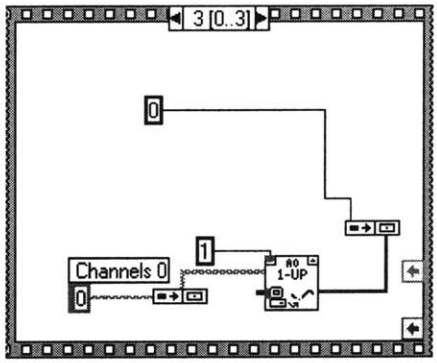
3 [0..3]
0
Channels 0
0
1
AO
1-UP

Appendix I

Accelerometer Feedback LabView Programs

Accelerometer Feedback Interface

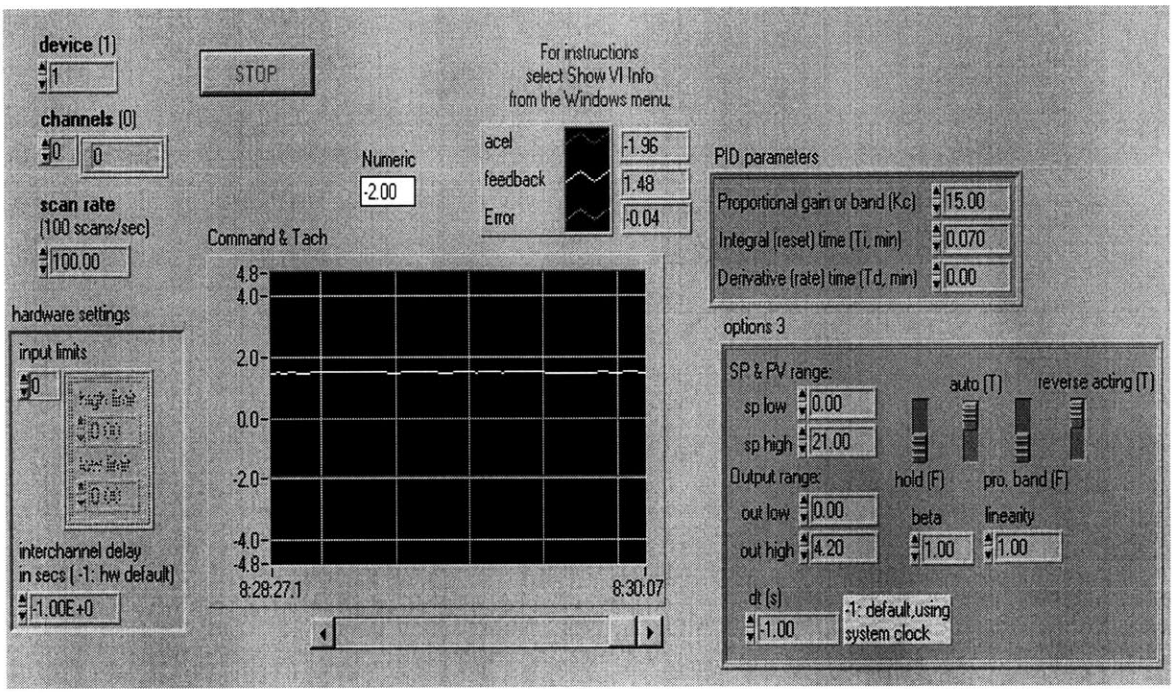

Accelerometer Feedback Diagram

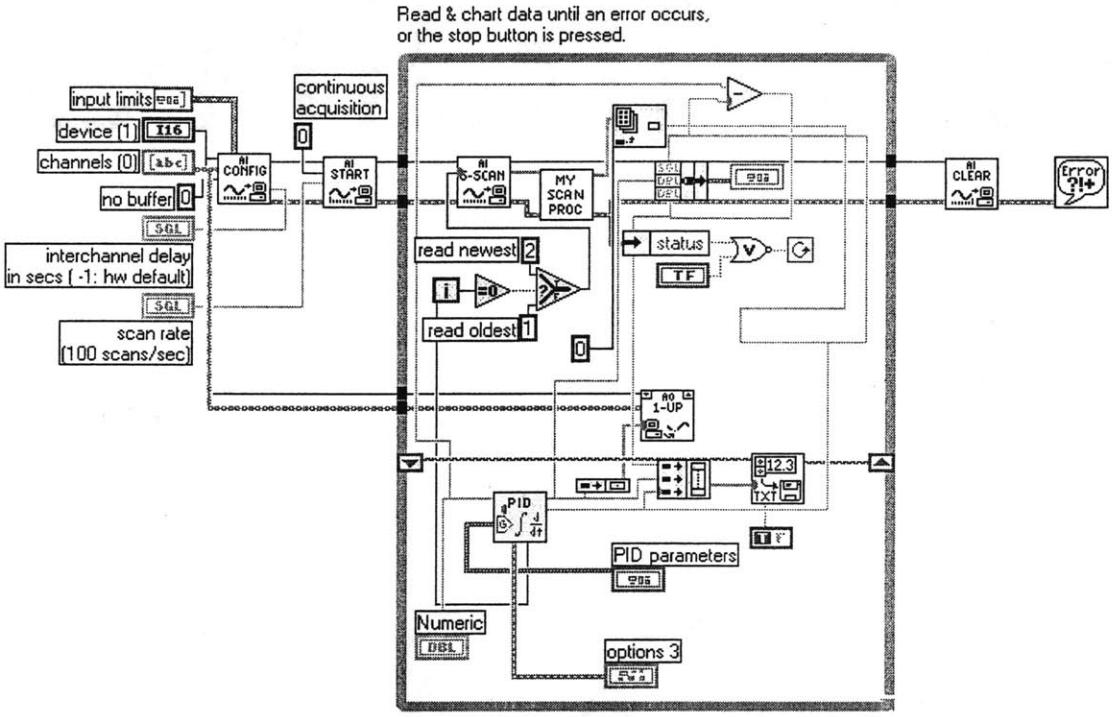

Appendix J

Optic Encoder and Accelerometer Data Sheets

(Appendix J contains illegible text/images)

PACKARD

Panel Mount Optical Encoders

Technical Data

HEDS-5700 Series

Features

- **Two Channel Quadrature Output with Optional Index Pulse**
- **Available with or without Static Drag for Manual or Mechanized Operation**
- **High Resolution – Up to 512 CPR**
- **Long Rotational Life, >1 Million Revolutions**
- **-20 to 85°C Operating Temperature Range**
- **TTL Quadrature Output**
- **Single 5 V Supply**
- **Available with Color Coded Leads**

Description

The HEDS-5700 series is a family of low cost, high performance, optical incremental encoders with mounted shafts and bushings. The HEDS-5700 is available with tactile feedback for hand operated panel mount applications, or with a free spinning shaft for applications requiring a pre-assembled encoder for position sensing.

The encoder contains a collimated LED light source and special detector circuit which allows for high resolution, excellent encoding performance, long rotational life, and increased reliability. The unit outputs two digital waveforms which are 90 degrees out of phase to provide position and direction information. The HEDS-5740 Series provides a third Index Channel.

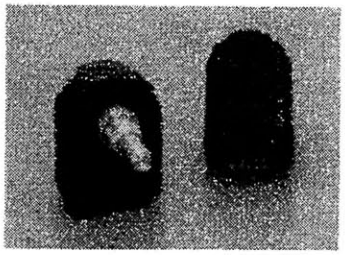

Package Dimensions

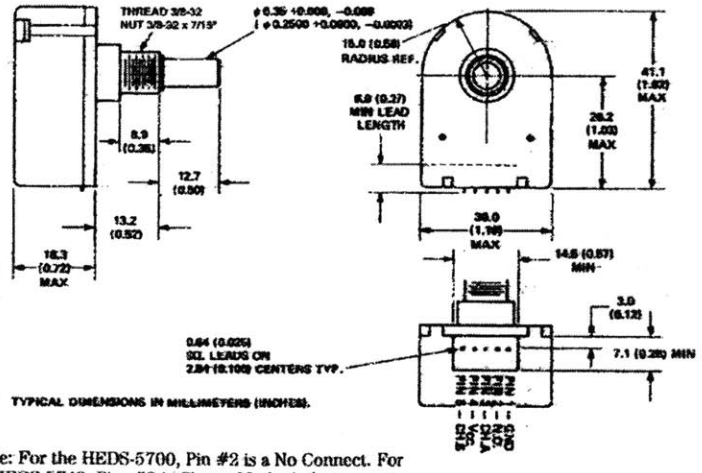

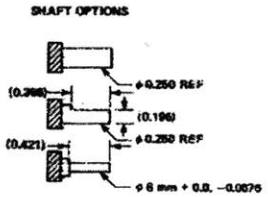

OPTIONAL WIRING COLOR CODE TABLE	
COLOR	OUTPUT
WHITE	A
BROWN	B
RED	V_{CC}
BLACK	GND
BLUE (THREE CHANNEL)	I

*Note: For the HEDS-5700, Pin #2 is a No Connect. For the HEDS-5740, Pin #2 is Channel I, the index output.

5965-5871E

The HEDS-5700 is quickly and easily mounted to a front panel using the threaded bushing, or it can be directly coupled to a motor shaft (or gear train) for position sensing applications.

Applications

The HEDS-5700 with the static drag option is best suited for applications requiring digital information from a manually operated knob. Typical front panel applications include instruments, CAD/CAM systems, and audio/video control boards.

The HEDS-5700 without static drag (free spinning) is best suited for low speed, mechanized operations. Typical applications are copiers, X-Y tables, and assembly line equipment.

Absolute Maximum Ratings

Parameter	Symbol	Min.	Max.	Units	Notes
Storage Temperature	T_s	-40	+85	°C	
Operating Temperature	T_A	-20	+85	°C	
Vibration			20	g	20 Hz - 2 kHz
Supply Voltage	V_{CC}	-0.5	7	V	
Output Voltage	V_O	-0.5	V_{CC}	V	
Output Current per Channel	I_O	-1	5	mA	
Shaft Load – Axial			1	lb	
– Radial			1	lb	

Recommended Operating Conditions

Parameter	Symbol	Min.	Max.	Units	Notes
Temperature	T	-20	+85	°C	Noncondensing Atmosphere
Supply Voltage	V_{CC}	4.5	5.5	V	Ripple < 100 mV_{p-p}
Rotational Speed -- Drag			300	RPM	
-- Free Spinning			2000	RPM	

Electrical Characteristics Over Recommended Operating Range, Typical at 25°C

Parameter	Symbol	Min.	Typ.	Max.	Units	Notes
Supply Current	I_{CC}		17	40	mA	Two Channel
			57	85		Three Channel
High Level Output Voltage	V_{OH}	2.4			V	I_{OH} = -40 µA Max.
Low Level Output Voltage	V_{OL}			0.4	V	I_{OL} = 3.2 mA

Note: If more source current is required, use a 3.2 K pullup resistor on each output.

Mechanical Characteristics

Parameter		Min.	Typ.	Max.	Units	Notes
Starting Torque	– Static Drag		0.47		oz in	
	– Free Spinning			0.14	oz in	
Dynamic Drag	– Static Drag		1.1		oz in	100 RPM
	– Free Spinning		0.70		oz in	2000 RPM
Rotational Life	– Static Drag	1×10^6			Revolutions	1 lb Load
	– Free Spinning	12×10^6			Revolutions	4 oz Radial Load
Mounting Torque of Nut				13	lb in	

Output Waveforms

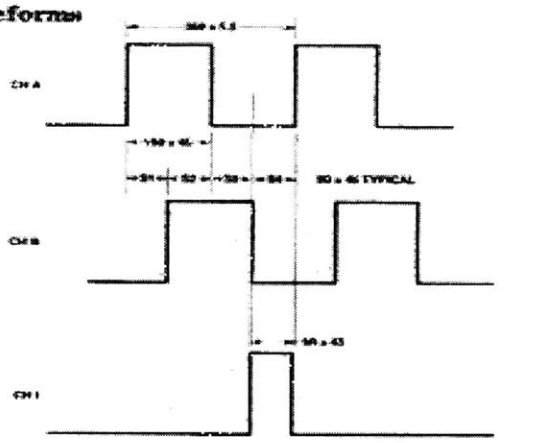

NOTE:
ALL VALUES ARE IN ELECTRICAL DEGREES. THERE ARE 360° e = 1 CYCLE OF RESOLUTION.
SHOWN ARE WORST CASE OVER ONE REVOLUTION.
CH B LEADS CH A FOR COUNTERCLOCKWISE ROTATION.
CH A LEADS CH B FOR CLOCKWISE ROTATION.

Ordering Information

HEDS-57[ ][ ]-[ ][ ][ ]

Outputs
0 - 2 Channel
4 - 3 Channel

Mechanical Configuration
0 - Pins
1 - 6" Coded Leads

Resolutions (Cycles Per Revolution)
HEDS-570X 2 Channel

K - 96 CPR	G - 360 CPR
C - 100 CPR	H - 400 CPR
D - 192 CPR	A - 500 CPR
E - 200 CPR	I - 512 CPR
F - 256 CPR	

HEDS-574X Three Channel*

F - 256 CPR	A - 500 CPR
G - 360 CPR	I - 512 CPR

Drag Option
0 - Free Spining
1 - Static Drag

Shaft Configuration
0 - 1/4" dia. with no flat
1 - 6 mm dia. with no flat
2 - 1/4" dia. with flat

*Please contact factory for other resolutions.

2-118

ANALOG DEVICES

High Accuracy ±1 *g* to ±5 *g* Single Axis *i*MEMS® Accelerometer with Analog Input

ADXL105*

FEATURES
- Monolithic IC Chip
- 2 mg Resolution
- 10 kHz Bandwidth
- Flat Amplitude Response (±1%) to 5 kHz
- Low Bias and Sensitivity Drift
- Low Power 2 mA
- Output Ratiometric to Supply
- User Scalable *g* Range
- On Board Temperature Sensor
- Uncommitted Amplifier
- Surface Mount Package
- +2.7 V to +5.25 V Single Supply Operation
- 1000 *g* Shock Survival

APPLICATIONS
- Automotive
- Accurate Tilt Sensing with Fast Response
- Machine Health and Vibration Measurement
- Affordable Inertial Sensing of Velocity and Position
- Seismic Sensing
- Rotational Acceleration

FUNCTIONAL BLOCK DIAGRAM

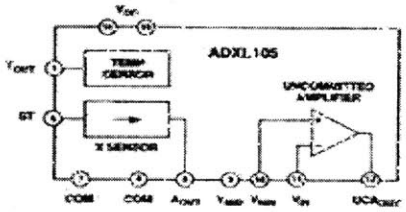

GENERAL DESCRIPTION

The ADXL105 is a high performance, high accuracy and complete single-axis acceleration measurement system on a single monolithic IC. The ADXL105 offers significantly increased bandwidth and reduced noise versus previously available micromachined devices. The ADXL105 measures acceleration with a full-scale range up to ±5 *g* and produces an analog voltage output. Typical noise floor is 225 $\mu g/\sqrt{Hz}$ allowing signals below 2 mg to be resolved. A 10 kHz wide frequency response enables vibration measurement applications. The product exhibits significant reduction in offset and sensitivity drift over temperature compared to the ADXL05.

The ADXL105 can measure both dynamic accelerations, (typical of vibration) or static accelerations (such as inertial force, gravity or tilt).

Output scale factors from 250 mV/*g* to 1.5 V/*g* are set using the on-board uncommitted amplifier and external resistors. The device features an on-board temperature sensor with an output of 8 mV/°C for optional temperature compensation of offset vs. temperature for high accuracy application.

The ADXL105 is available in a hermetic 14-lead surface mount Cerpak with versions specified for the 0°C to +70°C, and −40°C to +85°C temperature ranges.

Call in BOS technical dept. 617-761-7534
761-7000

in general: 1800-ANALOGD

*Patent Pending.
*i*MEMS is a registered trademark of Analog Devices, Inc.

REV. A

One Technology Way, P.O. Box 9106, Norwood, MA 02062-9106, U.S.A.
Tel: 781/329-4700 World Wide Web Site: http://www.analog.com
Fax: 781/326-8703

ADXL105—SPECIFICATIONS (T_A = T_{MIN} to T_{MAX}, T_A = +25°C for J Grade Only, V_S = +5 V, @ Acceleration = 0 g, unless otherwise noted)

Parameter	Conditions	ADXL105JA Min	Typ	Max	Units
SENSOR INPUT					
Measurement Range[2]		±5	±7		g
Nonlinearity	Best Fit Straight Line		0.2		% of FS
Alignment Error[3]			±1		Degrees
Cross Axis Sensitivity[4]	Z Axis, @ +25°C		±1	±5	%
SENSITIVITY[5] (Ratiometric)	At A_{OUT}				
Initial	V_S = 5.0 V	225	250	275	mV/g
		85	105	130	mV/g
vs. Temperature[3,6]			±0.5		%
ZERO g BIAS LEVEL[7] (Ratiometric)	At A_{OUT}				
Zero g Offset Error	From +2.5 V Nominal	-625		+625	mV
vs. Supply		-25		+25	mV/V_{DC}/V
vs. Temperature[3,7]			50		mV
NOISE PERFORMANCE					
Voltage Density[7]	@ +25°C		225	525	$\mu g/\sqrt{Hz}$
Noise in 100 Hz Bandwidth			2.25		mg rms
FREQUENCY RESPONSE					
3 dB Bandwidth		10	12		kHz
Sensor Resonant Frequency		13	15		kHz
TEMP SENSOR[8] (Ratiometric)					
Output Error at +25°C	From +2.5 V Nominal	-100		+100	mV
Nominal Scale Factor			8		mV/°C
Output Impedance			10		kΩ
V_{REF}[9] (Ratiometric)					
Output Error	From +2.5 V Nominal	-15		+15	mV
Output Impedance			16		kΩ
SELF-TEST (Proportional to V_{DD})					
Voltage Delta at A_{OUT}	Self-Test "0" to "1"	100		500	mV
Input Impedance[2]		30	50		kΩ
DIGITAL					
Output Drive	I = ± 50 µA	0.50		V_S - 0.5	V
Capacitive Load Drive		1000			pF
UNCOMMITTED AMPLIFIER					
Initial Offset		-25		+25	mV
Initial Offset vs. Temperature			5		µV/°C
Common-Mode Range		1.0		4.0	V
Input Bias Current[9]			25		nA
Open Loop Gain			100		V/mV
Output Drive	I = ± 160 µA	0.25		V_S - 0.25	V
Capacitive Load Drive		1000			pF
POWER SUPPLY					
Operating Voltage Range		2.70		5.25	V
Quiescent Supply Current	At 5.0 V		1.9	2.6	mA
	At 2.7 V		1.3	2.0	mA
Turn-On Time			700		µs
TEMPERATURE RANGE					
Operating Range J		0		+70	°C
Specified Performance A		-40		+85	°C

NOTES

[1]Guaranteed by tests of zero g bias, sensitivity and output swing.

[2]Alignment of the X axis is with respect to the long edge of the bottom half of the Cerpak package.

[3]Cross axis sensitivity is measured with an applied acceleration on the Z axis of the device.

[4]This parameter is ratiometric to the supply voltage V_{DD}. Specifications is shown with a 5.0 V V_{DD}. To calculate approximate values at another V_{DD}, multiply the specification by V_{DD}/5 V.

[5]Sensitivity refers to the maximum change in parameter from its initial value at +25°C to its worst-case value at T_{MIN} to T_{MAX}.

[6]See Figure 3.

[7]See Figure 2.

[8]CMOS and TTL Compatible.

[9]MOS input bias current is typical at final test.

[10]Min and max specifications are guaranteed. Typical specifications are not tested or guaranteed.

[11]Specifications subject to change without notice.

ABSOLUTE MAXIMUM RATINGS*

Acceleration (Any Axis, Unpowered for 0.5 ms) . . . . . 1000 *g*
Acceleration (Any Axis, Powered for 0.5 ms) . . . . . 500 *g*
$+V_S$ . . . . . −0.3 V to +7.0 V
Output Short Circuit Duration
(Any Pin to Common) . . . . . Indefinite
Operating Temperature . . . . . −55°C to +125°C
Storage Temperature . . . . . −65°C to +150°C

*Stresses above those listed under Absolute Maximum Ratings may cause permanent damage to the device. This is a stress rating only; the functional operation of the device at these or any other conditions above those indicated in the operational sections of this specification is not implied. Exposure to absolute maximum rating conditions for extended periods may affect device reliability.

Package Characteristics

Package	θ_{JA}	θ_{JC}	Device Weight
14 Lead Cerpak	110°C/W	30°C/W	<2 Grams

ORDERING GUIDE

Model	Temperature Range	Package Option
ADXL105JQC	0°C to +70°C	QC-14
ADXL105AQC	−40°C to +85°C	QC-14

CAUTION

ESD (electrostatic discharge) sensitive device. Electrostatic charges as high as 4000 V readily accumulate on the human body and test equipment and can discharge without detection. Although the ADXL105 features proprietary ESD protection circuitry, permanent damage may occur on devices subjected to high energy electrostatic discharges. Therefore, proper ESD precautions are recommended to avoid performance degradation or loss of functionality.

Drops onto hard surfaces can cause shocks of greater than 1000 *g* and exceed the absolute maximum rating of the device. Care should be exercised in handling to avoid damage.

PIN FUNCTION DESCRIPTIONS

Pin No.	Name	Description
1	T_{OUT}	Temperature Sensor Output
2, 3, 5	NC	No Connect
4	COM	Common
6	ST	Self-Test
7	COM	Common (Substrate)
8	A_{OUT}	Accelerometer Output
9	V_{MID}	$V_{DD}/2$ Reference Voltage
10	V_{NIN}	Uncommitted Amp Noninverting Input
11	V_{IN}	Uncommitted Amp Inverting Input
12	UCA_{OUT}	Uncommitted Amp Output
13, 14	V_{DD}	Power Supply Voltage

PIN CONFIGURATION

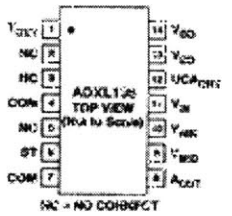

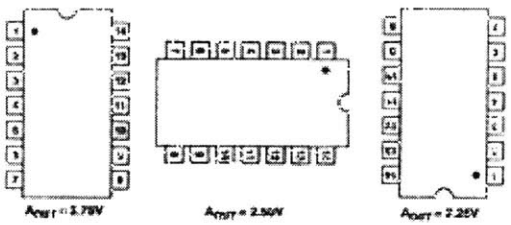

Figure 1. ADXL105 Response Due to Gravity

ADXL105—Typical Performance Characteristics

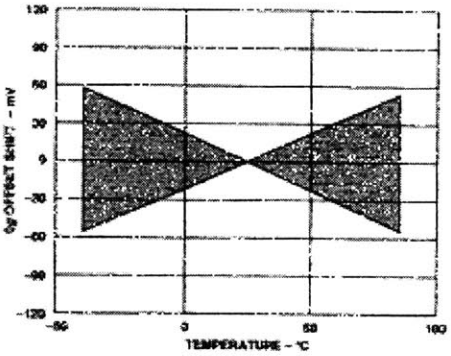

Figure 2. Typical 0 g Shift vs. Temperature*

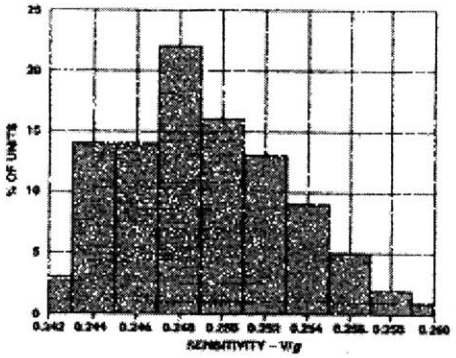

Figure 5. Sensitivity Distribution*

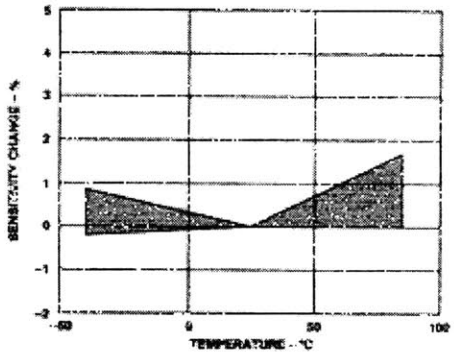

Figure 3. Typical Sensitivity Shift vs. Temperature*

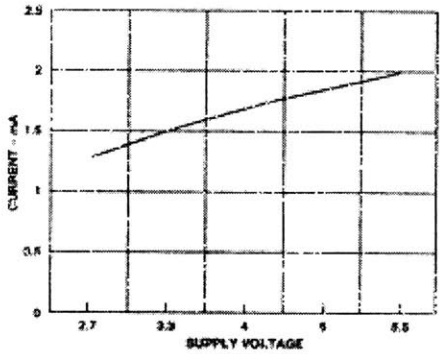

Figure 6. Typical Supply Current vs. Supply Voltage

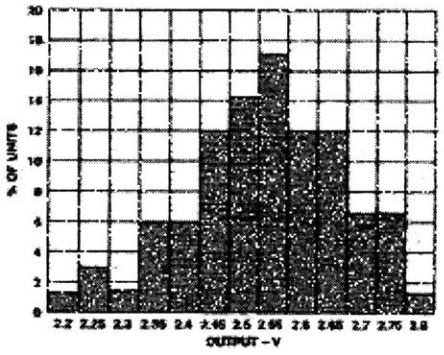

Figure 4. 0 g Output Distribution*

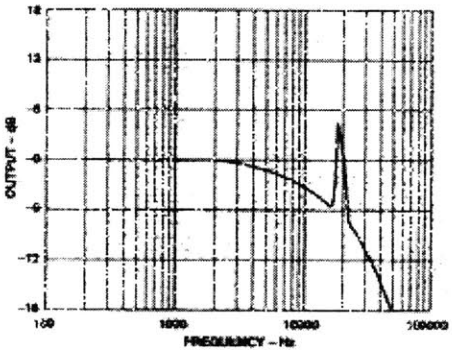

Figure 7. Noise Graph

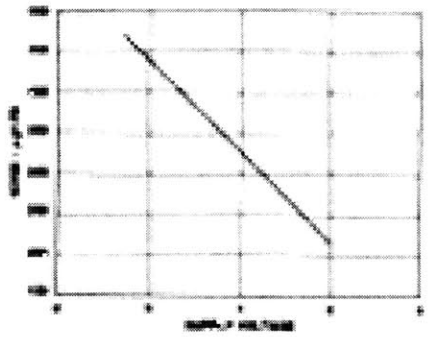

Figure 8. Typical Noise Density vs. Supply Voltage

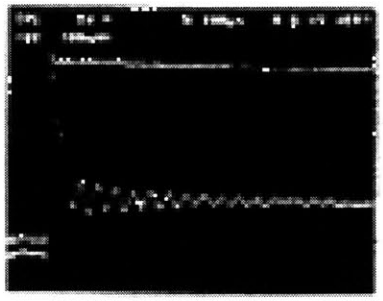

Figure 11. Typical Self-Test Response at V_{DD} = 5 V

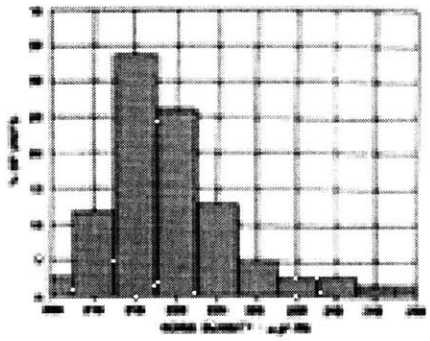

Figure 9. Noise Distribution*

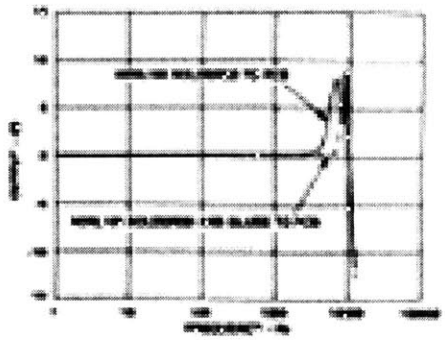

Figure 12. Frequency Response

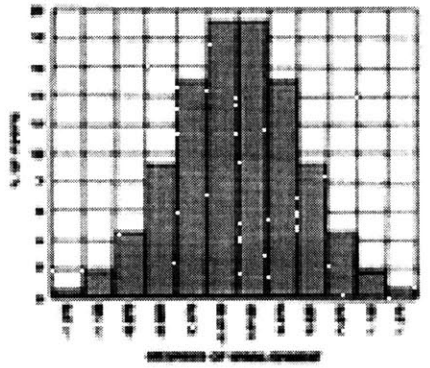

Figure 10. Rotational Die Alignment*

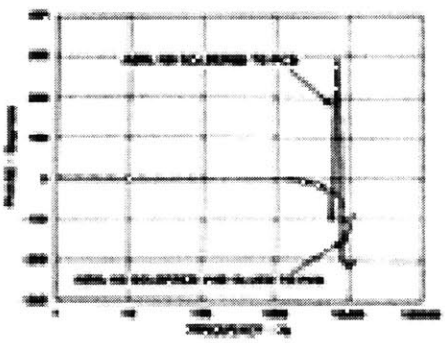

Figure 13. Phase Response

ADXL105

THEORY OF OPERATION

The ADXL105 is a complete acceleration measurement system on a single monolithic IC. It contains a polysilicon surface-micromachined sensor and BiMOS signal conditioning circuitry to implement an open loop acceleration measurement architecture. The ADXL105 is capable of measuring both positive and negative accelerations to a maximum level of ±5 g. The accelerometer also measures static acceleration such as gravity, allowing it to be used as a tilt sensor.

The sensor is a surface micromachined polysilicon structure built on top of the silicon wafer. Polysilicon springs suspend the structure over the surface of the wafer and provide a resistance against acceleration-induced forces. Deflection of the structure is measured with a differential capacitor structure that consists of two independent fixed plates and a central plate attached to the moving mass. A 180° out-of-phase square wave drives the fixed plates. An acceleration causing the beam to deflect, will unbalance the differential capacitor resulting in an output square wave whose amplitude is proportional to acceleration. Phase sensitive demodulation techniques are then used to rectify the signal and determine the direction of the acceleration.

An uncommitted amplifier is supplied for setting the output scale factor, filtering and other analog signal processing.

A ratiometric voltage output temperature sensor measures the exact die temperature and can be used for optional calibration of the accelerometer over temperature.

V_{DD}

The ADXL105 has two power supply (V_{DD}) pins, 13 and 14. The two pins should be connected directly together. The output of the ADXL105 is ratiometric to the power supply. Therefore a 0.22 µF decoupling capacitor between V_{DD} and COM is required to reduce power supply noise. To further reduce noise, insert a resistor (and/or a ferrite bead) in series with the V_{DD} pin. See the EMC and Electrical Noise section for more details.

COM

The ADXL105 has two common (COM) pins, 4 and 7. These two pins should be connected directly together and Pin 7 grounded.

ST

The ST pin (Pin 6) controls the self-test feature. When this pin is set to V_{DD}, an electrostatic force is exerted on the beam of the accelerometer causing the beam to move. The change in output resulting from movement of the beam allows the user to test for mechanical and electrical functionality. This pin may be left open-circuit or connected to common in normal use. The self-test input is CMOS and TTL compatible.

A_{OUT}

The accelerometer output (Pin 8) is set to a nominal scale factor of 250 mV/g (for V_{DD} = 5 V). Note that A_{OUT} is guaranteed to source/sink a minimum of 50 µA (approximately 50 kΩ output impedance). So a buffer may be required between A_{OUT} and some A-to-D converter inputs.

V_{REF}

V_{REF} is nominally $V_{DD}/2$. It is primarily intended for use as a reference output for the on board uncommitted amplifier (UCA) as shown in Figures 14a and 14b. Its output impedance is approximately 10 kΩ.

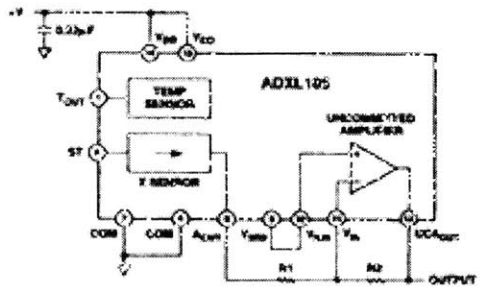

GAIN	SCALE – mV/g	R1	R2
1	250	80kΩ	120kΩ
2	500	80kΩ	320kΩ
3	750	80kΩ	560kΩ
4	1000	80kΩ	800kΩ

a. Using the UCA to Change the Scale Factor

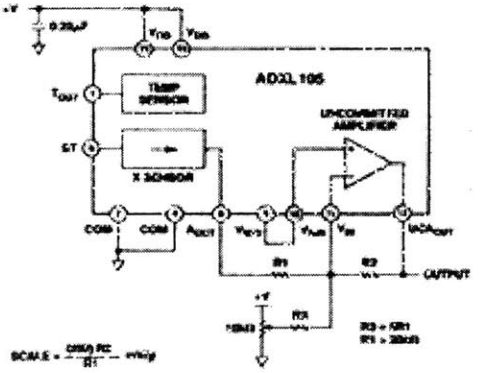

b. Using the UCA to Change the Scale Factor and Zero g Bias

Figure 14. Application Circuit for Increasing Scale Factor

T_{OUT}

The temperature sensor output is nominally 2.5 V at +25°C and typically changes 8 mV/°C, and is optimized for repeatability rather than accuracy. The output is ratiometric with supply voltage.

Uncommitted Amplifier (UCA)

The uncommitted amplifier has a low noise, low drift bipolar front end design. The UCA can be used to change the scale factor of the ADXL105 as shown in Figure 14. The UCA may also be used to add a 1- or 2-pole active filter as shown in Figures 15a through 15d.

Output Scaling

The acceleration output (A_{OUT}) of the ADXL105 is nominally 250 mV/*g*. This scale factor may not be appropriate for all applications. The UCA may be used to increase the scale factor. The simplest implementation would be as shown in Figure 14*a*. Since the 0 *g* offset of the ADXL105 is 2.5 V ± 625 mV, using a gain of greater than 4 could result in having the UCA output at 0 V or 5 V at 0 *g*. The solution is to add R3 and VR1, as shown in Figure 14*b*, turning the UCA into a summing amplifier. VR1 is adjusted such that the UCA output is $V_{DD}/2$ at 0 *g*.

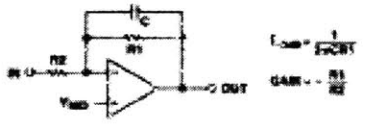

a. 1-Pole Low-Pass Filter

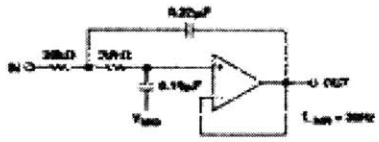

b. 2-Pole Bessel Low-Pass Filter

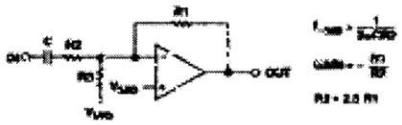

c. 1-Pole High-Pass Filter

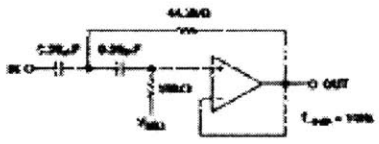

d. 2-Pole Bessel High-Pass Filter

Figure 15. UCA Used as Active Filters

Device Bandwidth vs. Resolution

In general the bandwidth selected will determine the noise floor and hence, the measurement resolution (smallest detectable acceleration) of the ADXL105. Since the noise of the ADXL105 has the characteristic of white Gaussian noise that contributes equally at all frequencies, the noise amplitude may be reduced by simply reducing the bandwidth. So the typical noise of the ADXL105 is:

$$Noise\ (rms) = (225\ \mu g/\sqrt{Hz}) \times (\sqrt{Bandwidth \times K})$$

Where

K = 1.6 for a single-pole filter

K = 1.4 for a 2-pole filter

So given a bandwidth of 1000 Hz, the typical rms noise floor of an ADLX105 will be:

$$Noise = (225\ \mu g/\sqrt{Hz}) \times (\sqrt{1000 \times 1.6})$$

$$= 9\ m g\ rms \text{ for a single-pole filter}$$

and

$$Noise = (225\ \mu g/\sqrt{Hz}) \times (\sqrt{1000 \times 1.4})$$

$$= 8.4\ m g\ rms \text{ for 2-pole filter}$$

Often the peak value of the noise is desired. Peak-to-peak noise can only be estimated by statistical means. Table I may be used for estimating the probabilities of exceeding various peak values given the rms value. The peak-to-peak noise value will give the best estimate of the uncertainty in a single measurement.

Table I. Estimation of Peak-to-Peak Noise

Nominal Peak-to-Peak Value	% of Time that Noise Will Exceed Peak-to-Peak Value
2 × rms	32%
3 × rms	13%
4 × rms	4.6%
5 × rms	1.2%
6 × rms	0.27%
7 × rms	0.047%
8 × rms	0.0063%

The UCA may be configured to act as an active filter with gain and 0 *g* offset control as shown in Figure 16.

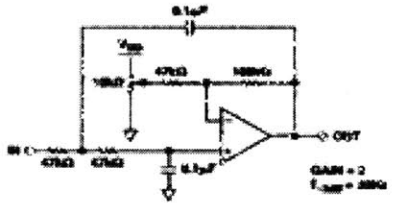

Figure 16. UCA Configured as an Active Low-Pass Filter with Gain and Offset

EMC and Electrical Noise

The design of the ADXL105 is such that EMI or magnetic fields do not normally affect it. Since the ADXL105 is ratiometric, conducted electrical noise on V_{DD} does affect the output. This is particularly true for noise at the ADXL105's internal clock frequency (200 kHz) and its odd harmonics. So maintaining a clean supply voltage is key in preserving the low noise and high resolution properties of the ADXL105.

One way to ensure that V_{DD} contains no high frequency noise is to add an R-C low-pass filter near the V_{DD} pin as shown in Figure 17. Using the component values shown in Figure 17, noise at 200 kHz is attenuated by approximately –23 dB. Assuming the ADXL105 consumes 3 mA, there will be a 100 mV drop across R1. This can be neglected simply by using the ADXL105's V_{DD} as the A-to-D converter's reference voltage as shown in Figure 17.

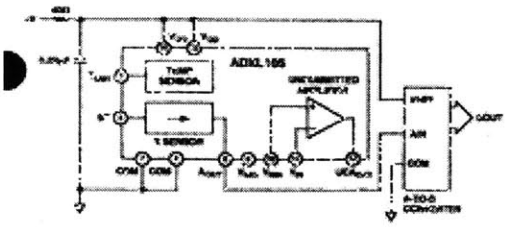

Figure 17. Reducing Noise on V_{DD}

Dynamic Operation

In applications where only dynamic accelerations (vibration) are of interest, it is often best to ac-couple the accelerometer output as shown in Figures 15c and 15d. The advantage of ac coupling is that dc offset variability (part to part) and drifts are eliminated.

Low Power Operation

The most straightforward method of lowering the ADXL105's power consumption is to minimize its supply voltage. By lowering V_{DD} from 5 V to 2.7 V the power consumption goes from 9.3 mW to 3.5 mW. There may be reasons why lowering the supply voltage is impractical in many applications, in which case the best way to minimize power consumption is by power cycling.

The ADXL105 is capable of turning on and giving an accurate reading within 700 µs (see Figure 18). Most microcontrollers can perform an A-to-D conversion in under 25 µs. So it is practical to turn on the ADXL105 and take a reading in under 750 µs. Given a 100 Hz sample rate the average current required at 2.7 V would be:

$$100\ samples/s \times 750\ \mu s \times 1.3\ mA = 97.5\ \mu A$$

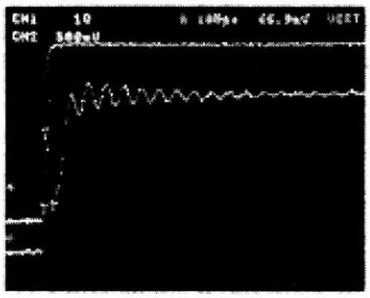

Figure 18. Typical Turn-On Response at V_{DD} = 5 V

Note that if a filter is used in the UCA, sufficient time must be allowed for the settling of the filter as well.

Broadband Operation

The ADXL105 has a number of characteristics that permits operation over a wide frequency range. Its frequency and phase response is essentially flat from dc to 10 kHz (see Figures 12 and 13). Its sensitivity is also constant over temperature (see Figure 3). In contrast, most accelerometers do not have linear response at low frequencies (in many cases, no response at very low frequencies or dc), and often have a large sensitivity temperature coefficient that must be compensated for. In addition, the ADXL105's noise floor is essentially flat from dc to 5 kHz where it gently rolls off (see Figure 7). The beam resonance at 16 kHz can be seen in Figure 7 where there is a small noise peak (+5 dB) at the beam's resonant frequency. There are no other significant noise peaks at any frequency.

The resonant frequency of the beam in the ADXL105 determines its high frequency limit. However the resonant frequency of the Cerpak package is typically around 7 kHz. As a result, it is not unusual to see 6 dB peaks occurring at the package resonant frequency (as shown in Figures 12 and 13). Indeed, the PCB will often have one or more resonant peaks well below 7 kHz. Therefore, if the application calls for accurate operation at or above 6 kHz the ADXL105 should be glued to the PCB in order to eliminate the amplitude response peak due to the package, and careful consideration should be given to the PCB mechanical design.

CALIBRATING THE ADXL105

The initial value of the offset and scale factor for the ADXL105 will require dc calibration for applications such as tilt measurement.

For low g applications, the force of gravity is the most stable, accurate and convenient acceleration reference available. An approximate reading of the 0 g point can be determined by orienting the device parallel to the Earth's surface and then reading the output. For high accuracy, a calibrated fixture must be used to ensure exact 90 degree orientation to the 1 g gravity signal.

An accurate sensitivity calibration method is to make a measurement at +1 g and −1 g. The sensitivity can be determined by the two measurements. This method has the advantage of being less sensitive to the alignment of the accelerometer because the on axis signal is proportional to the Cosine of the angle. For example, a 5° error in the orientation results in only a 0.4% error in the measurement.

To calibrate, the accelerometer measurement axis is pointed directly at the Earth. The 1 g reading is saved and the sensor is turned 180° to measure −1 g. Using the two readings and sensitivity is calculated:

$$Sensitivity = [1\ g\ Reading - (-1\ g\ Reading)]/2\ V_{DC}$$

OUTLINE DIMENSIONS

Dimensions shown in inches and (mm).

14-Lead Cerpak
(QC-14)